Distribution and fate of methane
released from submarine sources
–
Results of measurements using an improved *in situ* mass
spectrometer

Dissertation

zur Erlangung des Doktorgrades der Naturwissenschaften

(Dr. rer. nat.)

dem Fachbereich 5 (Geowissenschaften) der Universität

Bremen vorgelegt von

Torben Gentz

Bremen, Januar 2013

1. Gutachter: Herr Prof. Dr. Michael Schlüter

2. Gutachter: Herr Prof. Dr. Gerhard Bohrmann

Content

Chapter 1: Introduction

Chapter 2: Methodological overview, objectives and outline of the manuscripts

Chapter 5: Manuscript in preparation - mapping, quantification and inventory calculation of a methane plume by in situ mass spectrometry above a gas seepage.

Chapter 6: Synthesis

Summary

Methane (CH_4) is the most frequent organic compound in the atmosphere and its influence on the global climate is subject of currently conducted scientific discussion. Despite its limited content in the atmosphere (1787 ppbv in 2003), it contributes to ~15 % of the global warming as a result of its 20 to 40 times higher global warming potential compared to carbon dioxide (CO_2) on a 100 year timescale. One source of atmospheric methane is the release of biogenic and/or thermogenic CH_4 from the oceans seafloor, which is currently one of the research priorities of the marine geosciences. These submarine sources are characterized by rising gas bubbles or diffusive methane flux into the water column. It is estimated that these point sources release a total of ~30 Tg CH_4 per year into the ocean, and after its biological oxidation or dissolving in the water, ~10 Tg CH_4 are released into the atmosphere per year. Additionally, due to the warming of the oceans, an increasing release of methane can be expected as a result of the melting of permafrost and gas hydrates. Steep gradients over very short distances (< 20 m) and high time-based variability (few hours) are known from dissolved methane concentrations in the water column above these submarine CH_4 sources. Due to the limited number of samples taken by conventional *ex situ* methods, an accurate quantification of the methane distribution could hardly be estimated.

Nevertheless, one objective of the present thesis was the detailed spatial representation of the dissolved CH_4 in the water column originates from submarine seeps as well as the study of relevant pathways such as vertical or horizontal transport, dilution and its microbial oxidation.

Therefore, the first part of the dissertation deals with the optimization and establishment of a novel underwater mass spectrometer (UWMS, Inspectr200-200, Applied Microsystems Limited™) designed for inline, real time and *in situ* sampling in high frequency. Analysis and evaluation of several thousand samples per day take place in one step, so that one obtains the measurement result *in situ* and, unlike using conventional methods, without delay, and thus the sampling strategies can be adapted to the existing environment. Additionally, through the use of this novel analytical tool, potential sources of errors that occur during sampling or transport to

the laboratories are eliminated. In order to be able to use the potential of this mass spectrometer for scientific research questions, it was necessary to optimize the detection limit for the trace gases that were to be determined. For this purpose, a Stirling cooler was applied, which serves as a trapping system for water vapour and thus leads to optimized conditions for the analysis. In particular for CH_4, the detection limit could be decreased from more than 100 nmol L^{-1} to 16 nmol L^{-1}.

Within the framework of this thesis two gas ebullition areas were studied in detail. While one, which is located in the continental shelf northwest of Spitsbergen, is in the center of scientific attention, the gas ebullition area that was studied in the North Sea has not yet been examined until now with regard to the methane release into the water column and its subsequent pathways.

The global climatic change in the Arctic regions can be increasingly monitored. Thus years an increase in ocean temperature was observed in the last 30, which potentially leads to destabilization of gas hydrates and reduced methane storage capacity of the sediments. In the studied area with a size of 175 km² and an average water depth of 245 m, 10 gas ebullition locations, which were possibly induced by these climatic changes, were detected by using hydroacoustic methods. In this study, the release of dissolved CH_4 into the water column and its subsequent lateral and vertical transportation, microbial oxidation and dilution were investigated. For this purpose, methane concentrations, isotopic ratios and oxidation rates were determined and compared with hydroacoustic and oceanographic data. The study area is influenced by the northwards flowing West Spitsbergen current (WSC), which leads to a stratification (about 20 m above ground) of the water column due to salinity differences. With the help of detailed sampling and a subsequent modeling, we determined that ~80 % of the methane contained in the ascending gas bubbles is dissolved under the pycnocline into the surrounding water and leads to a locally increased CH_4 concentration. Even though rise heights of up to 50 m under the sea surface were detected by means of hydroacoustics, a direct transport of methane into the atmosphere via gas bubbles can be excluded due to the fast dissolution of the gaseous CH_4 into the ambient water.

Therefore, the vertical transport of dissolved CH_4 was studied in more detail as a potential source for atmospheric methane. The observed pycnocline represents a limitation for the vertical transportation of dissolved CH_4. Therefore, dissolved methane is mostly laterally transported underneath the pycnocline to greater depths and is, as shown by the determinations of the oxidation rates, microbiological oxidized over time. As long as there is a stratification of the water column, the transport of methane in the gas bubbles (about ~20 % of the entire amount of CH_4) into the water masses above the pycnocline and the subsequent dissolution of the gas bubbles represent the only potential pathway of methane into the atmosphere.

The investigations at the gas seepage area in the Netherland economic zone in the North Sea reveal significant differences regarding to the fate of dissolved CH_4 in the water column. It has been shown in previous studies that most probably the gas source is a gas reservoir at a sediment depth of 600 m, which reaches the sediment surface through fractures (gas chimneys) in the sediment structure. Our video observations indicated 113 gas streams with an estimated release of 35.3 $\pm$ 17.65 t CH_4 yr^{-1}. The dissolved methane concentration in various depths was measured in high resolution with the optimized *in situ* mass spectrometer. This data set, consisting of 11.900 single measurements sampled in between 24 hours, represents the dissolved CH_4 concentration above a gas seepage in up to 750 times higher temporal and spatial resolution than would be possible by conventional methods. Highest methane concentrations (~3.5 µmol L^{-1}) were detected in the surrounding water of the gas bubble streams and the inventory in the entire water column was calculated to a total amount of ~6.4*10^5 µmol. Due to the unique measurements, these results are not yet comparable with other gas seep areas. During the time of measurement the oceanographic data reveal a pycnocline, which we indicated as the main forcing factor for the pathway of methane at the gas seepage in the shelf area offshore West Spitsbergen. However, due to the short distance to the seabed (~10 m), a high grade of gas bubble dissolution takes place in the mixed layer above the pycnocline, and we consider that ~40 % of the total seabed released methane could enter the

atmosphere via this indirect pathway. Additionally, we measured direct CH_4 transport via gas bubbles of ~25 % by discrete gas bubble sampling at the sea surface, which emphasize, that 65 % (23 $\pm$ 11.5 t CH_4 yr^{-1}) of the entire seabed released CH_4 potentially contributing to the atmospheric methane budget, which is far above most studied gas seepages.

With the help of the optimized mass spectrometer it became possible for the first time to obtain distribution patterns of dissolved CH_4 in the water column in high resolution. With respect to the geochemical functionality of these increasingly important methane sources, the research conducted in this dissertation contribute to improve our knowledge of the entry of CH_4 into the water column as well as its fate. Therefore, the applied novel technique can contribute to "revolutionize our understanding of the behavior of seep plumes" as suggested by Judd and Hovland (2007).

Zusammenfassung

Methan (CH_4) ist die häufigste organische Verbindung in der Atmosphäre und dessen Beeinflussung auf das globale Klima ist Gegenstand momentan geführter wissenschaftlicher Diskussionen. Trotz seiner geringen Konzentration in der Atmosphäre (1787 ppb in 2003) trägt es durch sein 20 bis 40 fach höheres Treibhauspotenzial gegenüber Kohlendioxid (CO_2) bezogen auf einen Zeitraum von 100 Jahren mit ~15 % zur globalen Erwärmung bei. Eine Quelle für atmosphärisches Methan, die einen aktuellen Forschungsschwerpunkt der marinen Geowissenschaften darstellt, ist die Freisetzung von biogenem und/oder thermogenem Methan in Form von Gasblasen oder mittels Fluiden aus dem Meeresboden. Diese Quellen sind durch den Aufstieg und biogeochemischen Umsatz von Methan in den obersten Stockwerken mariner Sedimente charakterisiert. Es wird geschätzt, dass diese, vornehmlich an dem Kontinentalschelf vorkommenden Punktquellen zusammen ~30 Tg Methan pro Jahr in das Meer eintragen und nach biologischer Oxidation und /oder Lösung im umgebenden Wasser ~10 Tg Methan pro Jahr in die Atmosphäre emittierter. An diesen submarinen Methanquellen sind starke Konzentrationsgradienten auf sehr kurzen Distanzen (< 20 m) und hoher zeitlicher Variabilität (wenige Stunden) in der überliegenden Wassersäule beobachtet worden. Aufgrund der limitierten Anzahl an Probennahmen von konventionellen *ex situ* Messmethoden und der damit verbundenen geringen räumlichen und zeitlichen Auflösung reichen diese Methoden nur sehr schwer aus, um die Methanverteilung an diesen Quellen adäquat zu quantifizieren. Ziel dieser Doktorarbeit war jedoch die detaillierte räumliche Abbildung der aus kalten Kohlenwasserstoffquellen stammenden, im Wasser gelösten Methanfracht und deren Budgetierung, sowie der Untersuchung relevanter Prozesse wie Methantransport, -verdünnung und seiner mikrobiellen Oxidation.

Daher beschäftigt sich der erste Teil der Dissertation mit der Etablierung und Optimierung eines neuartigen Unterwasser-Massenspektrometers (Inspectr200-200, Applied Microsystems Limited ™) zur hochauflösenden Vermessung von Methanmustern in der Wassersäule. Analyse und Auswertung von mehreren tausend Proben pro Tag erfolgen mit diesem Gerät in einem Schritt, so dass man, im Gegensatz zu konventionellen Methoden ohne Zeitverzug ein Messergebnis erhält und somit Beprobungsstrategien auf die vorliegenden Gegebenheiten angepasst

werden können. Durch die in situ Nutzung entfallen ebenfalls potentielle Fehlerquellen und zeitintensive Schritte wie die Probenahme vor Ort, der Transport zu den Laboratorien und die anschließende Messung. Um das Potential dieses Massenspektrometers jedoch für unsere wissenschaftlichen Fragestellungen nutzen zu können, war es erforderlich, die Nachweisgrenze für die zu ermittelnden Spurengase (Methan, Kohlenstoffdioxid) herabzusetzen. Dazu wurde ein Stirlingkühler eingebaut, der als Filter für den in der Analyseeinheit vorhandenen Wasserdampf fungiert und so zu optimierten Analysebedingungen führt. Insbesondere für Methan konnte die Nachweisgrenze mit dieser Weiterentwicklung von über 100 nmol L^{-1} auf 16 nmol L^{-1} herabgesetzt werden.

Mit diesem neuartigen und optimierten Messgerät wurden zwei submarine Ausgasungsstellen im Detail untersucht. Während die eine am Kontinentalhang nordwestlich vor Spitzbergen aufgrund ihrer exponierten Lage im Fokus der Wissenschaft steht, ist die in der Nordsee untersuchte Ausgasungsstelle bisher nicht bezüglich des Methaneintrages in die Wassersäule und anschließenden Verbleib betrachtet worden.

Die arktischen Regionen erwärmen sich verstärkt im Zuge des globalen Klimawandels. So wurde in den letzten 30 Jahren ein Anstieg der Meerestemperatur observiert, was zu einer Destabilisation von Gashydraten und verminderter Aufnahmefähigkeit von Methan im Sediment führen kann. In dem Untersuchungsgebiet mit einer Größe von 175 km² und einer durchschnittlichen Wassertiefe von 245 m wurden 10 Ausgasungsstellen mit hydroakustischen Methoden detektiert, die eventuell durch diese Klimaveränderungen iniziert worden sind. In dieser Studie wurde das Einbringen von gelösten Methan in der Wassersäule sowie dessen anschließenden lateralen sowie vertikalen Transport, mikrobielle Oxidation und Verdünnung betrachtet. Dazu wurden Konzentrationen, Isotopie sowie Oxidationsraten von Methan bestimmt und mit hydroakustischen sowie ozeanographischen Daten verglichen. Das Untersuchungsgebiet ist durch den

nordwärts fließenden West Spitzbergen Strom beeinflusst was zu einer Stratifizierung (ca. 20 m über Grund) der Wassersäule führt. Mit einer detaillierten Probennahme und einer auf diesen Resultaten aufbauenden Modellierung wurde ermittelt, dass sich das in den aufsteigenden Gasblasen enthaltene Methan zu ~80 % unterhalb der Pyknokline in das umgebene Wasser löst. Auch wenn mittels Hydroakustik Aufstiegshöhen von Gasblasen bis zu 50 m Wassertiefe ermittelt worden sind, kann ein direkter Transport von Methan über Gasblasen in die Atmosphäre durch die schnelle Lösung des Methans aus den Gasblasen in das umgebene Wasser ausgeschlossen werden. Daher wurde der vertikale Transport des gelösten Methans als potentielle Quelle für atmosphärisches Methan eingehender betrachtet. Aufgrund der erhobenen Daten konnte ermittelt werden, dass die vorliegende Pyknokline eine Limitation für den vertikalen Transport von gelöstem Methan darstellt. Daher kann das unterhalb der Pyknokline gelöste Methan nicht zum atmosphärischen Methanbudget beitragen, sondern lateral in größere Tiefen verfrachtet wird und dort, wie die Oxidationsratenbestimmungen zeigen, mit der Zeit mikrobiell oxidiert. Durch die Stratifizierung der Wassersäule stellt der Transport von Methan in den Gasblasen in die Wassermassen oberhalb der Pyknokline (~20 % des Gesamtmethans) und dessen anschließende Lösung den einzigen potentiellen Weg für das am Meeresboden ausgasende Methan in die Atmosphäre dar.

Im Gegensatz zu den submarinen Methanquellen vor Spitzbergen zeigen die Untersuchungen an der Ausgasungsstelle im niederländischen Ökonomiegebiet der Nordsee stark abweichende Ergebnisse bezüglich des Verbleibes von Methan. In vorhergehenden seismischen Untersuchungen wurde ermittelt, dass die Quelle für das am Meeresboden austretende Methan ein Gasreservoir in ~600 m Tiefe ist. Durch Risse in der Sedimentstruktur erreicht dieses Methan die Sedimentoberfläche und tritt dort in Form von Gasblasen aus. Mittels Videoobservation des Meeresbodens haben wir 113 Ausgasungsstellen identifiziert und die austretende Menge an Methan auf 35.3 ± 17.6 Tonnen pro Jahr quantifiziert. Die gelöste Methanfraktion wurde hier mit dem optimierten Massenspektrometer *in situ* in sehr hoher Auflösung gemessen. Es wurden innerhalb von 24 Stunden 11.900 Einzelmessungen aus 6 unterschiedlichen Tiefen aufgenommen, was eine höhere zeitliche und räumliche Auflösung der gelösten Methankonzentration über einem

submarinen Gasaustritt darstellt, als es jemals mit konventionellen Messmethoden möglich sein würde. Mit diesem Datensatz konnte erstmals die Methanverteilung hochaufgelöst und somit in 3-D dargestellt werden. Das somit ermittelte Inventar der gelösten Methanfraktion in der Wassersäule beträgt ~$6.4*10^5$ µmol. Aufgrund der einzigartigen Messungen sind diese Ergebnisse noch nicht vergleichbar mit anderen untersuchten submarinen Methanquellen. Höchste Konzentrationen (~ 3.5 µmol L^{-1}) wurden ca. 1 m über dem Meeresbodens im Gasblasenstrom detektiert und, im Gegensatz zu der Ausgasungsstelle vor Spitzbergen wurden auch in geringen Wassertiefen (8 m) Methankonzentrationen von bis zu 0.65 µmol L^{-1} gemessen. Während der Einsätze zeigten die ozeanographischen Daten eine Pyknokline, die wir als den entscheidenden Faktor für den weiteren Verbleib von Methan bei den untersuchten Gasaustrittsstellen vor Spitzbergen bestimmt haben. Jedoch liegt die Pyknokline in der Nordsee sehr bodennah (~ 10 m über dem Meeresboden) und somit können bis zu 40 % des am Meeresboden freigesetzten Methans indirekt durch Gasblasendissoziation oberhalb der Pyknokline in die Atmosphäre gelangen. Zusätzlich zum indirekten Transport haben wir, durch diskrete Probennahme der oberflächennahen Gasblasen, direkten Methantransport durch Gasblasen nachweisen können. Somit erhalten wir als Ergebnis, dass ~65 % (23 + 11.5 t CH_4 yr^{-1}) des gesamten am Meeresboden freigesetzten Methans in die Atmosphäre gelangen kann, was weit über dem liegt, was für viel andere Gasaustrittsstellen angenommen wird.

Mit dem optimierten Massenspektrometer konnten somit erstmals detaillierte Verteilungsmuster des gelösten Methans in der Wassersäule durch submarine Quellen erstellt werden. Im Hinblick auf die geochemische Funktionsweise dieser stark an Bedeutung wachsenden Methanquellen tragen die in dieser Dissertation durchgeführten Studien dazu bei, den potentiellen Eintrag von Methan in die Wassersäule zu quantifizieren sowie dessen Verbleib besser zu ermitteln. Daher kann diese Arbeit einen Beitrag zu der von Judd und Hovland (2007) beschriebenen „Revolution unseres Verständnisses des Verhaltens von submarinen Methanausgasungstellen" leisten.

List of figures

List of tables

Chapter 1

~ Introduction ~

108.70 pm

Molecular structure of methane

1.1 Global methane inventory

1.1.1 Methane in the atmosphere

In the atmosphere, CH_4 acts besides CO_2 and water vapour as a greenhouse gas and influences the global climate (Houghton 2001). It is largely transparent to incoming solar radiation (UV, visible, and near IR radiation) but absorbs and re-radiates the resulting reflected far infrared thermal radiation (4 – 100 µm wavelength). The average atmospheric concentration of the greenhouse gas methane has increased by 1060 ppb (151 %) since year 1750 (Houghton 2001) which lead to a more rapid depletion of the hydroxyl radicals and subsequent longer CH_4 residence times. Thus, insolation and radiation back to space are out of balance (Lelieveld et al. 1998). Therefore, increasing methane concentrations in the atmosphere contribute to global warming (Houghton 2001). On a 100 year timescale the global warming potential of methane is at least 20 - 40 times higher than of carbon dioxide and CH_4 emissions represent the second largest contribution (about 15 %) to historical warming after CO_2 (Shindell et al. 2009). The atmospheric CH_4 concentration with a lifetime of 8.7 ± 1.3 y (Lelieveld et.al. 2002) is low in the southern hemisphere and higher in the northern hemisphere which reflects the distribution of anthropogenic sources (Fig. 1-1). Even though there is a decrease in the growth rate of methane concentrations in the atmosphere that is not yet fully understood (Dlugokencky et al. 2003), up to 610 Tg CH_4 are introduced from several sources into the atmosphere annually (Fig.1-2) (IPCC report 2007).
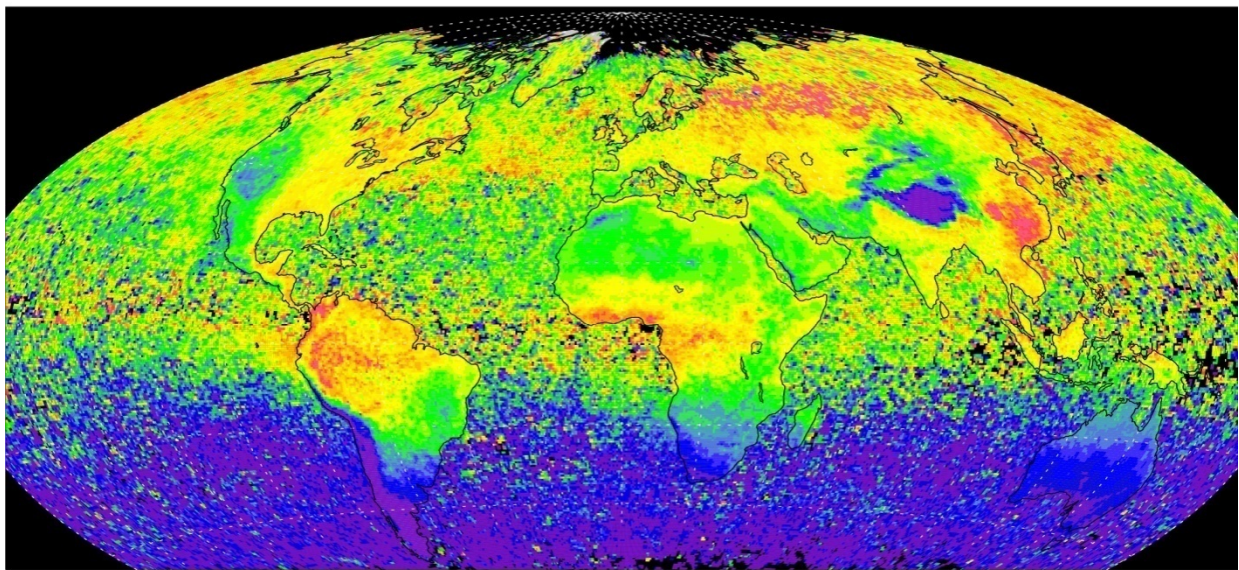
Fig. 1-1 *Global map of the distribution of atmospheric methane (2003) revealed by the Scanning Imaging Absorption Spectrometer for Atmospheric Chartography (SCIAMACHY) on board of the European environment satellite (ENVISAT).*

1.1.2 Methane: Sources and sinks

The CH_4 sources which contribute to the atmospheric methane inventory can be divided into anthropogenic and natural sources (Fig. 1-2).

$$CH_4 + {}^*OH \rightarrow H_2O + {}^*CH_3$$

Stratospheric 30 - 40

Trophospheric 428 - 511

Atmosphere

Total sources + Total sinks = Imbalance
503 – 610   492- 581   -12 to 33

Soils 26 - 34

Anthropogenic ~60 %
Coal mining 30 – 48
Energy 74 – 77
Landfills & Waste 35 – 69
Gas, oil industry 36 – 68
Ruminants 76 – 92
Rice agriculture 31 – 112
Biomass burning 14 – 88
Others 2 - 22

Natural ~40 %:
Wetlands 100 – 231
Termites 20 – 29
Hydrates 4 – 5
Oceans 4 – 15
Others ???

Marine Seeps ???

Fig. 1-2 *Relative contribution of methane sources and sinks to the global atmospheric budget. Information obtained from IPCC (2007). Methane as gas bubbles (white circles) or as fluids from marine seeps are not considered in the report. Units in Tg CH_4 yr^{-1}*

About 60 % of the global atmospheric methane is emitted from anthropogenic sources (black arrow Fig. 1-2) including e.g., rice agriculture, landfills and waste

treatment, biomass burning, and fossil fuel combustion (Houweling et al. 2000). Natural sources of CH_4 (blue arrow in Fig. 1-2) such as wetlands, oceans, forests, fire, termites, and geological sources contribute the rest to the atmospheric methane. The major CH_4 sinks (green arrows in Fig. 1-2) are the photochemical oxidation of CH_4 through reaction with OH^- radicals (up to 80 % of the total), biological CH_4 oxidation in soils, and loss to the stratosphere (Khalil and and Rasmussen 1983). Several studies shown in IPCC-report (2007) indicate an imbalance between the sources and sinks of atmospheric methane. One reason could be the increased impact of the global pre-industrial emissions of CH_4 that are estimated to be 200 to 250 Tg y^{-1} (Chappellaz et al. 1993; Etheridge et al. 1998; Ferretti et al. 2005; Houweling et al. 2000; Valdes et al. 2005).

In addition, CH_4 deriving through faults and fractured rocks from geological features like mud volcanoes on land and at the seafloor, submarine gas seepage, micro seepage over dry lands, and geothermal seeps is getting in focus as a potential source. Emissions into the atmosphere from these sources are estimated based are supposed to range between 40 and 60 Tg CH_4 y^{-1} which would represent a significant role in the global carbon cycle (Kvenvolden and Rogers 2005) but is not yet considered in the global methane inventory by the IPCC (Etiope and Favali 2004; Etiope and Klusman 2002; Kvenvolden and Rogers 2005).This budget of methane could be divided in submarine and terrestrial sources. In example, Judd and Hovland, (2007) estimated that the submarine sources with a strength of 10 to 30 Tg CH_4 yr^{-1} would nearly double the estimated amount of methane from the ocean of 11 to 18 Tg yr^{-1} (Bange et al. 1994) to a total amount 21 – 48 Tg yr^{-1} which is at least 4 -9 % of the total flux to the atmosphere.

.

1.2 Submarine seepage as a methane source, study area

Submarine seepages getting in scope of the marine science as a significant source for the atmospheric CH_4 inventory and are frequently highlighted in the scientific literature (Judd and Hovland 2007; Suess 2010). While terrestrial sources of hydrocarbons including methane are well characterized, most submarine sources (red arrow Fig. 1-2) remain poorly quantified. The main reasons for this are the technical difficulty of sampling and the very high temporal dynamics of submarine cold seeps. Therefore, the estimations of the amount of gas discharge from submarine methane sources into the ocean (8 - 65 Tg CH_4 yr^{-1}) and subsequent release into the atmosphere (0.4 – 48 Tg CH_4 yr^{-1}) varies in large ranges (Hovland et al. 1993; Judd and Hovland 2007; Judd 2004; Judd et al. 2002; Kvenvolden and Rogers 2005).

In addition, these estimations do not consider the potential source of up to 995 Gt (Burwicz et al. 2011) of methane released from destabilizing CH_4 hydrates in the sediments induced by present climate change (Ruppel 2011; Shakhova et al. 2010; Westbrook et al. 2009).

1.2.1 Worldwide distribution of cold seeps

In the mid 1960´s the development of side-scan sonar and later multibeam echo sounder, manned and remotely operating vehicles (ROVs) or autonomous underwater vehicles (AUVs) enabled the detailed inspection of the seabed (Judd and Hovland 2007). Since this time examples for geological marine CH_4 emissions like seeps, mud volcanoes, anthropogenic gas release areas or pockmarks were discovered worldwide and mostly on the continental margins (Fig. 1-3; Judd and Hovland 2007; Suess 2010). Due to the ongoing examination of the seafloor the number of discovered seep areas or mud volcanoes will increase in the future, which consolidates the importance of these methane sources.

Beside the supposed affect of the widespread and dynamic sources to the atmospheric CH_4 budget they play a significant role in ocean processes, as for instance ocean acidification (Biastoch et al. 2011). They are often related to gas hydrate deposits (Bohrmann and Torres 2006) and can be seen as "open pressure valves" in the Earth's crust.
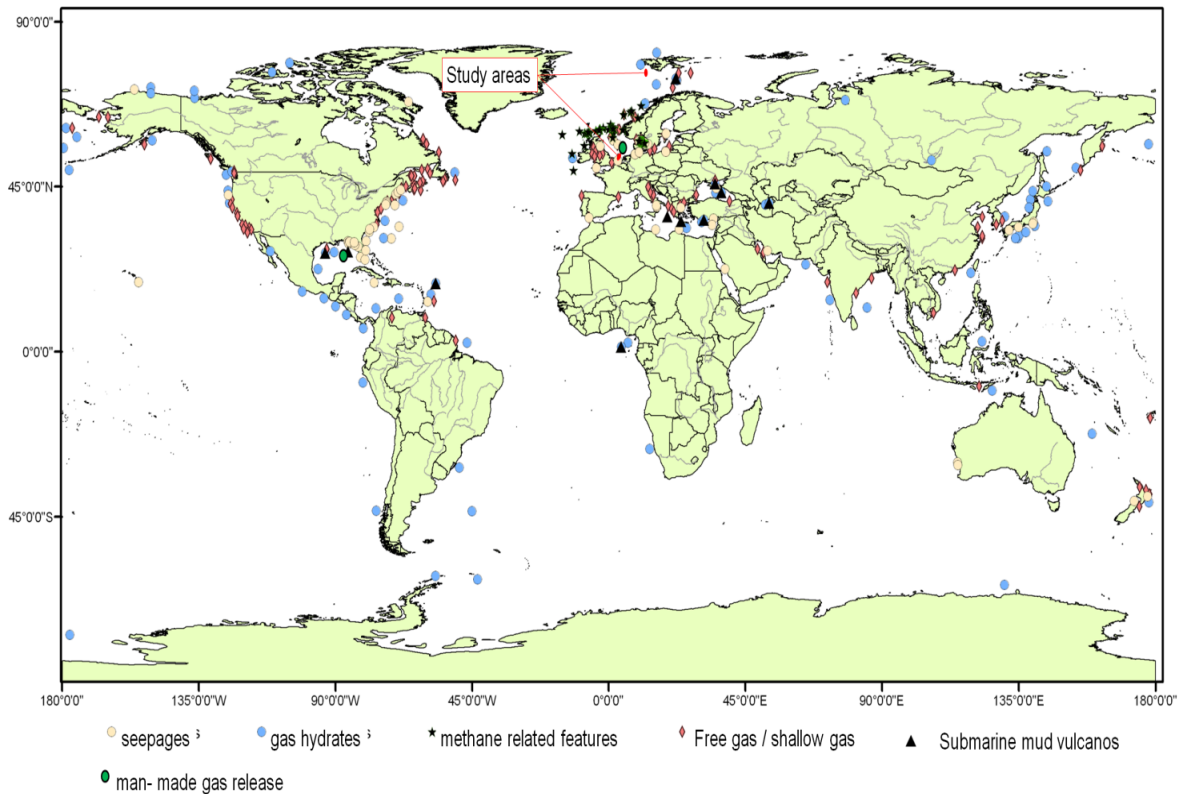
Fig. 1-3: *Worldwide distribution of submarine mud volcanos (Milkov 2000), gas hydrates (Kvenvolden et al. 2001), free gas occurrence (Fleischer et al. 2001), and pockmarks (Hovland et al. 2002).*

Prominent locations where methane release as fluid flow or gas bubbles in the water column has been observed are for example the Håkon Mosby Mud Volcano (Damm and Budéus 2003; Felden et al. 2010; Sauter et al. 2006), the Cascadia margin (Suess et al. 2001), the Tommeliten field in the North Sea (Hovland and Sommerville 1985), the Santa Barbara Basin (Fischer 1978; Leifer and Clark 2002), the Black Sea (Limonov et al. 1997) and the West Spitsbergen continental margin (Hustoft et al. 2009b; Knies et al. 2004).

1.2.2 Formation, storage and migration of methane in the sediments

In the marine sediments hydrocarbons, dominantly CH_4, are produced via two main pathways: the microbial degradation of organic matter in shallow sediments, or the thermocatalytic breakdown of complex organic molecules as part of petroleum-generating processes occurring deep within sedimentary basins. (Fig. 1-4) (Floodgate and Judd 1992; Judd 2004).

Fig. 1-4 *Schematic view of the formation (modified after Froelich et al. 1979) and the subsequent pathways of methane in the sediment (modified after Judd 2004). Crystallographic image of gas hydrates after Bohrmann and Torres (2006).*

An essential requirement for the formation of methane in sediments, whether by microbial or thermogenic processes, is an abundance (at least 0.5 %) of organic matter (Judd 2004). Therefore, to understand the **microbial formation** of CH_4 by methanogens we have to follow the sequence of redox processes with different

electron acceptors during decomposition of the particulate organic matter (POM; Fig. 1-4) presented in fundamental works by Froelich et al. (1979). Particulate organic matter sinks down in the water column and is buried in marine sediments. Due to the high production rates and shallow water depths highest fluxes of POM to the seabed are measured at the continental shelves (Judd and Hovland, 2007). In the open ocean, most of the POM is aerobically oxidized in the water column and the fluxes to the seafloor are thus low (Suess 1980).

In the oxic zone of the sediment POM is degraded by aerobic respiration (Fig. 1-4 left side). This process reveals the highest energy yield (ΔG_0= -479 kJ mol^{-1} C) for bacteria and therefore, they are most active close to the seabed. After oxygen depletion usually in the first millimeters of sediment (Sauter et al. 2001), remineralization of POM proceeds through anaerobic respiration (Canfield and Thamdrup 2009; Froelich et al. 1979). The successive processes involved in POM degradation are nitrate reduction (ΔG_0= -453 kJ mol^{-1} C), manganese oxide reduction (ΔG_0= -349 kJ mol^{-1} C), iron oxide reduction (ΔG_0= -114 kJ mol^{-1} C) and sulfate reduction (ΔG_0= -77 kJ mol^{-1} C), which are distributed in a characteristic vertical pattern within the seabed (Fig. 1-4). During dissimilatory metal reduction, solid phase iron (Fe(III)) and manganese (Mn(IV)) are reduced, and Fe^{2+} and Mn^{2+} are released to the pore water. Organoclastic sulfate reduction usually occurs in sediments below the Fe(II)/Fe(III) redox boundary (Fig. 1-4). Below sulfate concentrations of 200 µmol L^{-1} the degradation of POM via methanogenic pathways with competitive substrates (CO_2 and CH_3COO^-) and non competitive substrates (e.g., CH_3OH, CH_3NH_2 or $(CH_3)_2S$) takes place (Whiticar 1999; Whiticar and Faber 1986). Three possible processes for methane production are known and can be distinguished by their hydrogen isotopic ratio (Whiticar 1999):

Hydrogenotrophic $\quad\quad CO_2 + 4\ H_2 \rightarrow CH_4 + 2\ H_2O$ (ΔG_0= -130 kJ mol^{-1} C) (1)

Acetotrophic $\quad\quad CH_3COO^- + H_2O \rightarrow CH_4 + HCO_3$ (ΔG_0= -30 kJ mol^{-1} C) (2)

Methylotrophic $\quad CH_3\text{-A} + H_2O \rightarrow CH_4 + CO_2 + \text{A-H}$ (ΔG_0= -106 kJ mol^{-1}C) (3)
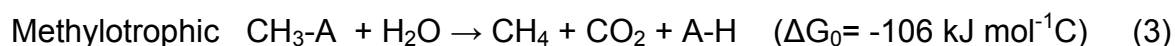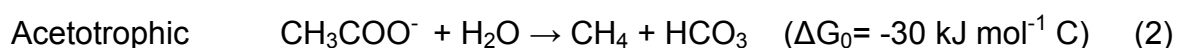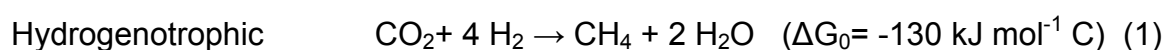
If organic matter is not microbially remineralized in shallow sediments of up to 2 km (Judd 2004) and buried by subsequent sedimentation to greater depth it may be degraded by **thermocatalytic** processes deep within the sediments where high temperatures caused by the geothermic gradient (~ 30 °C km^{-1}) are observed (Claypool 1974; Schoell 1988). With increasing depth POM is converted into "kerogens", a mixture of high molecular weight organic materials which are classified into groups according to their morphology, color in white and ultra-violet light, and chemical composition (the C, H and O content). Depending on the origin of the organic matter and the depth, the thermocatalytic breakdown (`cracking´) of the kerogens releases various hydrocarbon compounds and may accumulate in deep petroleum reservoirs (Fig. 1-4) (Cornford 2009). The geological processes occurring throughout all the stages of the POM breakdown are known as diagenesis, catagenesis and metagenesis. Related to the increasing temperature and the origin of the kerogen liquids like crude oil are produced first, then condensates ($C_8 - C_{15}$) as well as gases like ethane, propane, iso-butane and at the end methane. These processes are mostly consist in fine-grained sedimentary rocks like mudstones, claystones, shales or certain limestones (Floodgate and Judd 1992).

After generation of methane formed by any of the processes outlined above, migration occurs by bulk flow driven by a pressure gradient or buoyancy as well as diffusion within pore waters (Floodgate and Judd 1992; Kubala et al. 2003). Generally the migration is an upward process from the source rocks in which it is generated towards the surface. Due to the highest buoyancy force and the ability of diffusion lighter hydrocarbons are more able to migrate upwards than crude oils and may become trapped in shallow gas reservoirs (< 1000 m) below impermeable sediments (Fleischer et al. 2001). Beside this reservoir, large quantities of CH_4 are sequestered in gas hydrates (Hesse and Harrison 1981; Shipley et al. 1979; Trehu et al. 2006). This reservoir is formed under certain conditions like high hydrostatic pressure, low temperatures and salinity, oversaturation of low molecular-weight hydrocarbons and an adequate supply of pore water (Bohrmann and Torres 2006). At the studied areas in this thesis we assume that the methane from these reservoirs

reaches the seabed by fracture zones or faults in deeper sediment which is mostly observed at submarine gas ebullition areas (Rajan et al. 2012; Schroot et al. 2005;Westbrook et al. 2009). Nevertheless, mud volcanoes like the Håkon Mosby Mud Volcano provide other major pathways (Etiope and Milkov 2004), which is, however not in scope of this thesis.

The origins of methane (thermogenic or microbial) can be interpreted by the carbon and hydrogen isotope signatures and the relative proportions of methane and the higher hydrocarbon gases isotope analysis (Faber et al. 1992; Schoell 1980; Whiticar and Snowdon 2000). Biogenic CH_4 is usually depleted in higher homologues (high C_1/C_{2+} ratios) and shows a very low $\delta^{13}C$ due to microbial isotope fractionation and hence the enrichment of light ^{12}C atoms (Claypool and Kaplan, 1974; Whiticar et al., 1986; Whiticar, 1999) whereas the isotopic composition of thermogenic hydrocarbons is characterized by a relative enrichment in the heavy ^{13}C atoms which leads to high $\delta^{13}C$ values. Nevertheless, at these methane seeps generally a mixture of different gas types i.e. thermogenic and biogenic source types is likely (Knies et al. 2004) or fractionation occur in the directly in the sediments (Prinzhofer and Pernaton 1997) which challenging the interpretation of the isotopic signature of CH_4.

1.2.3 Fate of methane at the seabed and in the water column

Methane generated in, or migrating through to the seabed can be utilized by methanotrophic archaea as a chemosynthetic energy source. The zone of CH_4 depletion corresponds to the zone of sulfate depletion and is called the sulfate/methane transition zone (SMTZ) (Iversen and Jorgensen 1985; Reeburgh 1976).

$$CH_4 + SO_4^{2-} + 2\,H^+ \rightarrow CO_2 + H_2S + 2\,H_2O \qquad (\Delta G^0 = -27\ kJ\ mol^{-1}) \qquad (4)$$
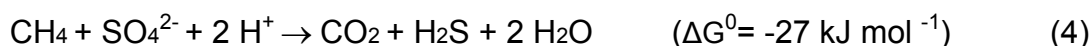
This process (reaction 4) is called the anaerobic oxidation of methane (AOM) coupled to sulfate reduction (Boetius et al. 2000). It was suggested that AOM proceeds via the co-consumption of methane and sulfate by a syntrophic consortium of methanotrophic archaea and sulfate reducing bacteria that occur in aggregates (Boetius et al. 2000). During AOM hydrogen sulfide and bicarbonate are released to the ambient pore water. The former promotes an entire ecosystem including chemoautotrophic bacteria (e.g., *Beggiatoa sp.*) or metazoan organisms, such as pogonophorans and mussels/clams, which live in symbiosis with these bacteria (Sahling et al. 2003). In seep areas often large mats of bacteria are observed (Fig. 1-4). Methane, which enters the aerobic zone of the seabed and/or the water column, can be consumed with a high energy yield (reaction 5) by methanotrophic microorganims involving several genera (e.g., Methylosinus, Methylocystis, Methanomonas), but the understanding of the kinetics of microbial CH_4 oxidation in oxic environments is poor (Reeburgh 2007).

$$CH_4 + 2\,O_2 \rightarrow CO_2 + 2\,H_2O \qquad (\Delta G^0 = -818\ kJ\ mol^{-1}) \qquad (5)$$

Therefore, where the rate of methane production in relation of migration exceeds the rate of microbial utilization, seepage into the water column occurs (Judd et al. 2004). Besides the aerobic oxidation of CH_4 by microorganism, dilution by mixing of the water column, vertical and horizontal transports as well as escape to the atmosphere are potential pathways for the fate of methane. A detailed estimation of the main pathway of CH_4 consumption with regards to the hydrographic settings at one gas ebullition are a offshore Spitsbergen is presented in chapter 4.

1.3 Study areas

This thesis deals with two marine regions where gas ebullition from the seabed into the water column had been observed in previous studies. The study area close to Spitsbergen was chosen due to the hypothesis of increased release of methane into the water column due to ocean warming which can is observed in higher latitudes (Steele et al. 2008). Due to the shallow water depth of ~40 m the gas ebullition area in the North Sea has a high potential for CH_4 flux from the seabed to the atmosphere.

1.3.1 Gas seeps offshore Spitsbergen

The Spitsbergen continental margin is a prominent gas seep area. In previous studies gas accumulation in shallow sediments, as well as gas hydrates had been observed (Hustoft et al. 2009a; Knies et al. 2004; Westbrook et al. 2008). The study area is located northwest of Spitsbergen around 20 km west of Prins Karls Forland between Kongsfjorden and Isfjorden (Fig. 1-5 A). It consists of a shelf bank with mean water depths of 245 m and is located at the shelf close to the shelf edge with relatively steep slope gradient in the east (Figs. 1-5 A and B). To the north the study area is adjacent to the shelf edge with less steep gradients than in the east. The sediments consist of a prominent moraine system formed by glacial erosion or glaciotectonic detachment of larger blocks or sediments. The gas hydrate stability zone begins below 400 m (Westbrook et al. 2009) and Rajan et al., (2012) indicated through high-resolution mapping of the sediment that shallow gas accumulations and pockmarks are present in this area. Westbrook et al., (2009) detected gas ebullition into the water column at more than 250 sites in an area of 665 km² (Fig. 1-5 B). In this thesis we investigated a subregion of the area studied by Westbrook et al. (2009) where we observed 10 gas flares up to 50 m to the sea surface (Fig. 1-5 C).
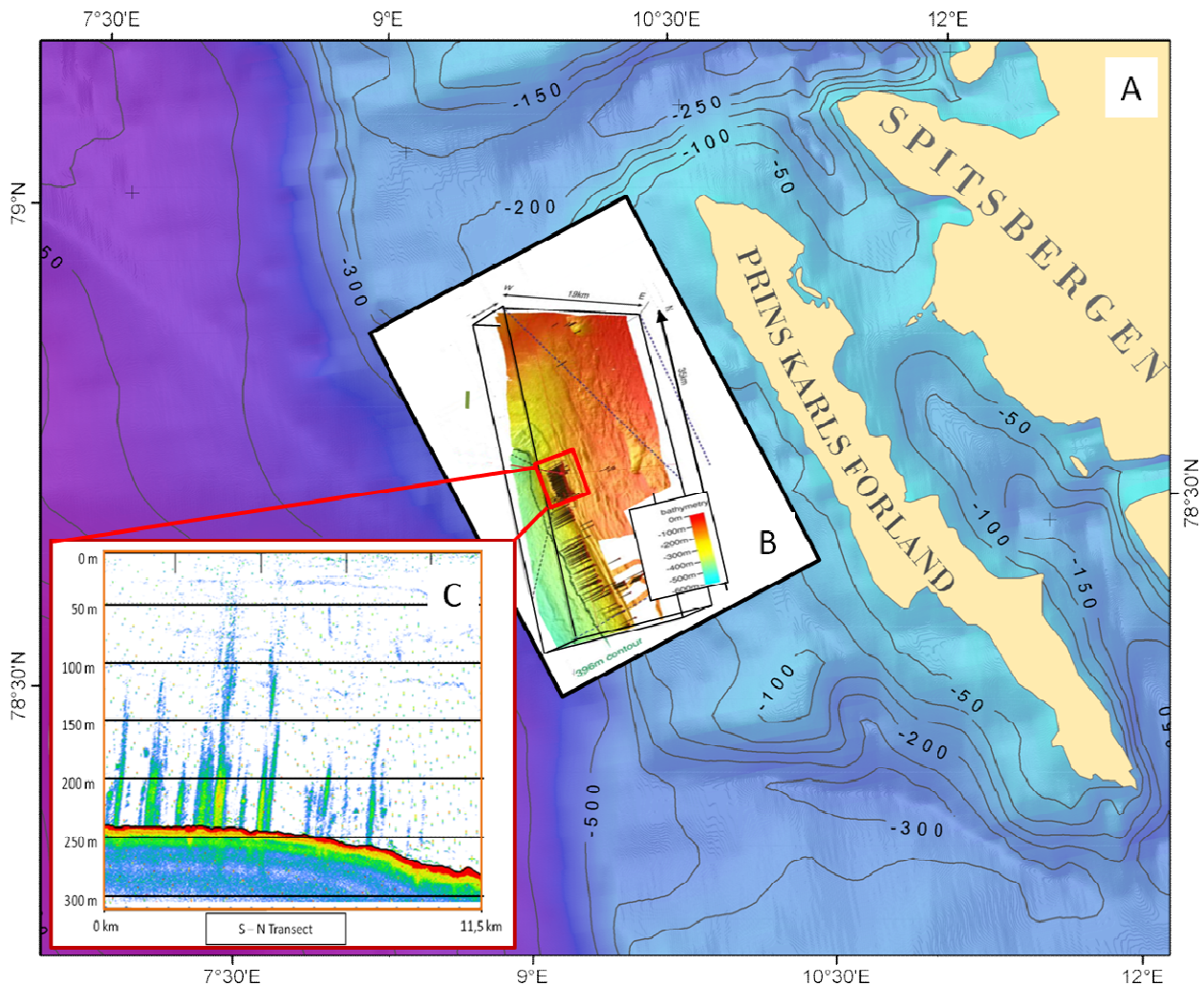
Fig. 1-5 *(A) Location of survey area west of Spitsbergen (B) Positions of 250 plumes acoustically imaged with the EK60 sonar, depicted by "pins", superimposed on perspective view of the bathymetry of part of the area of plume occurrence. Modified after Westbrook et al. (2009). (C) Part of record from an EK60 acoustic survey from HE333, showing the gas flares observed in the detailed investigated area (red corner in B). The seabed, at around 245 m depth, is shown by the strong (red) response.*

The hydrographic conditions in the study area are controlled by the intrusion of the West Spitsbergen Current (WSC), a shallow northward-flowing saline Atlantic water (AW) along the shelf edge (Schauer et al. 2004). The Coastal Current (CC) as an extension of the East Spitsbergen Current may also affect the study area and carries water with lower salinities and lower temperature than the Atlantic water (Saloranta and Svendsen 2001). Further, seasonal events like formation and melting of sea ice or glaciers, rivers run off from Spitsbergen and fjord outflow and special events like

storm activities affects the study area and reveal strong seasonal variation. During summer the WSC is stably stratified but vigorous convection vertically mixes the AW within the WSC during winter (Cisewski et al. 2003).

We focused in the investigation of the water column by hydroacoustic and geochemical methods during HE333.

1.3.2 Gas seepage in the North Sea

The North Sea study area is located on the European shelf in the Netherland part of the Southern Central North Sea, very close to the German border (Fig.1-6 A). The area is characterized by strong seasonal forcing of the water column stratification and shallow water depth of 30 - 45 m. On top of a Permian Zechstein salt dome, source rocks for hydrocarbons are observed. The area is characterized by gas basins, with mainly Carboniferous source rocks and there are a number of oil and condensate fields holding hydrocarbons from Jurassic source rocks (green area in Fig. 1-6 A). In our specific study area of 140000 m² in license block B13 seismic studies from Schroot et al, (2005) show shallow gas fields, with reservoirs of Pliocene to Pleistocene age at depths of 600–700 m (Fig.1-6). The sedimentary postdates the Mid- Miocene unconformity, a surface which is buried at 1000 to 1500 m depth in the north of the Netherlands North Sea (Schroot et al. 2005; Schroot and Schuttenhelm 2003). The sediment structure also points at Pleistocene gas events (Schroot et al. 2005; Stuart and Huuse 2012). Analyses of multiple corers during HE362 showed that the shallow subsurface (<0.3 m) consists of sandy sediment. Via echo-sounding two active gas seeps areas were observed in 2005 (Schroot et al. 2005), 2010 (HE337) and 2011 (HE362, Fig. 1-6 B) and qualified via video observation (HE362, Fig. 1-6 C). During the cruise HE362 gas bubbles were observed to reach the sea surface. We focused in the high resolution investigation of the water column by hydroacoustic and geochemical methods during HE362.
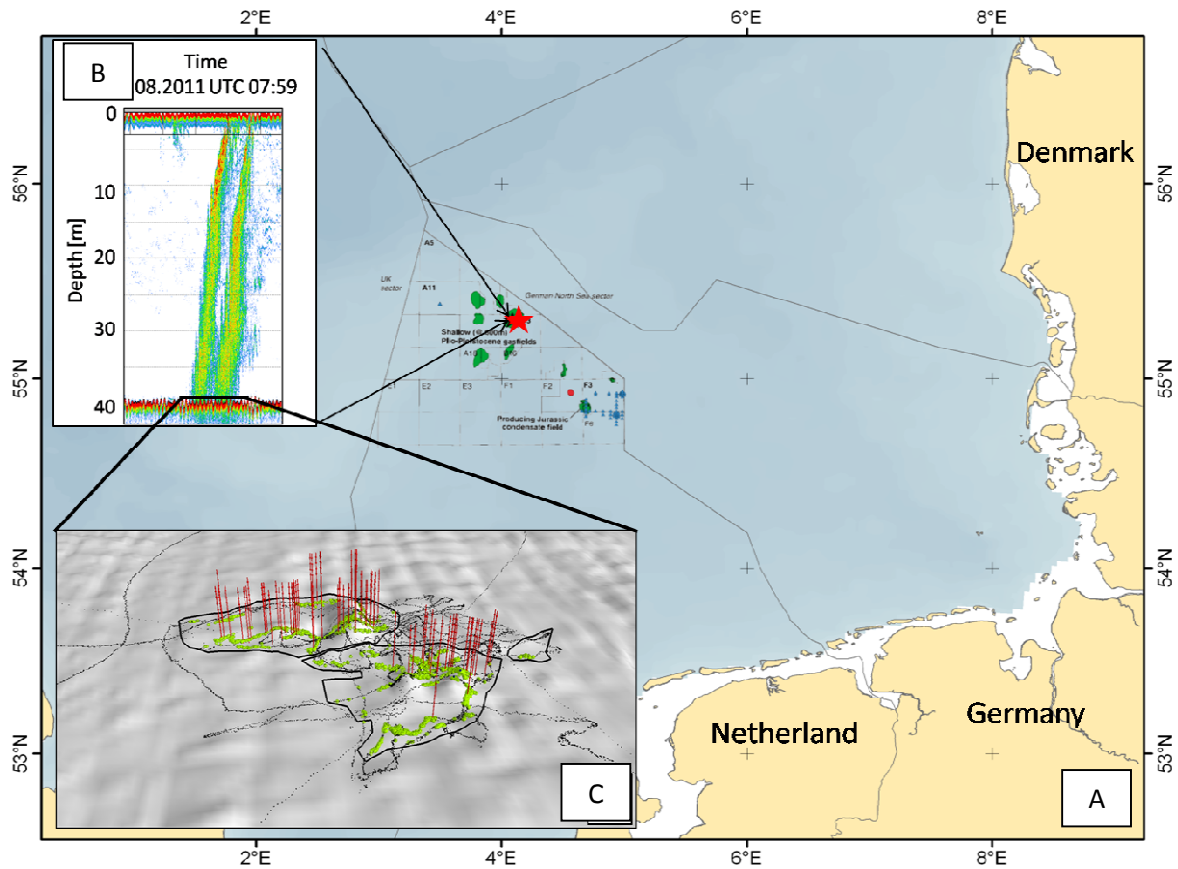
Fig. 1-6 _(A) Location of the study area (red star in license block B13) in a region of known shallow gas accumulation (green dots). (B) Two gas flares were observed via hydroacoustic in the study area. (C) 113 single gas streams (red lines) as well as areas of bacterial mats (green dots) were qualified via video observation._
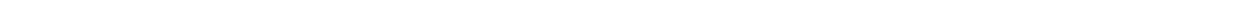
2 Methodological overview

2.1 Techniques for the investigation of submarine gas release.

The investigation of the release of methane and other trace gases from gassy sediments, hydrocarbon reservoirs, and pipelines, or through dissociation of gas hydrates is a major objective in basic and applied research. At such sites, analyses of gases are required in order to calculate budgets, evaluate the fate of gases due to microbial turnover processes as well as estimating the air-sea exchange of trace gases (Hovland and Judd 1988; Leifer and Boles 2005; McGinnis et al. 2006; McGinnis et al. 2011; Niemann et al. 2005; Rehder et al. 1998; Sahling et al. 2008; Sauter et al. 2006; Suess et al. 1999; Tortell and Long 2009).

Techniques like floating chambers at the water surface are applied for the calculation of the air-sea exchange (Bastviken et al. 2004), and the ebullition of gas bubbles from the seabed is quantified by bubble collectors at the sediment surface (e.g., Leifer and Boles 2005). However, most studies on ebullition of gas from the seafloor and its fate in the water column are based on geo- and hydroacoustic systems like multibeam echo sounder or fish finder sonar. Those are applied for the detection of shallow gas, gas seeps or gas flares (Fleischer et al. 2001; Hovland and Judd 1988; McGinnis et al. 2006).

Most investigations of dissolved CH_4 concentrations and budgets in the water column above gas ebullition include water sampling (e.g., by rosette water sampler, Hydro-Bios, Kiel, Germany), the phase separation by head-space as well as vacuum-ultrasonic techniques, and the subsequent gas chromatography (GC) for (gas) analysis onboard the research vessel or in the laboratory (Kampbell et al. 1989; Lammers and Suess 1994; Wiesenburg and Guinasso 1979). Compared to the currently used hydroacoustic techniques, this procedure provides higher quantitative information about the concentration of dissolved CH_4 in the water column. Nevertheless, using water samplers might cause contamination during sample collection and handling (Chapter 2.2) which obtain an potential uncertainty for subsequent modeling (e.g., Leifer and Judd 2002; McGinnis et al. 2006) of the methane dissolution from saturated gas bubbles. In addition, this method is technically challenging, costly and rather time consuming, which limits the number of sampling sites and therefore the spatial and temporal resolution.

Especially in gas ebullition areas where the spatial extent of discharge sites is highly variable and may change over time, the resolution of the conventional method is not sufficient to fully describe the two- or three-dimensional structure of methane plumes in the water column.

These restrictions stimulated the development of continuous underway measurement systems (Butler and Elkins 1991; Gueguen and Tortell 2008; Johnson et al. 1999; Saltzman et al. 2009; Tortell 2005) and underwater gas analyzers for *in situ* measurements of O_2, CH_4, volatile organic compounds as well as CO_2 (Boulart et al. 2010; Camilli and Hemond 2002; Emerson et al. 2002; Mcmurtry et al. 2005; Prien 2007; Short et al. 2006; Tortell 2005; Wankel et al. 2010).

Beside other novel techniques (Chapter 2.3) like metal-oxide semiconductors (Franatech GmbH) or sensors using infrared spectroscopy (Contros GmbH), specific membrane inlet systems and underwater mass spectrometers (UWMS) such as the Inspectr200-200 (Chapter 2.4), the THETYS, or the NEREUS (Bell et al. 2007; Camilli and Hemond 2004; Hemond and Camilli 2002; Kibelka et al. 2004; Short et al. 1999; Wenner et al. 2004) were designed especially for the detection of the trace gas methane. Due to the fast sampling frequency on a time scale of a few seconds for all gases, UWMSs are valuable important tools to locate and quantify point sources in highly dynamic environments and to assess their role in the global carbon cycle.

2.2 Established methods for the dissolved methane quantification.

Conventional methods consist of discrete water sampling, subsequent phase separation and gas analysis via gas chromatography.

Water sampling is performed using rosette water samplers. This device usually consists of up to 24 bottles (e.g., Niskin™ 5 L), which can be closed from board in various depths as well as a conductivity / temperature and depth profiler (CTD; e.g., Seabird™ 911) to provide information about the hydrography of the water column. Onboard, the water samples from the Niskin bottles have to be taken immediately in order to prevent contamination by air bubbles. The subsequent application of a GC requires the phase transfer of gases from the dissolved to the gaseous phase. For this purpose, head-space as well as vacuum-ultrasonic techniques are applied (Kampbell et al. 1989; Lammers and Suess 1994; Wiesenburg and Guinasso 1979). For the head-space method, a head-space of ca. 5 mL volume is generated by inserting argon, helium or nitrogen gas and the simultaneous removal of an equivalent sample volume. After at least 5 hours of equilibration, the gas concentration in the head space is analyzed by gas chromatography. For this purpose, a Thermo Finnigan (Waltham, USA) TraceGC equipped with a flame-ionization detector and a Porapak Q column can be used. To measure background concentrations of methane (3.5 nmol L^{-1}) the vacuum-ultrasonic technique is favourable (Lammers and Suess 1994). Based on the methane concentration in the head-space and the CH_4 concentration in the aqueous phase, which is computed using the Bunsen coefficient according to Wiesenburg and Guinasso (1979), the methane concentration in the water sample can be derived. The standard deviation of duplicate analyses is 5 – 10 %. This high overall error is almost exclusively due to the gas extraction procedure and not to the GC precision, which has an error of only 1 %.

Head-space techniques and vacuum-degassing are very suitable for analysis of discrete water samples but require considerable time for phase separation and chemical analysis. In addition, the sampling is affected by degassing due to decompression during the retrieval of the sample and due to the temperature increase in the water column as well as onboard (Leifer and Judd 2002; Schlüter et al. 1998). Furthermore, potentially trapped gas bubbles may dissolve during the ascent of the water sample to the surface.

2.3 Novel *in situ* Analyzer

Novel analysis techniques which detect the dissolved concentration of one or more gases *in situ* in high spatial resolution represent attractive alternatives to the conventional *ex situ* gas measurement procedures. Due to the *in situ* applications the analysis is unaffected by contamination during sample collection and handling. Furthermore, *in situ* sensors do not require reagent or sample preparation for analyses of gaseous or aqueous samples, which reduces the sampling time, man power and laboratory costs.

The novel *in situ* analyzer has to fulfill the following requirements:

- Robustness for the use in harsh environment
- The energy consumption needs to be low to allow long term measurements
- A low detection limit for trace gases
- Sampling rates should be high and respond times correspondingly short
- Application of the device should be inexpensive
- Maintenance of the analyzer should be easy and short in time.

To fulfill most of these requirements, three general techniques for the detection of methane have been developed (table 2-1). These are the bio-sensors using methane-oxidizing bacteria (Turner et al. 2000), the partitioning of the gas into an indicator layer (Buerck et al. 2001), and extraction of the dissolved CH_4 into the gas phase prior to transduction. Most applied devices use the extraction of dissolved CH_4 into the gas phase and subsequent detection via photoacoustic detectors, metal-oxide semiconductors (e.g., Franatech), infrared spectroscopy (e.g., Contros GmBH), or mass spectrometry (Bell et al. 2007; Camilli and Hemond 2004; Hemond and Camilli 2002; Kibelka et al. 2004; Short et al. 1999; Wenner et al. 2004).

An intensive state of the art and usability study of the 11 known *in situ* methane sensors and technologies in 2010 (table 2-1) was performed by Boulart et al. (2010).

To classify the different stages of the development of the sensors a Technology Readiness Level (TRL) is applied (Boulart et al. 2010). The TRL is based on the performance of the instrument with regard to requirements of a particular application, reliability of data, and adaptation of the system to field conditions (table 2-1).

It is shown that the instruments with the membrane inlet system are most developed (table 2-1), especially the membrane inlet systems coupled to a mass spectrometer.

In this thesis the *in situ* mass spectrometer of the University of South Florida (USA, marked yellow in table 2-1) was used. After several improvements it fulfilled the requirements from the technical perspective to raise the TRL to the highest level of 9.

TRL 1 Basic principles of technology; observed and reported
TRL 2 Technology concept and/or application formulated
TRL 3 Analytical and laboratory studies to validate analytical predictions
TRL 4 Component and/or basic sub-system technology valid in laboratory environment
TRL 5 Component and/or basic sub-system technology valid in relevant environment
TRL 6 System/sub-system technology model or prototype demonstrated in relevant environment
TRL 7 System technology prototype demonstrated in an operational environment
TRL 8 System technology qualified through test and demonstration
TRL 9 System technology qualified through successful mission operations

Sensor	Measurement/ environments	Technology	Membrane/ Sensitive layer	Concentration range	Limit of detection	T 90	T°C	Depth range	Power supply	Manufacturer/ Research Institute/ Reference	TRL
METS-CAPSUM	Gas phase/water column	SnO_2 semi-conductors	Silicon rubber (5-100 µm)	10 nM-150 mM	10 nM	1-30 min	2-40°C	0-3500 m	35-100 mA at 12 V	Capsum GmbH/ Franatech GmbH [26]	TRL 7
HydroC/CH$_4$	Gas phase/water column	Direct IR absorption spectroscopy (3.4 µm)	Modified silicon rubber (2-100 µm)	30 nM-500 µM	<10 ppm (<6 nM)	17-30 s	0-50°C	0-6000 m	250 mA at 12 V	Contros GmbH http://www.contros.eu	TRL 7
Deep-sea methane sensor	Gas phase/water column	Laser absorption spectroscopy (3.3 µm)	Silicon-membrane tubes	40-320 ppm (25-200 nM)	40 ppm (25 nM)			0-2000 m		Hokkaido University (Japan) [15]	TRL 6/7
Deep-sea gas analyzer*	Gas phase/water column	NIR-off-axis integrated-cavity output spectroscopy	Silicon rubber			less than 1 min	0-45°C	0-2000 m	Internal battery	Iginc (USA)	TRL 6/7*
Equilibrator	Gas phase/surface water	Photoacoustic spectroscopy	Glass marbles in tube	up to 400 µM	20 µM	12 min at 7 m depth**				[33]	TRL 6
In situ mass spectrometer	Gas phase/water column	In situ mass spectrometer	Semi-permeable membrane inlet	no data	Sub-ppm (<1 nM)			0-30 m (200 m possible)	20 W	WHOI (USA) [36]	TRL 8
In situ mass spectrometer	Gas phase/water column	In situ mass spectrometer	PDMS membrane inlet	no data	1-5 ppb (<1 nM)			0-30 m (200 m possible)	20 W	University of South Florida (USA) [35]	TRL 8
Biosensor	Dissolved phase/sediments, pore water	Amperometry	Silicon membrane	up to 350 µM	5 µM			surface		University of Aarhus (Denmark) [19]	TRL 5/6
Biosensor	Dissolved phase/sediments, pore water	Dissolved oxygen sensor	"bacterial beads"	0.4-2 mM	100 µM	100 s		surface		[44]	TRL 5/6
FEWS	Dissolved phase/water column	Evanescent wave spectroscopy	Optical fiber/ sensitive layer					Possibly up to 6000 m		[50]	TRL 2/3
SERS	Dissolved phase/water column	Surface-enhanced Raman scattering	Silver-colloid SERS substrate		nM-µM			Possibly up to 6000 m		Technical University Berlin (Germany) [60]	TRL 4/5
SPR	Dissolved phase/water column	Surface-plasmon resonance	PDMS/crypto-phane-A	0-400 nM	0.2 nM	2-5 min	45°C	Surface	1 mW	[64] (Appendix 2)	TRL 4/5

* Note that for the dissolved gas analyzer, it is difficult to state the TRL as there are no real environmental trials. The suggested TRL is based on comparison with similar systems employing gas-permeable membranes.
** No indication is given whether or not the response time is the T 90.

Table 2-1 Compilation of in situ methane sensors and technologies, modified after Boulart (2010) including the explanation of the TRL levels, modified from a UK Defence Procurement Agency version.

2.4 Used *in situ* mass spectrometer

Membrane inlet systems in combination with mass spectrometers provide a powerful technology to measure dissolved gases which can be applied for several scientific questions. In the marine sciences, the membrane inlet mass spectrometry (MIMS) allows the simultaneous quantification of a multitude of gases in the water column on time scales of a few seconds (Schlüter and Gentz 2008). Whereas in environmental research MIMS is very successfully applied in soil science or for studies on microbial turnover processes (Benstead and Lloyd 1996; Lloyd et al. 1996; Sheppard and Lloyd 2002), it is a rather new application in marine and limnic research. Studies by Tortell (2005) showing O_2, dimethyl sulphide (DMS) or N_2 concentrations in surface waters or by Hartnett and Seitzinger (2003) investigating nitrogen concentrations in sediment cores underlined the suitability of MIMS for geochemical investigations in marine and limnic environments (Hartnett and Seitzinger 2003). Fast technical developments in the field of Harsh Environment Mass Spectrometry (HEMS) allows to measure a wide range of gases by MIMS on board of small research vessels or even on mobile underwater platforms like AUVs (Autonomous Underwater Vehicles) or submersibles (Short et al. 1999, 2006). For this purpose specific membrane inlet systems for underwater mass spectrometer (UWMS) like the Inspectr200-200 were designed (Kibelka et al. 2004; Short et al. 1999). These UWMS can be operated in water depths of several hundred meters.

In 2005 the Alfred Wegener Institute for Polar and Marine Research (AWI, Bremerhaven, Germany) bought a novel underwater mass spectrometer (Inspectr200-200) from AML Oceanographic (formerly Applied Microsystems). This underwater mass spectrometer was developed by the University of South Florida (Center for Ocean Technology) and SRI International (Stanford Research Institute; Short et al., 1999) and significantly improved in terms of the detection limit and safety during this study. This UWMS is verified up to 200 m water depth. The Inspectr200-200 consists of two cylindrical housings (sensor unit and sampling unit) and an external peristaltic pump. The pressure housing of the sensor unit has an outer diameter of 190mm and a length of 1195 mm. It consists of an Inficon (Bad Ragaz, Switzerland) Transpector CPM 200 quadrupole mass spectrometer, a Varian (Palo Alto, USA) turbo pump, a roughing pump as well as an embedded PC, a Pirani pressure sensor (PSG502, Inficon™), a solenoid valve (EVI 005 M, Pfeiffer

vacuum™) and a microcontroller. The housing of the sample unit has a outer diameter of 190 mm and a length of 290mm. It consists of a heated membrane inlet system (MIS) and a personally developed cryotrap (Ricor™ 1/2W Micro Stirling Cooler K508). To transfer the gases from the sample unit housing to the sensor unit a vacuum line made of $^1/_8$" stainless steel capillary was mounted. During operation of the Inspectr200-200, water is pumped by an additional peristaltic pump from the outside into the pressure housing through the membrane inlet system (MIS) where gas permeation takes place. Within the MIS, the water is in contact with a polydimethylsiloxane (PDMS) tubular membrane. Through a $^1/_8$" capillary, the PDMS membrane is coupled to the high vacuum section supplied by the turbo pump.

To avoid the collapse of the PDMS tube under hydrostatic pressures of up to 20 bar (equivalent to ca. 200 m water depths), the membrane is supported at the inside by a stainless steel spring. Gases (excluding water vapour), permeating through the PDMS membrane are detected by the Inficon CPM 200 residual gas analyzer. The water vapour in the vacuum line is trapped in the affiliated cryotrap, which leads to an improved detection limit to all other gases especially methane. To ensure constant and reproducible physical-chemical conditions for the gas transfer through the membrane, the flow rate of water is controlled by the peristaltic pump, and the membrane inlet system includes a heater and a thermocouple. The temperature of the MIS is adjusted and regulated by a micro-controller. We operated the MIS at a constant temperature of 50 °C and applied a constant flow rate of 3 mL min^{-1}.

The atomic mass-to-charge ratio (*m/z*) of 1 to 200 is covered by the Transpector CPM 200 and, according to Lloyd and Scott (1983) CH_4, N_2, O_2, Ar, and CO_2 were quantified by the ion current detected at *m/z* ratios of 15, 28, 32, 40, and 44, respectively. Depending on the running mode, a full dataset is recorded in between a few seconds. A detailed consideration of the Inspectr200-200 is given by Short et al. (1999) and the gas permeation within the membrane inlet system is described by Bell et al. (2007). Detailed information of the redesign and the calibration of the mass spectrometer are described in chapter 3 and Schlüter and Gentz (2008).

2.5 Objectives of this thesis and overview of the manuscripts

Nowadays, submarine methane release and its present and future contribution to the global carbon cycle is highly debated in the scientific community. Nevertheless, the mechanism of methane release and its fate in the water column are poorly understood. Sampling by conventional techniques is rather time-consuming, which resolves in a low resolution of available data. In order to get a higher data resolution a new *in situ* analysis technique was developed and extensively tested in the frame of this thesis. Within these step forward, important open questions related to the pathways of CH_4 in the water column can be answered by detailed mapping of the methane concentration in combination with other geochemical, biological, and hydrological investigations. These included following steps:

- Improving the *in situ* mass spectrometer in terms of its detection limit with respect to several gases, especially for methane
- Quantifying the methane distribution and its fate in gas ebullition areas
- Detecting, mapping and calculating of the methane inventory in the water column above gas seeps in high resolution.

Therefore, three manuscripts were written by me as first author in context of this thesis. All manuscripts are topically linked to each other. All studies presented here were designed and mainly written by myself supervised by Michael Schlüter and benefited from the contribution of the respective co-authors in sampling as well as discussion of data and writing. The first methodological manuscript (chapter 3) is published in May 2012 in *Limnology and Oceanography-Methods* (DOI:10.4319/lom.2012.10.317) and deals with the improvement of the UWMS with respect to the detection limit and safety. The laboratory experiments were planned and done by myself. Michael Schlüter contributed to data interpretation and writing of the manuscript. The second manuscript (chapter 4) has been submitted in December 2012 for peer-review to the journal "*Continental Shelf Research*" and shows data collected with the improved mass spectrometer. These data were complemented with other geochemical analyses in order to characterize the pathways of methane in the water column at a gas seep area offshore Spitsbergen. The sampling strategy was planned by me and Michael Schlüter. Field work and data acquisition were realized by

me, Ellen Damm and Susan Mau. I interpreted the data and wrote the manuscript with support of my co-authors Ellen Damm, Jens Schneider von Deimling, Susan Mau and Michael Schlüter. The third manuscript (chapter 5) is in preparation for the journal "*Earth and Planetary Science Letters".* The study deals with a very detailed area of 0.14 km² where gas flares through the water column to the surface were observed. By the use of the improved mass spectrometer combined with video observation, hydroacoustic as well as geophysical data, the distribution of dissolved methane in the water column was visualized in high-resolution and, subsequent its inventory calculated. Responsible for the cruise HE362 as cruise leader I planned the sampling strategy. The field work and data acquisition was realized by me with support of Roi Martinez and Till Oehler. I interpreted the data and wrote the manuscript with contributions of Sören Krägewski and Roi Martinez.

Additional to these manuscripts I contribute to a manuscript as a co-author. This manuscript is in the second peer review process with *Journal of Marine Systems* and deals with impacts of submarine groundwater discharge on the meiofaunal community. My contribution was a first data set of CH_4 flux measurement at the sediment-water-transition zone by benthic chamber measurements. Furthermore, I sampled, analyzed and interpreted methane samples taken in sediments in the "affected" and "unaffected" study area by groundwater discharge.

Underwater cryotrap - membrane inlet system (CT-MIS) for improved *in situ* analysis of gases (chapter 3).

Torben Gentz & Michael Schlüter

This chapter focuses on the improvement and the redesign of an *in situ* mass spectrometer (Inspectr 200-200) described in Short et al. (2001). A stirling cooler acting as a novel robust, low-power cryotrap represents an important security system in case of membrane failure. In addition, the cooler removes more than 98% of the water vapour in the analytical line, which leads to better conditions for the ionization of the molecules at the ion source. In this way the detection limits for major and trace gases are considerably improved. For the trace gas CH_4, the detection limit was lowered by this improvement from 100 to 16 nmol L^{-1}, which allows the measurement of the dissolved CH_4 distribution in the water column above gas seeps as well as in coastal areas.

A water column study of methane around gas flares located at the West Spitsbergen continental margin. (chapter 4).

Torben Gentz, Ellen Damm, Susan Mau, Jens Schneider von Deimling, Michael Schlüter

In this chapter, detailed sampling of methane combined with other geochemical methods, hydroacoustic and geophysical data was done in a small gas bubble ebullition area. The data were used to analyze the dissolution of methane from submarine gas bubbles released into the water column and the following pathways like microbiological oxidation, dilution by mixing as well as vertical and horizontal transport with regards to the hydrographic settings. The study area of 175 km² is located at the West Spitsbergen continental margin and is strongly influenced by the West Spitsbergen Current. In previous investigations gas accumulation in shallow sediments and gas ebullition into the water column have been observed (Rajan et al. 2012; Westbrook et al. 2009). The geophysical data reveal a pycnocline in salinity ~20 m above the seafloor, which limits the vertical transport of dissolved CH_4. Our data combined with a gas bubble model suggests that ~80 % of the CH_4 dissolution from gas bubbles into the ambient water takes place below the pycnocline and ~99 % of this CH_4 is lateral transported northwards to greater depths and oxidized by time. Related to the hydrographic conditions in summer we assume that gas bubbles which penetrate the pycnocline and dissolved methane above reveal the only pathway of seabed-released CH_4 as potential source for atmospheric methane.

High resolution determination and inventory calculation of methane in the water column at a gas seepage area in the North Sea via *in situ* mass spectrometry (chapter 5).

Torben Gentz, Sören Krägewski, Roi Martinez, Michael Schlüter

Several submarine geological sources of methane like cold streams, coastal anoxic sediments or mud volcanoes are recognized as significant contributors to the oceanic CH_4 pool. Unfortunately, most sources (like the here presented gas seepage) remain poorly quantified in terms of the fate of methane after seabed release and the resulting potential climate impact. This is caused, among other reasons, that conventional methods hardly reach the spatial and temporal resolution necessary for a detailed inventory calculation of the dissolved methane above gas seepage. Therefore, we used the improved mass spectrometer (chapter 3) *in situ* in various depths for the determination, mapping and quantification of the potential release from a gas seepage area in high resolution. Due to the *in situ* use, the technique is unaffected by potential sampling artifacts and reveals an up to 750 times higher sampling frequency compared to conventional methods. Additionally, we used the acquired knowledge about the limitation of vertical dissolved CH_4 transport by pycnocline (chapter 4) to optimize the sampling strategy. During three deployments in a detailed area of 400 x 410 m in the Netherlands part of the southern North Sea we measured ~11900 samples which lead to detail mapping and subsequent 3-D visualization of the dissolved CH_4 concentration in the water column above the gas seep. Based on the video taken from the sediment 113 active CH_4 streams with a total amount seabed methane release of 35.3 $\pm$ 17.65 t CH_4 yr^{-1} were detected in an "affected" area of 3800 m² in size. Highest dissolved CH_4 concentrations (up to ~3500 nmol L^{-1}) were measured near the seabed in the gas seep area and the inventory in the water column is calculated to ~$6.4*10^5$ μmol with an air sea exchange flux of up to ~210 $\pm$ 63 μmol m^{-2} d^{-1}. As the observed pycnocline in 29 m water depth limits the vertical transport of dissolved CH_4 we divided the inventory in bottom water below and mixed water layer above the pycnocline. Based on these results, we consider an indirect CH_4 transport of ~40 % of the total seabed released methane through dissolution of gas bubbles in the mixed water layer. Additionally, we indicated direct methane transfer via gas bubbles ~25 % by discrete gas bubble sampling at the sea surface, which emphasize that ~65 % (23 $\pm$ 11.5 t CH_4 y^{-1}) of the entire CH_4 emission potentially contributing to the atmospheric CH_4 budget, which is far above most studied gas seepages.

Submarine Groundwater Discharge to the Baltic coastal zone: impacts on the meiofaunal community.

L. Kotwicki, K. Grzelak, M. Czub, O. Dellwig, T. Gentz, B. Szymczycha, M. Böttcher

The discharge of groundwater into the sea is widespread. Overlooking this process may lead to serious misinterpretations of ecological data, particularly in studies of coastal pollution, benthic zonation and productivity, or flux of dissolved substances within and between bottom sediments and overlying water. Freshwater discharges change the salinity, temperature and nutrient regimes and affect near-shore environments. However, the effects of this kind of disturbance on shallow sandy bottom fauna have been little studied.

This work reports the spatial effects of a groundwater discharge on the abundance and structure of the meiofauna community in the shallow area of Puck Bay (the Baltic Sea). During several field expeditions in the years 2009 and 2010, it was found that low-saline groundwater escapes into the bay from permeable, sandy, near-shore sediments. Salinity decreased to 0.1 PSU in pore waters near the surface, and the load of metabolites increased. Groundwater had a clear effect on meiofauna assemblages in the research area, reflected by a significant decline of certain meiofauna taxa, mainly nematodes and harpacticoids. It is clear that groundwater discharge phenomena should be considered in future ecological studies.

References: Chapter 1 and 2

Bange, H. W., U. H. Bartell, S. Rapsomanikis, and M. O. Andreae. 1994. Methane in the Baltic and North Seas and a Reassessment of the Marine Emissions of Methane. GLOBAL BIOGEOCHEMICAL CYCLES 8: 465-480.

Bastviken, D., J. Cole, M. Pace, and L. Tranvik. 2004. Methane emissions from lakes: Dependence of lake characteristics, two regional assessments, and a global estimate. GLOBAL BIOGEOCHEMICAL CYCLES 18.

Bell, R. J., R. T. Short, F. H. W. Van Amerom, and R. H. Byrne. 2007. Calibration of an in situ membrane inlet mass spectrometer for measurements of dissolved gases and volatile organics in seawater. Environ Sci Technol 41: 8123-8128.

Benstead, J., and D. Lloyd. 1996. Spatial and temporal variations of dissolved gases (CH4, CO2, and O2) in peat cores. Microbial Ecol 31: 57-66.

Biastoch, A. and others 2011. Rising Arctic Ocean temperatures cause gas hydrate destabilization and ocean acidification. Geophys Res Lett 38.

Boetius, A. and others 2000. A marine microbial consortium apparently mediating anaerobic oxidation of methane. Nature 407: 623-626.

Bohrmann, G., and M. E. Torres. 2006. Gas Hydrates in Marine SedimentsMarine Geochemistry, p. 481-512. In H. D. Schulz and M. Zabel [eds.]. Springer Berlin Heidelberg.

Boulart, C., D. P. Connelly, and M. C. Mowlem. 2010. Sensors and technologies for in situ dissolved methane measurements and their evaluation using Technology Readiness Levels. Trends in Analytical Chemistry 29: 186-195.

Buerck, J., S. Roth, K. Kraemer, M. Scholz, and N. Klaas. 2001. Application of a fiber-optic NIR-EFA sensor system for in situ monitoring of aromatic hydrocarbons in contaminated groundwater. J Hazard Mater 83: 11-28.

Burwicz, E. B., L. H. Rupke, and K. Wallmann. 2011. Estimation of the global amount of submarine gas hydrates formed via microbial methane formation based on numerical reaction-transport modeling and a novel parameterization of Holocene sedimentation. Geochim Cosmochim Ac 75: 4562-4576.

Butler, J. H., and J. W. Elkins. 1991. An Automated Technique for the Measurement of Dissolved N2o in Natural-Waters. Marine Chemistry 34: 47-61.

Camilli, R., and H. Hemond. 2002. NEREUS engineering concept for an underwater mass spectrometer. Trends in analytical chemistry, 23: 307-313.

Canfield, D. E., and B. Thamdrup. 2009. Towards a consistent classification scheme for geochemical environments, or, why we wish the term 'suboxic' would go away. Geobiology 7: 385-392.

Chappellaz, J. A., I. Y. Fung, and A. M. Thompson. 1993. The Atmospheric Ch4 Increase since the Last Glacial Maximum. Tellus Series B-Chemical and Physical Meteorology 45: 228-241.

Cisewski, B., G. Budeus, and G. Krause. 2003. Absolute transport estimates of total and individual water masses in the northern Greenland Sea derived from hydrographic and acoustic Doppler current profiler measurements. J Geophys Res-Oceans 108.

Claypool, G. E. 1974. The origin and distribution of methane in marine sediments. Natural gases in marine sediments: 99-139.

Cornford, C. 2009. Source Rocks and Hydrocarbons of the North Sea, p. 376-462. Petroleum Geology of the North Sea. Blackwell Science Ltd.

Damm, E., and G. Budéus. 2003. Fate of vent-derived methane in seawater above the Håkon Mosby mud volcano (Norwegian Sea). Marine Chemistry 82: 1-11.

Dlugokencky, E. J. and others 2003. Atmospheric methane levels off: Temporary pause or a new steady-state? Geophys Res Lett 30.

Emerson, S., C. Stump, B. Johnson, and D. M. Karl. 2002. In situ determination of oxygen and nitrogen dynamics in the upper ocean. Deep-Sea Res Pt I 49: 941-952.

Etheridge, D. M., L. P. Steele, R. J. Francey, and R. L. Langenfelds. 1998. Atmospheric methane between 1000 AD and present: Evidence of anthropogenic emissions and climatic variability. J Geophys Res-Atmos 103: 15979-15993.

Etiope, G., and P. Favali. 2004. Geologic Emissions of Methane from lands and seafloor: mud volcanoes and observing systems. Environ Geol 46: 987-987.

Etiope, G., and R. W. Klusman. 2002. Geologic emissions of methane to the atmosphere. Chemosphere 49: 777-789.

Etiope, G., and A. V. Milkov. 2004. A new estimate of global methane flux from onshore and shallow submarine mud volcanoes to the atmosphere. Environ Geol 46: 997-1002.

Faber, E., W. Stahl, and M. Whiticar. 1992. Distinction of bacterial and thermogenic hydrocarbon gases. Bacterial gas: Paris, Editions Technip: 63-74.

Felden, J., F. Wenzhofer, T. Feseker, and A. Boetius. 2010. Transport and consumption of oxygen and methane in different habitats of the Hakon Mosby Mud Volcano (HMMV). Limnology and Oceanography 55: 2366-2380.

Ferretti, D. F. and others 2005. Unexpected changes to the global methane budget over the past 2000 years. Science 309: 1714-1717.

Fischer, P. J. 1978. Natural gas and oil seeps,Santa Barbara Basin, California.

Fleischer, P., T. H. Orsi, M. D. Richardson, and A. L. Anderson. 2001. Distribution of free gas in marine sediments: a global overview. Geo-Mar Lett 21: 103-122.

Floodgate, G. D., and A. G. Judd. 1992. The origins of shallow gas. Continental Shelf Research 12: 1145-1156.

Froelich, P. N. and others 1979. Early Oxidation of Organic-Matter in Pelagic Sediments of the Eastern Equatorial Atlantic - Suboxic Diagenesis. Geochim Cosmochim Ac 43: 1075-1090.

Gueguen, C., and P. D. Tortell. 2008. High-resolution measurement of Southern Ocean CO2 and O2/Ar by membrane inlet mass spectrometry. Marine Chemistry 108: 184-194.

Hartnett, H. E., and S. P. Seitzinger. 2003. High-resolution nitrogen gas profiles in sediment porewaters using a new membrane probe for membrane-inlet mass spectrometry. Marine Chemistry 83: 23-30.

Hemond, H., and R. Camilli. 2002. NEREUS: engineering concept for an underwater mass spectrometer. Trac-Trend Anal Chem 21: 526-533.

Hesse, R., and W. E. Harrison. 1981. Gas Hydrates (Clathrates) Causing Pore-Water Freshening and Oxygen Isotope Fractionation in Deep-Water Sedimentary Sections of Terrigenous Continental Margins. Earth Planet Sc Lett 55: 453-462.

Houghton, J. T. 2001. Climate change 2001 : the scientific basis ; contribution of Working Group I to the third assessment report of the Intergovernmental Panel on Climate Change. Cambridge Univ. Press.

Houweling, S., F. Dentener, and J. Lelieveld. 2000. Simulation of preindustrial atmospheric methane to constrain the global source strength of natural wetlands. J Geophys Res-Atmos 105: 17243-17255.

Hovland, M., J. V. Gardner, and A. G. Judd. 2002. The significance of pockmarks to understanding fluid flow processes and geohazards. Geofluids 2: 127-136.

Hovland, M., and A. G. Judd. 1988. Seabed Pockmarks and Seepages. Graham and Trotman, London,: 293pp.

Hovland, M., A. G. Judd, and R. A. Burke. 1993. The Global Flux of Methane from Shallow Submarine Sediments. Chemosphere 26: 559-578.

Hovland, M., and J. H. Sommerville. 1985. Characteristics of two natural gas seepages in the North Sea. Mar Petrol Geol 2: 319-326.

Hustoft, S., S. Bunz, J. Mienert, and S. Chand. 2009a. Gas hydrate reservoir and active methane-venting province in sediments on < 20 Ma young oceanic crust in the Fram Strait, offshore NW-Svalbard. Earth Planet Sc Lett 284: 12-24.

Hustoft, S., B. Dugan, and J. Mienert. 2009b. Effects of rapid sedimentation on developing the Nyegga pockmark field: Constraints from hydrological modeling and 3-D seismic data, offshore mid-Norway. Geochem Geophy Geosy 10.

Intergovernmental Panel on Climate Change (2007) IPCC fourth assessment report (AR4). Working Group 1, The Physical Science Basis

Iversen, N., and B. B. Jorgensen. 1985. Anaerobic Methane Oxidation Rates at the Sulfate Methane Transition in Marine-Sediments from Kattegat and Skagerrak (Denmark). Limnology and Oceanography 30: 944-955.

Johnson, K. M., A. Kortzinger, L. Mintrop, J. C. Duinker, and D. W. R. Wallace. 1999. Coulometric total carbon dioxide analysis for marine studies: measurement and internal consistency of underway TCO2 concentrations. Marine Chemistry 67: 123-144.

Judd, A. G. 2004. Natural seabed gas seeps as sources of atmospheric methane. Environ Geol 46: 988-996.

Judd, A. G., and M. Hovland. 2007. Seabed fluid flow the impact of geology, biology and the marine environment. Cambridge University Press.

Judd, A. G., M. Hovland, L. I. Dimitrov, S. G. Gil, and V. Jukes. 2002. The geological methane budget at Continental Margins and its influence on climate change. Geofluids 2: 109-126.

Kampbell, D. H., J. T. Wilson, and S. A. Vandegrift. 1989. Dissolved-Oxygen and Methane in Water by a Gc Headspace Equilibration Technique. Int J Environ an Ch 36: 249-257.

Khalil, M.A.K., Rasmussen, R.A., 1983. Sources, Sinks, and Seasonal Cycles of Atmospheric Methane. J. geophys. Res. 88, 5131-5144.

Kibelka, G. P. G., R. T. Short, S. K. Toler, J. E. Edkins, and R. H. Byrne. 2004. Field-deployed underwater mass spectrometers for investigations of transient chemical systems. Talanta 64: 961-969.

Knies, J., E. Damm, J. Gutt, U. Mann, and L. Pinturier. 2004. Near-surface hydrocarbon anomalies in shelf sediments off Spitsbergen: Evidences for past seepages. Geochem Geophy Geosy 5.

Kubala, M., M. Bastow, S. Thompson, I. Scotchman, and K. Oygard. 2003. Geothermal regime, petroleum generation and migration. The Millennium Atlas: Petroleum Geology of the Central and Northern North Sea. Geological Society, London: 289-315.

Kvenvolden, K. A., T. D. Lorenson, S. Geological, C. Western, and P. Marine Geology. 2001. A global inventory of natural gas hydrate occurrence. USGS WR CMG.

Kvenvolden, K. A., and B. W. Rogers. 2005. Gaia's breath - global methane exhalations. Mar Petrol Geol 22: 579-590.

Lammers, S., and E. Suess. 1994. An Improved Headspace Analysis Method for Methane in Seawater. Marine Chemistry 47: 115-125.

Leifer, I., and J. Boles. 2005. Measurement of marine hydrocarbon seep flow through fractured rock and unconsolidated sediment. Mar Petrol Geol 22: 551-568.

Leifer, I., and J. Clark. 2002. Modeling trace gases in hydrocarbon seep bubbles. Application to marine hydrocarbon seeps in the Santa Barbara Channel. Geol Geofiz 43: 613-621.

Leifer, I., and A. G. Judd. 2002. Oceanic methane layers: the hydrocarbon seep bubble deposition hypothesis. Terra Nova 14: 417-424.

Lelieveld, J. O. S., P. J. Crutzen, and F. J. Dentener. 1998. Changing concentration, lifetime and climate forcing of atmospheric methane. Tellus B 50: 128-150.

Lelieveld, J., Crutzen, P.J., Dentener, F.J., 2002. Changing concentration, lifetime and climate forcing of atmospheric methane. Tellus B 50, 128-150.

Limonov, A. F., T. C. E. Van Weering, N. H. Kenyon, M. K. Ivanov, and L. B. Meisner. 1997. Seabed morphology and gas venting in the Black Sea mudvolcano area: Observations with the MAK-1 deep-tow sidescan sonar and bottom profiler. Marine Geology 137: 121-136.

Lloyd, D.; Scott, R. I. Direct measurement of dissolved gases in microbiological systems using membrane inlet mass spectrometry. J. Microbiol. Methods. Vol. 1983, 1, 313–328.

Lloyd, D., K. Thomas, D. Price, B. Oneil, K. Oliver, and T. N. Williams. 1996. A membrane-inlet mass spectrometer miniprobe for the direct simultaneous measurement of multiple gas species with spatial resolution of 1 mm. Journal of Microbiological Methods 25: 145-151.

McGinnis, D. F., J. Greinert, Y. Artemov, S. E. Beaubien, and A. Wuest. 2006. Fate of rising methane bubbles in stratified waters: How much methane reaches the atmosphere? J Geophys Res-Oceans 111.

McGinnis, D. F. and others 2011. Discovery of a natural CO2 seep in the German North Sea: Implications for shallow dissolved gas and seep detection. Journal of geophysical research 116.

McMurtry, G. M., J. C. Wiltshire, and A. Bossuyt. 2005. A deep ocean mass spectrometer to monitor hydrocarbon seeps and pipelines. 24th International Conference on Offshore Mechanics and Arctic Engineering.

Milkov, A. V. 2000. Worldwide distribution of submarine mud volcanoes and associated gas hydrates. Marine Geology 167: 29-42.

Niemann, H. and others 2005. Methane emission and consumption at a North Sea gas seep (Tommeliten area). Biogeosciences 2: 335-351.

Prien, R. D. 2007. The future of chemical in situ sensors. Marine Chemistry 107: 422-432.

Prinzhofer, A., and E. Pernaton. 1997. Isotopically light methane in natural gas: bacterial imprint or diffusive fractionation? Chem Geol 142: 193-200.

Rajan, A., J. Mienert, and S. Bünz. 2012. Acoustic evidence for a gas migration and release system in Arctic glaciated continental margins offshore NW-Svalbard. Mar Petrol Geol 32: 36-49.

Reeburgh, W. S. 1976. Methane Consumption in Cariaco Trench Waters and Sediments. Earth Planet Sc Lett 28: 337-344.

---. 2007. Oceanic methane biogeochemistry. Chem Rev 107: 486-513.

Rehder, G., R. S. Keir, E. Suess, and T. Pohlmann. 1998. The multiple sources and patterns of methane in North Sea waters. Aquat Geochem 4: 403-427.

Ruppel, C. 2011. Methane hydrates and contemporary climate change. Nat. Educ. Knowl 2: 12.

Sahling, H. and others 2008. Pockmarks in the Northern Congo Fan area, SW Africa: Complex seafloor features shaped by fluid flow. Marine Geology 249: 206-225.

---. 2003. Depth-related structure and ecological significance of cold-seep communities - a case study from the Sea of Okhotsk. Deep-Sea Res Pt I 50: 1391-1409.

Saloranta, T. M., and H. Svendsen. 2001. Across the Arctic front west of Spitsbergen: high-resolution CTD sections from 1998-2000. Polar Res 20: 177-184.

Saltzman, E. S., W. J. De Bruyn, M. J. Lawler, C. A. Marandino, and C. A. Mccormick. 2009. A chemical ionization mass spectrometer for continuous underway shipboard analysis of dimethylsulfide in near-surface seawater. Ocean Sci 5: 537-546.

Sauter, E. J. and others 2006. Methane discharge from a deep-sea submarine mud volcano into the upper water column by gas hydrate-coated methane bubbles. Earth Planet Sc Lett 243: 354-365.

Sauter, E. J., M. Schluter, and E. Suess. 2001. Organic carbon flux and remineralization in surface sediments from the northern North Atlantic derived from pore-water oxygen microprofiles. Deep-Sea Res Pt I 48: 529-553.

Schauer, U., E. Fahrbach, S. Osterhus, and G. Rohardt. 2004. Arctic warming through the Fram Strait: Oceanic heat transport from 3 years of measurements. J Geophys Res-Oceans 109.

Schlüter, M., and T. Gentz. 2008. Application of Membrane Inlet Mass Spectrometry for Online and In Situ Analysis of Methane in Aquatic Environments. J Am Soc Mass Spectr 19: 1395-1402.

Schlüter, M., P. Linke, and E. Suess. 1998. Geochemistry of a sealed deep-sea borehole on the Cascadia Margin. Marine Geology 148: 9-20.

Schoell, M. 1980. The Hydrogen and Carbon Isotopic Composition of Methane from Natural Gases of Various Origins. Geochim Cosmochim Ac 44: 649-661.

---. 1988. Origins of Methane in the Earth - a Selection of Lectures from the Annual-Meeting of the Geological-Society-of-America, Phoeniz, Arizona, 26-29 October 1987 - Preface. Chem Geol 71: R7-R7.

Schroot, B. M., G. T. Klaver, and R. T. E. Schuttenhelm. 2005. Surface and subsurface expressions of gas seepage to the seabed - examples from the Southern North Sea. Mar Petrol Geol 22: 499-515.

Schroot, B. M., and R. T. E. Schuttenhelm. 2003. Expressions of shallow gas in the Netherlands North Sea. Neth J Geosci 82: 91-105.

Shakhova, N., I. Semiletov, A. Salyuk, V. Yusupov, D. Kosmach, and Ö. Gustafsson. 2010. Extensive Methane Venting to the Atmosphere from Sediments of the East Siberian Arctic Shelf. Science 327: 1246-1250.

Sheppard, S. K., and D. Lloyd. 2002. Direct mass spectrometric measurement of gases in soil monoliths. Journal of Microbiological Methods 50: 175-188.

Shindell, D. T., G. Faluvegi, D. M. Koch, G. A. Schmidt, N. Unger, and S. E. Bauer. 2009. Improved Attribution of Climate Forcing to Emissions. Science 326: 716-718.

Shipley, T. H. and others 1979. Seismic Evidence for Widespread Possible Gas Hydrate Horizons on Continental Slopes and Rises. Aapg Bulletin-American Association of Petroleum Geologists 63: 2204-2213.

Short, R. T., D. P. Fries, S. K. Toler, C. E. Lembke, and R. H. Byrne. 1999. Development of an underwater mass-spectrometry system for in situ chemical analysis. Meas Sci Technol 10: 1195-1201.

---. 2006. Development of an underwater mass spectrometry system for in-situ chemical analysis,. Meas. Sci. Technol. 10: 1195–1201.

Steele, M., W. Ermold, and J. Zhang. 2008. Arctic Ocean surface warming trends over the past 100 years. Geophys Res Lett 35: L02614.

Stuart, J. Y., and M. Huuse. 2012. 3D seismic geomorphology of a Large Plio-Pleistocene delta - 'Bright Spots' and Contourites in the Southern North Sea. Mar Petrol Geol.

Suess, E. 1980. Particulate organic carbon flux in the oceans-surface productivity and oxygen utilization. Nature 288: 260-263.

--- [ed.]. 2010. Handbook of Hydrocarbon and LipidMicrobiology. Springer Berlin,

Suess, E. and others 2001. Sea floor methane hydrates at Hydrate Ridge, Cascadia margin, p. 87-98. Natural Gas Hydrates: Occurrence, Distribution, and Detection. Geophys. Monogr. Ser. AGU.

---. 1999. Gas hydrate destabilization: enhanced dewatering, benthic material turnover and large methane plumes at the Cascadia convergent margin. Earth Planet Sc Lett 170: 1-15.

Tortell, P. D. 2005. Dissolved gas measurements in oceanic waters made by membrane inlet mass spectrometry. Limnol Oceanogr-Meth 3: 24-37.

Tortell, P. D., and M. C. Long. 2009. Spatial and temporal variability of biogenic gases during the Southern Ocean spring bloom. Geophys Res Lett 36: -.

Trehu, A. M. and others 2006. Hydrates. Oceanography 19: 124.

Turner, A. P. F., S. Laschi, and M. Mascini. 2000. Biosensors. Kirk-Othmer Encyclopedia of Chemical Technology. John Wiley & Sons, Inc.

Valdes, P. J., D. J. Beerling, and C. E. Johnson. 2005. The ice age methane budget. Geophys Res Lett 32.

Wankel, S. D. and others 2010. New constraints on methane fluxes and rates of anaerobic methane oxidation in a Gulf of Mexico brine pool via in situ mass spectrometry. Deep Sea Research Part II: Topical Studies in Oceanography 57: 2022-2029.

Wenner, P. G. and others 2004. Environmental chemical mapping using an underwater mass spectrometer. Trac-Trend Anal Chem 23: 288-295.

Westbrook, G. K. and others 2008. Estimation of gas hydrate concentration from multi-component seismic data at sites on the continental margins of NW Svalbard and the Storegga region of Norway. Mar Petrol Geol 25: 744-758.

---. 2009. Escape of methane gas from the seabed along the West Spitsbergen continental margin. Geophys Res Lett 36: -.

Whiticar, M. J. 1999. Carbon and hydrogen isotope systematics of bacterial formation and oxidation of methane. Chem Geol 161: 291-314.

Whiticar, M. J., and E. Faber. 1986. Methane Oxidation in Sediment and Water Column Environments - Isotope Evidence. Org Geochem 10: 759-768.

Whiticar, M. J., and L. R. Snowdon. 2000. Geochemical characterization of selected Western Canada oils by C-5-C-8 Compound Specific Isotope Correlation (CSIC) (vol 30, pg 1127, 1999). Org Geochem 31: 775-775.

Wiesenburg, D. A., and N. L. Guinasso. 1979. Equilibrium Solubilities of Methane, Carbon-Monoxide, and Hydrogen in Water and Sea-Water. J Chem Eng Data 24: 356-360.

Chapter 3 – Manuscript I

~ Cryotrap for *in situ* analysis ~

Published in Limnology and Oceanography: Methods
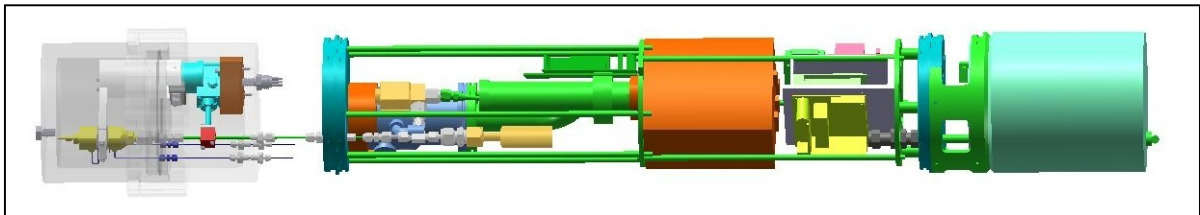
Schematic view of the improved mass spectrometer

Underwater cryotrap - membrane inlet system (CT-MIS) for improved *in situ* analysis of gases

Torben Gentz & Michael Schlüter

Alfred Wegener Institute for Polar and Marine Research, Am Handelshafen 12, D-27570 Bremerhaven, Germany

3.1 Abstract

Membrane inlet sensor techniques allow online, real-time and *in situ* analyses of gases during the investigation of aquatic environments. Of specific interest for research and applied objectives are quantifications of gases like methane, higher hydrocarbons, carbon dioxide, nitrogen, volatile organic compounds and pollutants. For these objectives, membrane inlet systems are coupled to optical or solid state sensors as well as mass spectrometers. Besides the gases of interest, large quantities of water vapour are passing through the membrane and are thus introduced into the sensor system. This downgrades the detection limit, affects the ionization efficiency of mass spectrometers or could cause the condensation of water within infrared sensors. In this study, we describe a novel robust, low-power cryotrap coupled to a membrane inlet system (CT-MIS), which is suitable to be used in harsh environments, including underwater applications. The entire system is of small size and weight, is operated at -85 °C and requires an energy consumption of less than 10 Watt. By using the cryotrap, we are able to reduce water vapour in the analytical line by more than 98%. The detection limits for major- and trace gases are considerably improved this way. For the trace gas CH_4, the detection limit was lowered from 100 to 16 nmol/L, which allows the measurement of methane in surface and bottom waters of coastal areas and lakes. In case of membrane failure, the CT-MIS acts as a security system by shock-freezing the water, thus blocking the capillary connection to the analyzer unit.

3.2   Introduction

The analysis of gases like carbon dioxide, methane, higher hydrocarbons, dimethylsulfide (DMS) as well as volatile organic compounds (VOCs) in marine or freshwater environments has been gaining attention as an increasing necessity within the last few years. Such gases are produced in the water column or released from sediments as well as anthropogenic sources. Examples for the release of gases from sediments are seeps, mud volcanoes or pockmarks, which are observed along coastal margins as well as in lakes (Hovland and Judd 1988; Milkov 2000). At such sites, analyses of gases like CH_4, higher hydrocarbons or natural CO_2 are required to be performed in order to calculate budgets, evaluate the fate of gases due to microbial turnover processes as well as estimating the air-sea exchange of trace gases (Hovland and Judd 1988; Leifer and Boles 2005b; McGinnis et al. 2006,2011; Niemann et al. 2005; Rehder et al. 1998; Sahling et al. 2008; Sauter et al. 2006; Suess et al. 1999; Tortell and Long 2009). Furthermore, economic demands related to geo-engineering issues, for example, require onsite and online gas analyses to monitor the release of CH_4, CO_2 or VOCs from underwater pipelines, wells, or geological sequestration sites (Camilli et al. 2009; Leifer and Boles 2005a; McMurtry et al. 2005).

For the investigation of gas concentrations in aquatic systems, techniques like water sampling by e.g., rosette water sampler, subsequent phase separation by head space technique as well as analyses by gas chromatography are well established (Kampbell et al. 1989). Unfortunately, these procedures are rather time consuming. Especially for settings where steep concentration gradients exist, for example at seeps or pockmarks, they limit the spatial resolution by which concentration fields can be described.

Furthermore, at sites where high gas concentrations are observed, the decompression of water samples during the sampler retrieval on board the vessel could cause a loss of gases (Schlüter et al. 1998). Such restrictions stimulated the development of continuous underway measurement systems (Butler and Elkins 1991; Gueguen and Tortell 2008; Johnson et al. 1999; Saltzman et al. 2009; Tortell 2005) and underwater gas analyzers for *in situ* measurements of O_2 (Oxygen), CH_4, VOC´s

and CO_2 (Boulart et al. 2008; Camilli and Hemond 2002; Emerson et al. 2002; McMurtry et al. 2005; Prien 2007; Short et al. 2006b; Wankel et al. 2010).

Whereas optodes for *in situ* measurement of O_2 rely on a chemical transducer and measurement of fluorescence, most other underwater gas analyzers require a gas extraction unit. Most of these units apply membrane inlet systems (MIS), which allow the phase separation of gases like CO_2, CH_4, DMS, radon or VOCs from water into the gaseous phase (Boulart et al. 2010; Johnson et al. 2000; Prien 2007). The gas phase separated by the MIS is introduced into an analytical unit, like a mass spectrometer, gas chromatograph, infrared spectrometer or solid-state gas sensors for detection of the composition of the gas mixture as well as gas concentrations.

Dependent on the field of application, research as well as industrial applications make use of different membrane materials and geometries (e.g., planar, tubular or coiled) when performing phase separation with membrane inlet systems. These membranes are made of polydimethylsiloxane (PDMS), Teflon (Teflon™, AF2400™) as well as materials like Nafion™, Celgard™ or Accurel™ (Melin and Tautenbach 2006). Common to these different materials are their non-porous or micro-porous properties, which are impermeable to the liquid phase, up to a certain pressure. The transfer of gases through solid state membranes like PDMS as well as Nafion™, or through micro-porous membranes like Accurrel™ or Celgard™, is described and modeled by concepts like permeation or pervapouration. A detailed consideration of different membrane materials and separation mechanisms considering analytical as well as industrial application is provided by Melin and Tautenbach (2006).

The mass transport of gas through a membrane depends on the membrane type as well as the specific properties of the gas. Most of the non-porous or micro-porous membranes are hydrophobic and preferentially exclude the polar water molecules over e.g., VOCs. However, they do not completely exclude water vapour (H_2O_v) and since it is the matrix, it is still the major gas species in the vacuum system (Tortell 2005). The H_2O_v affects gas analyses done by mass spectrometry, as well as the IR bands of the analyte during spectroscopy, downgrades the detection limit or could cause condensation of water inside the optical sensor section of the analyzer.

Regarding membrane inlet mass spectrometry (MIMS), additional disadvantages of high water vapour contents within the vacuum line are excessive pressure in the ion source of the mass spectrometer and decreased signal stability at Ar (argon, m/z 40), O_2 (m/z 32) and N_2 (nitrogen, m/z 28), for example (Bell et al. 2011; Lloyd et al. 1996; McCarthy and Gardner 2003; Tortell 2005).

In the laboratory, interferences due to a high amount of water vapour entering the sensor system can be avoided by absorbing agents (e.g., Dierite™), molecular sieves or cold traps. The detection limits for e.g., VOC´s, DMS, CH_4 or DMSP (dimethylsulfoniopropionate) are considerably improved by enriching, and subsequently releasing, analytes within the cryotrap (Damm et al. 2008; Desmarais 1978; Mendes et al. 1996a; Simmonds 1984). For the measurement of some analytes, the trapping of gases like water vapour or hydrogen sulfide (H_2S) improves the signal to noise ratio, the detection limit and the measurement precision (Kolb et al. 1996; Mendes et al. 1996b).

Compared to cryotraps applied in laboratories, issues like small size, low weight, small waste-heat production, robustness and especially low energy consumption are the required specifications in underwater applications. This article describes the design and performance of a novel underwater cryotrap membrane inlet system (CT-MIS), reaching temperatures of less than -85 °C to trap water vapour before entering the analytical line. The CT-MIS is self-contained and, with small modifications, can be coupled to different optical sensors in addition to mass spectrometers. For the assessment of the CT-MIS, the unit was coupled to the underwater mass spectrometer (UWMS) Inspectr200-200 (Bell et al. 2007, 2011; Short et al. 2001, 2006a; Wenner et al. 2004). We applied this system in the Baltic Sea and the North Sea for the analysis of Ar, O_2, N_2, CH_4 as well as CO_2 in the water column and also at the sediment-water interface.

For trapping water vapour from the gas phase prior to a chemical analysis utilizing gas chromatography, MIMS or IR spectrometry cryotraps of different types are applied. The design varies from U-shaped type capillaries submerged in Dewar flasks to advanced microjet cryotrap systems (Desmarais 1978; Kolb et al. 1996; Peters and

Yakir 2010; Van Der Laan-Luijkx et al. 2010). Techniques to cool down a section of the gas stream include the application of liquid N_2 or Ar contained in Dewar flasks and thermoelectric cooling by Peltier elements or high performance cryopumps. The cooling temperature depends on the mode of operation as well as the freezing point of the gases of interest. For example, to trap water vapour in a vacuum section (i.e. @0.0533 Pa = $4x10^{-4}$Torr) while connecting a membrane inlet system with a mass spectrometer, the cryotrap has to be operated at a temperature of about -80 °C (Wexler 1977).

For the application of cryotraps in laboratories, features the evapouration of cooling agents as well as size and weight of the device are of minor importance. In contrast, these features are essential for cryotraps which are applied on research vessels or mounted in a pressure housing for the use in underwater applications. In such applications, the use of cooling agents such as liquid ethanol or N_2 would lead to the formation of large gas volumes and could cause security risks or are inappropriate during operation.

Therefore, from a technical as well as analytical perspective, the following issues are considered mandatory for a stand-alone underwater cryotrap membrane inlet systems: (1) temperatures below -85°C have to be reached, (2) a small waste-heat production is required, (3) the energy consumption has to be below 10 W, (4) a service life time of more than 10 hours is favorable, (5) a short cool down time below 60 min is necessary, and (6) the system should be robust, of small dimensions and low weight for applications in harsh environments.

3.3   Materials and procedures

Since small sized, low energy, robust mechanical designs as well as liquid-free cooling systems are required, we considered the application of Stirling coolers and Peltier elements. Due to the low energy consumption, Stirling coolers would be a suitable choice for the application in underwater cryotraps. Peltier elements are inexpensive, do not contain moving parts and are small in size and of low weight, which are beneficial features for applications in harsh environments. Potential drawbacks of Peltier elements are the high electrical energy consumption as well as the high waste-heat production.

For the development of an underwater cryotrap, we compared a compact Stirling cooler (Ricor™ 1/2W Micro Stirling Cooler K508; Fig. 3-1 B) with an advanced three-layer Peltier cooler (Whatson Marlow™, MI4040), able to generate temperature differences of up to 120 °C. The K508 is a rotary compressor with a mechanically driven expander. Under ideal conditions (operating in a vacuum at an ambient temperature of 20 °C), a temperature of -196 °C is reached. Even under standard conditions (operating in air at an ambient temperature of 20 °C) temperatures of less than -93 °C were achieved. The weight of the K508 is about 450 g and the dimensions are 116 x 58 x 71 mm. The results of the Stirling cooler and the Peltier element are shown in more detail in the assessment section.

The cold part of the Stirling cooler is coupled to a $^1/_8$" capillary tube by an aluminium block of 20 x 20 x 20 mm (Fig. 3-1 B). The water vapour will be trapped in the inner part of this capillary tube. The block is divided in two parts, which are connected by screws in order to clamp down the capillary tube. The heat sink of the cooler is coupled to a copper block, which is tightly connected to the inside of the pressure housing (Fig. 3-1 B). The area of the copper block connected to the pressure housing measures about 4550 mm². This is sufficient for the heat to transfer from the cooler inside the pressure housing to the outside, and to minimize any warming of the interior of the pressure housing.
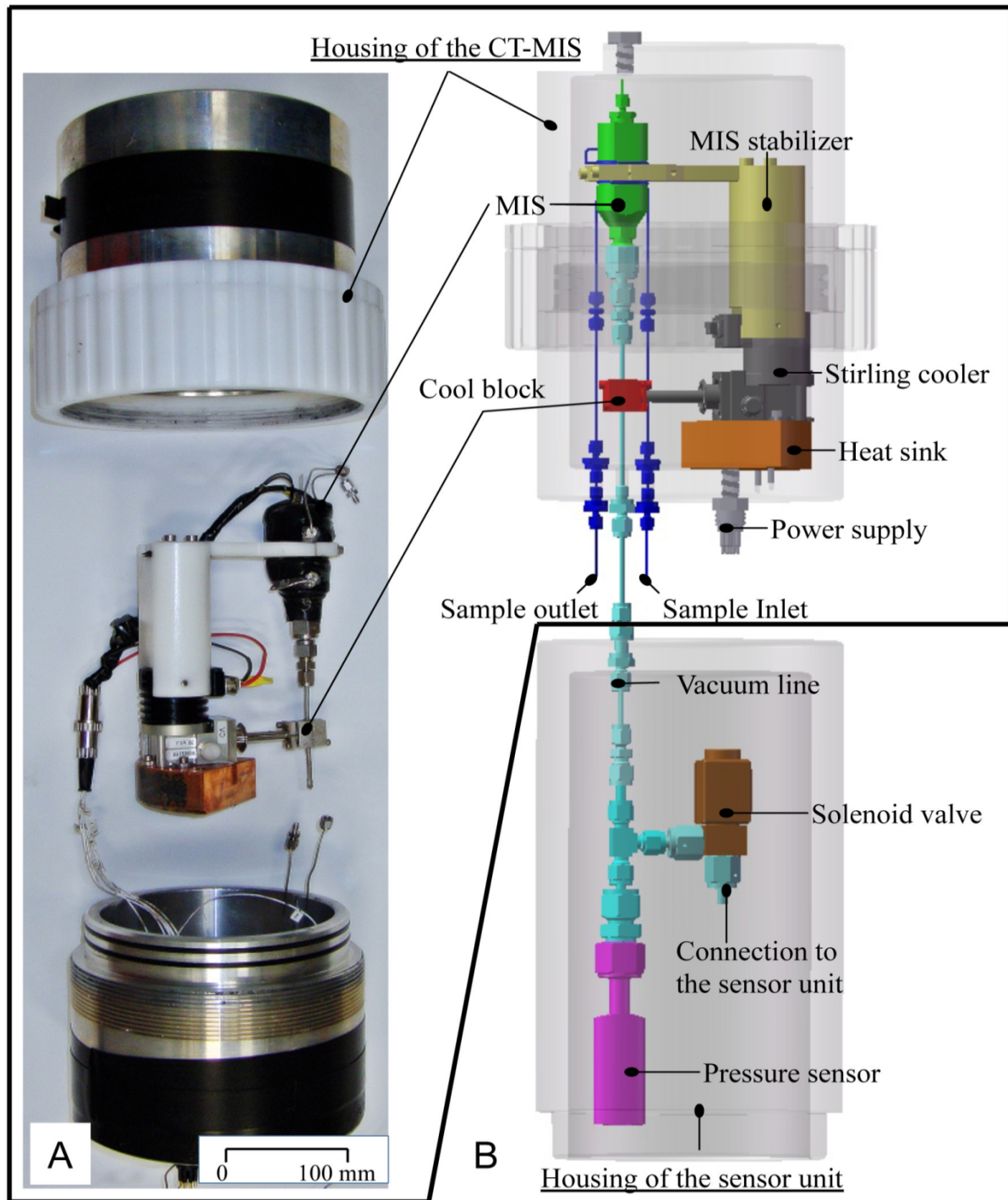
Fig. 3-1 (A) Image of the disassembled pressure housing (depth rate up to 200 m) and schematic drawing of the cryotrap membrane inlet system (CT-MIS). Main components of the CT-MIS are the Ricor™ cooler (K508) and the membrane inlet system (Short et al. 2001). (B) Schematic drawing the lower part of the sensor housing including the Pirani pressure sensor (PSG502- S, Inficon™) and the solenoid valve (EVI 005 M, Pfeiffer vacuum™).

For assessing the performance of the cryotrap, we coupled it to a membrane inlet system (MIS) developed by Short et al. (2001; Fig. 3-1 B). The membrane interface is made of a 13 mm long PDMS tubing (Helix Medical™), which is supported on the inside by a stainless steel spring (Gutekunst™) to sustain pressure of up to 20 bar (Bell et al. 2007; Short et al. 2001, 2006a; Wenner et al. 2004). To get stable conditions for the gas transfer through the membrane, the entire MIS is temperature-controlled and the water is pumped at a constant flow rate along the PDMS tubing.

The cooler and membrane inlet system are mounted in a pressure housing made of aluminium (Fig. 3-1 B). The housing has a length of 290 mm, an outer diameter of 190 mm and an inner diameter of 180 mm, and is certified to a water depth of 200 m. The housing can be split into two parts of similar length, which are connected by a cap nut made of Polyoxymethylene. This design allows easy access to the cryotrap and MIS for maintenance purposes.

An *in situ* peristaltic pump (KC Denmark™), mounted outside the pressure housing of the cryotrap, is applied to pump water through the membrane inlet system at a constant flow rate of e.g., 3 ml min^{-1}. For this purpose, two $^1/_{16}$" Swagelok™ connectors (SS-100-1-OR) and two stainless steel $^1/_{16}$" capillaries are mounted on the left hand side of the pressure housing for sample inlet and outlet (Fig. 3-1 B). To transfer the gases through the vacuum line connecting the CT-MIS with the gas analyzer, a $^1/_8$" capillary fixed by a $^1/_8$" Swagelok™ connector (SS-200-1-OR) was mounted to one side of the pressure housing. A SubConn™ connector (eight pin female, BH8F) used for data transfers and acting as a power supply for the heater as well as the cryotrap is mounted at the same side. Therefore, maintenance requires only to unlock the cap nut and to split the housing into two parts (Fig. 3-1 B).

In case of a rupture of the PDMS membrane, the cryotrap will act as a security system. The inflowing water will freeze in the capillary tube connected to the cool finger of the cryotrap, creating an "ice plug" which will block the inflow of liquid water for a few minutes (Schlüter and Gentz, 2008). Additional to the cryotrap, we installed a Pirani pressure sensor (PSG502-S, Inficon™, Fig. 3-1 A) in order to measure the absolute pressure in the vacuum line, and a high vacuum solenoid valve (EVI 005 M, Pfeiffer vacuum™; Fig. 3-1 A). In case of inflowing water, the fast responding Pirani

sensor registers the pressure increase in the vacuum section and triggers the solenoid valve, which uncouples the CT-MIS unit from the gas analyzer.

In our application, we mounted the sensor and solenoid valve into the pressure housing of the gas analyzer, which provides some additional milliseconds of response time (Fig. 3-1 A). Prior to the deployment of the underwater CT-MIS, we flushed the housing with Ar gas. This stabilizes the temperature at the cooling block since precipitation of the air water vapour is avoided. Furthermore, we coated the cooling block with 25 mm of strong insulating material (Armaflex^{TM}) to further improve the temperature stability.

3.4 Assessment

3.4.1 Specification of the cooling unit

For assessing the suitability and performance of the cooling unit to trap water vapour at a temperature of -85 °C, we compared a compact Stirling cooler (Ricor™ 1/2W Micro, K508) with a novel three layer Peltier cooler (Whatson Marlow™, MI4040). From the perspective of underwater deployments, criteria for this assessment were the mechanical robustness, the cool down time, the power consumption required to keep the temperature at -85 °C and the waste-heat of the cooler. Since the cryotrap had to be installed within a fully enclosed pressure housing, the waste-heat needed to be transferred from the inside of the housing into the water column.

In order to compare the two cooler systems, we mounted each of them with its heat sink on a copper block of 60 x 60 x 15 mm in the laboratory, and measured the temperature at the cool finger as well as the temperature at the heat sink (Fig. 3-2 A). The Stirling cooler reached the target temperature of -85 °C within less than 60 minutes (Fig. 3-2 A). This temperature as well as the temperature of the heat sink (about +40 °C) remained stable for more than 1300 minutes.

In comparison, the Peltier element reached a temperature of -55.3 °C after about two minutes. The temperature of the heat sink increased continuously and reached a

temperature of more than 80 °C after 13 min (Fig. 3-2 B). Since the cold side and the heat sink of the Peltier element are less than 14.1 mm apart, the area of the copper block had to be increased considerably to transfer the heat into the environment. To keep the temperature constant at the heat sink as well as the cold site of the Peltier element, we applied a water-cooled heat sink and installed the Peltier element in an Ar gas environment. This improved the performance of the Peltier element considerably. Nevertheless, for underwater applications, this would require an additional pump to circulate water from the outside into the pressure housing through the heat sink and back into the water column. This pump would entail additional energy requirements and result in considerable modifications of the pressure housing to avoid any risks of leaks.
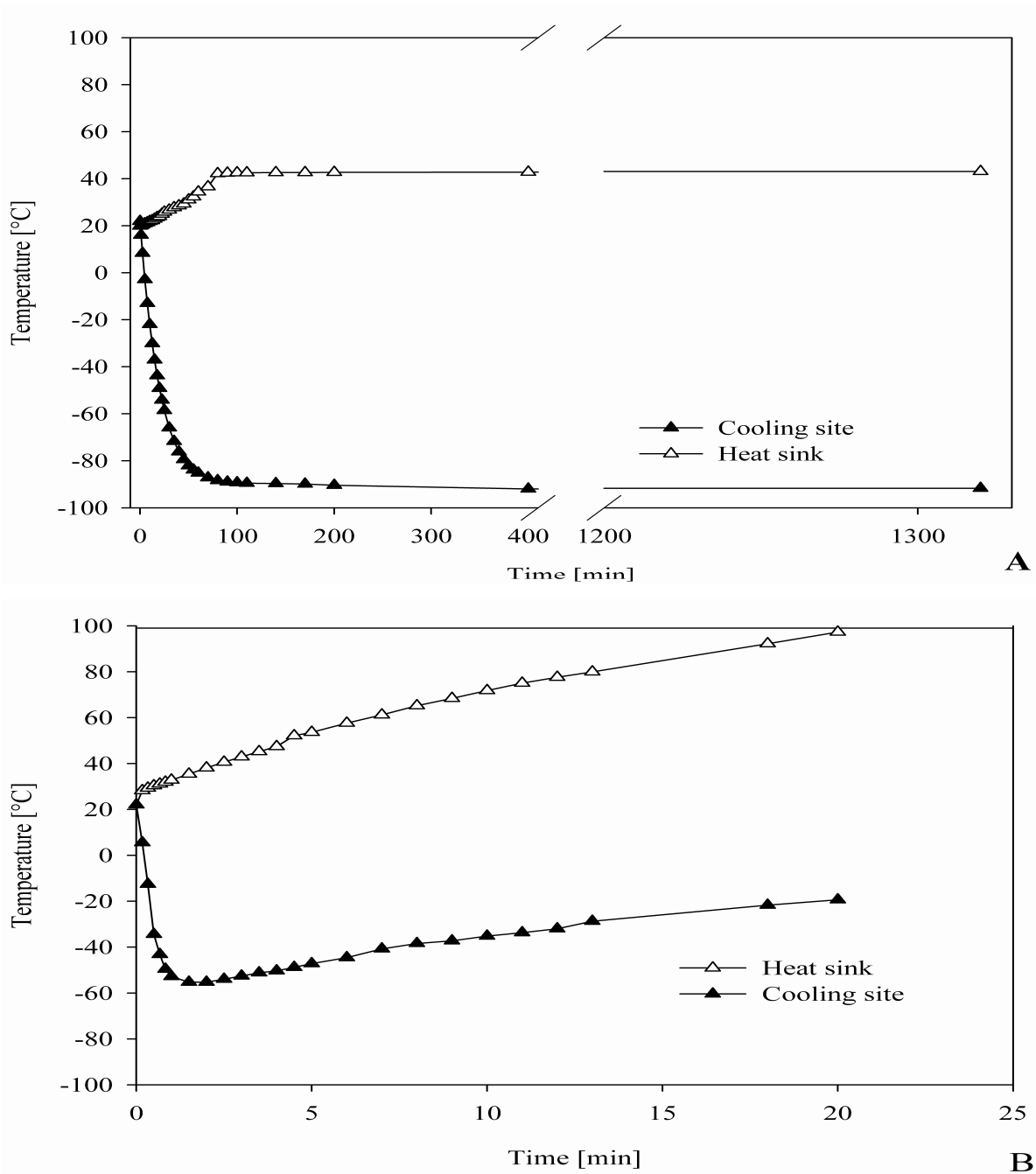
Fig. 3-2 *Comparison of the temperature measured versus time at the cooling site and heat sink of the Stirling cooler (A) and the Peltier element (B).*

To reach and keep the target temperature, the Peltier element required more than 80 W at 6.8 V. In contrast, the Stirling cooler required 6 W at 24 V to keep the cool finger at a temperature of -85 °C throughout. Based on these results, we decided to use the Stirling cooler within the CT-MIS.

3.4.2 Temporal development of the water vapour content within the vacuum line

We investigated the performance of the CT-MIS mounted in the pressure housing with respect to the reduction of the water vapour content in the vacuum section, the improvement of the signal detected by the gas analyzer, and the service life time. For this assessment, we connected the CT-MIS to the Inspectr200-200.

To investigate the development of the water vapour content versus time (Fig. 3-3), CH_4-free water was prepared by purging synthetic air through distillated water. The water vapour was measured by the mass spectrometer (intensities are displayed as ion current in ampere) at the m/z 18 with the highest relative abundance (also detectable at m/z 17 and m/z 16). Also, the absolute pressure (Torr) measured by the Pirani sensor and the temperature of the cryotrap are shown in figure 3.
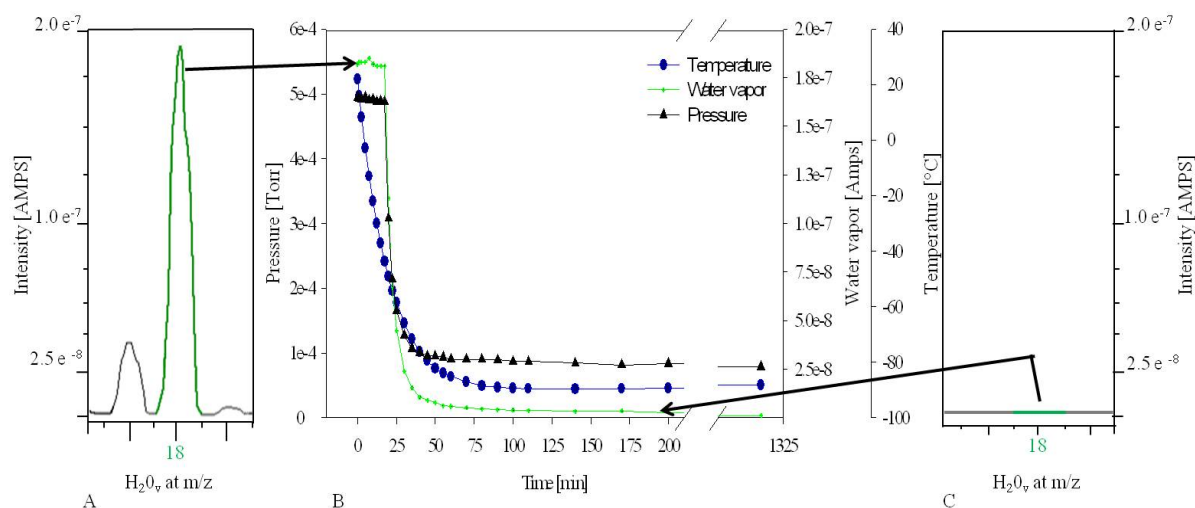

Fig. 3-3 *(A) Water vapour peak intensity at m/z 18 before the cooling. (B) Reduction of the internal pressure, water vapour intensities and temperature versus after the Stirling cooler was switched on. (C) Water vapour peak intensity at m/z 18 after a cooling time of 240 min. Comparing (A) and (C) results a signal reduction at m/z 18 of 96 %.*

Starting at an ambient temperature of 22 °C, the water vapour peak at m/z 18 having reached an intensity of ~ $1.8*10^{-7}$ Ampere (AMPS, Fig. 3-3 A). After 26 min, the cryotrap reached a temperature of -60°C, and a significant reduction of H_2O_v was observed (Fig. 3-3 B), which also caused a significant reduction of the absolute pressure in the vacuum section from $4.95*10^{-4}$Torr to $1.65*10^{-4}$ Torr. After one hour,

the target temperature of -85 °C was reached, the pressure is reduced to $0.902*10^{-4}$ Torr and about 96% of initial water vapour was trapped by the cryotrap. After 140 min, the absolute pressure was reduced by factor six to $0.842*10^{-4}$ Torr (Fig. 3-3 B). At this point, no significant peak was detected at m/z 18 (Fig. 3-3 C), which means that most of the H_2O_v (98 %) was trapped in the cryotrap. Due to this reduced pressure at the ion source, a higher electron emission current which would increase the ionization efficiency, and a higher voltage at the electron multiplier could be applied, which would improve the detection limit of all gases.

Compared to most cryotraps applied in laboratories, where e.g., U-shaped traps are used and the cooling section can be easily shifted, only a small section of the vacuum line was cooled down to trap H_2O_v in our underwater applications. Therefore, we investigated the impact of the deposition and formation of ice coatings within the capillary. For this purpose, we also used methane free water and measured the intensity at m/z ratios 40, 32, 28, 18 and 15 representatives for Ar, O_2, N_2, H_2O_v and CH_4 over several hours (Fig. 3-4 B). Here, special attention was paid to the change of background signal at m/z 15 (methane) and the signal stability of argon, oxygen and nitrogen. At the beginning of the cooling, interferences overlapped the background signal of methane at m/z 15 and a high signal/noise ratio was observed (Fig. 3-4 A). The interferences appeared due to a combination of the low mass "tail" of the very large m/z 16 peak arising from ionization of H_2O_v as well as from the ionization of O_2 (producing single charged atomic oxygen ^{16}O). Trapping the water vapour (Fig. 3-4 B) downgraded this interference, and the signal/noise ratio at m/z 15 is improved (Fig. 3-4 C). This effect, combined with a higher electron emission current, lowered the detection limit of the trace gas CH_4 from values of more than 100 nmol L^{-1} to 16nmol L^{-1} (Schlüter and Gentz 2008).

Considering the signal intensities observed for nitrogen, oxygen and argon over time suggested a linear signal reduction of 3.3% h^{-1} for ten hours (Fig. 3-4 B). Due to the contribution of O_2 at m/z 15, the same signal reduction was measured for methane. We assumed that this signal reduction was mainly due to the decreasing inner diameter of the capillary caused by the deposition of H_2O_v. This effect could be quantified and conveyed to the measured mass spectrometer intensities.
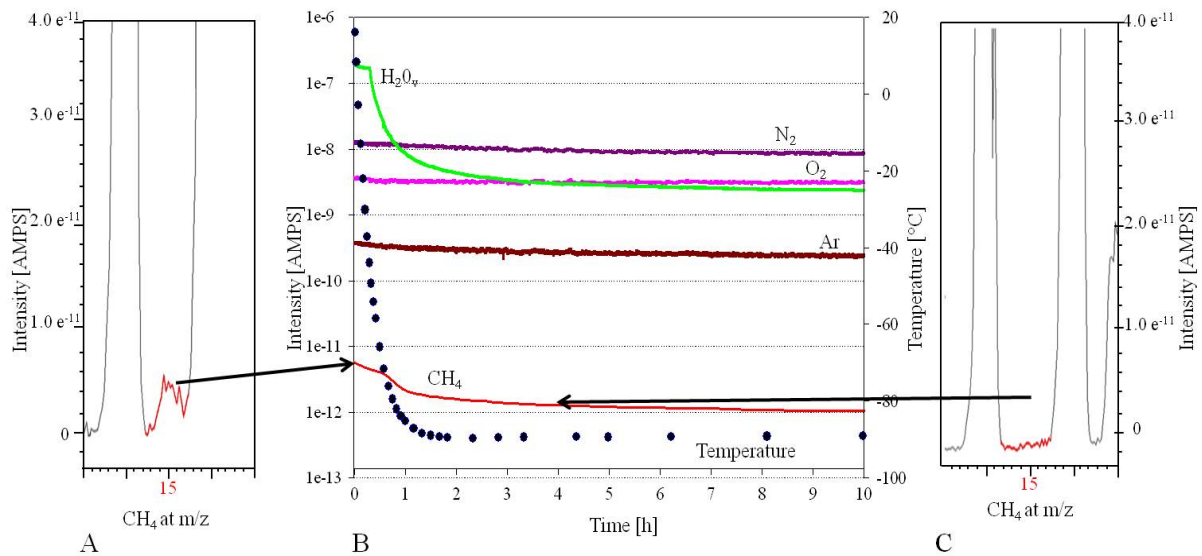
Fig. 3-4*. For the assessment of the peak stability of selected gases during the cooling by the CT-MIS methane free water was used. (A) Methane background signal at m/z 15 before cooling. (B) Ion current intensities versus time during the cooling process measured for methane free water at m/z rations of 28 (N2), 32 (O2), 40 (Ar), 18 (H2Ov) and 15 (CH4). (C) Methane background signal at m/z 15 after 240 min of cooling.*

For underwater applications, the system has to be started about 90 min prior to the deployment in order to ensure the drop down of H_2O_v. Based on our laboratory measurements as well as experience gained during our field assessments, the CT-MIS can be operated *in situ* for more than ten hours. After the maximum operating time, ice coating in the capillary of the cryotrap has to been removed by switching off the cooler, which causes the cool block to warm up and the ice coat to sublimate. The originating water vapour is removed by the turbo pump and roughing pump of the mass spectrometer. The entire maintenance procedure takes about one hour.

3.5   Applications

For field applications, we coupled the CT-MIS to the underwater mass spectrometer Inspectr 200-200. The gas analysis unit, as well as a benthic chamber system, an underwater peristaltic pump and the power supply (two *SeaBatteries^{Tm}*, SB24-40, 24 V, and 40 Ah) were mounted to a deployment frame (Fig. 3-5 A). We applied this system for investigating the distribution of CH_4 in the water column around gas seeps in the North Sea. To detect the release of gases from sediments in Gdansk Bay (Baltic Sea), a smaller frame consisting of the CT-MIS coupled to the mass spectrometer, the underwater pump and the power supply (one *SeaBatterie^{Tm}*, SB24-40, 24 V, 40 Ah) was used. The benthic chamber was placed manually into the sediment. During these *in situ* measurements, we monitored the water vapour content, the intensity of the gases CH_4, N_2, O_2, Ar and CO_2, the total energy consumption of the system, as well as the robustness of the CT-MIS.

3.5.1 In situ investigation of CH$_4$ in the water column around gas seeps (North Sea)

In the North Sea, ebullitions of gas bubbles from the seafloor have been observed along fracture zones where thermogenic gases or natural CO_2 are released, in regions where biogenic CH_4 is produced in surface sediments, as well as at gas releases of former wellheads (Clayton et al. 1997; Rehder et al., 1998; Schroot et al. 2005; McGinnis et al. 2011; Niemann et al. 2005; Von Deimling et al. 2011). During RV Heincke cruise HE337 in September/October 2010, we investigated hydrocarbon seeps associated with pockmark structures situated at a fracture zone in the Dutch sector of the North Sea (Schroot et al. 2005; Schroot and Schuttenhelm 2003a, 2003b).

Prior to the deployment, the seafloor around the pockmark area was mapped with a Kongsberg SIS multibeam system, and the Simrad EK 60 echo sounder was applied for the detection of gas flares in the water column (Fig. 3-5 B). The area of our detailed investigation had a size of 500 m x 400 m (Fig. 3-5 B). Within this area, the investigated pockmark, where an active release of gas bubbles was observed, had a diameter of less than 5 m.

For mapping the concentration field of dissolved CH_4, the CT-MIS coupled to the Inspectr200-200 was deployed in water depths of 10 m, 14 m, 24 m, and 34 m. When the system had reached the respective depth, the research vessel moved slowly around and across the site of gas seepage while gas concentrations were measured continuously every 1.8 s. One hour of measuring time was estimated for each water depth. The data was integrated into the Geo-Information-System ArcGIS 10 (ESRI™), and contour plots were computed by Kriging.

The *in situ* analysis provided very detailed information about the concentration field of CH_4 around gas flares (Fig. 3-5). Within the rather small sampling area of 280 m x 280 m (78400 m², Fig. 3-5 C), steep concentration gradients of more than 1200 nmol L^{-1} in less than 20 m were detected, and the methane concentrations varied from values of less than 16 nmol L^{-1} about 60 m adjacent to the pockmark to high concentrations of 1450 nmol L^{-1} within the gas flare.
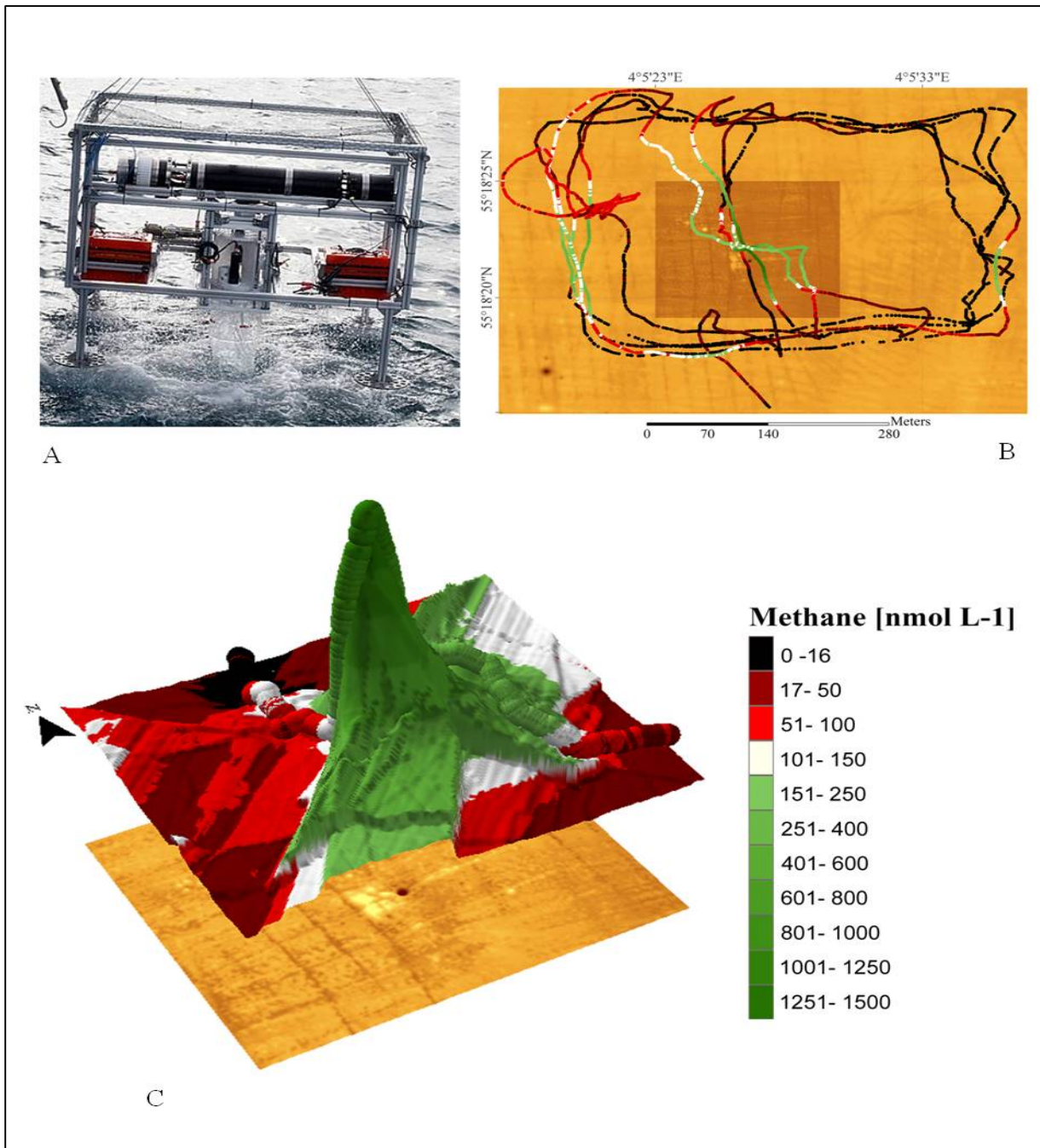
Fig. 3-5 *In situ methane measurements around a pockmark in the North Sea (A)*
Deployment frame were the CT-MIS is coupled to the underwater mass spectrometer.
(B) High resolution bathymetric map derived by a multibeam survey. The pockmark,
where methane is released from the seafloor, has a diameter of less than 5 m. (C)
Methane concentrations measured at 24 m water depth. Close to the pockmark, step
*gradients in the CH4 concentrations of more than 1430 nmol L-1 were observed.*

3.5.2 In situ measurement of gas fluxes across the sediment-water interface (Baltic Sea)

Several biogeochemical investigations used the flux of O_2 or nutrients through the sediment water interface to study the remineralization of organic matter or to quantify the rain rate of organic matter reaching the seafloor. The latter is investigated through the *in situ* measurement of O_2 by either applying benthic chamber systems or O_2 microprofiler, for example (Glud et al. 1994; Sauter et al. 2001).

Beside O_2 fluxes, only a rather limited number of investigations considered the flux of gases like CO_2, CH_4, DMS or N_2 through the sediment water interface (Felden et al. 2010; Lichtschlag et al. 2010; Niemann et al. 2005). For these purposes, benthic chamber systems are applied and water samples (typically 12 samples with a volume of 50 ml each) are collected within predefined time intervals by using a syringe sampler, for example. Fluxes are calculated based on the change of gas concentrations within the chamber over time. The limited number of samples and the sample volume restricts the detailed investigation of changes in concentration versus time as well as the number of gases, which can be analyzed.

Coupling the underwater gas analyzer system to a benthic chamber allows the continuous measurement of gas concentrations for gases like O_2, N_2, DMS and CH_4 over time, and thus allows the study of gas fluxes in coastal areas. In our application, the deployed cylindrical benthic chamber had an inner diameter of 290 mm and a height of 170 mm. It was manually placed into the sediment at a depth of 20 mm, and a stirrer prevented stratification inside the chamber. The entrapped bottom water was recirculated through the CT-MIS and back into the benthic chamber using an underwater peristaltic pump. During the measurements by the membrane inlet less than 1 % of the gases were extracted from the sampling water in the benthic chamber and the gas concentrations of Ar, O_2, CH_4 and CO_2 were measured every 1.8 s for more than 5.5 h.
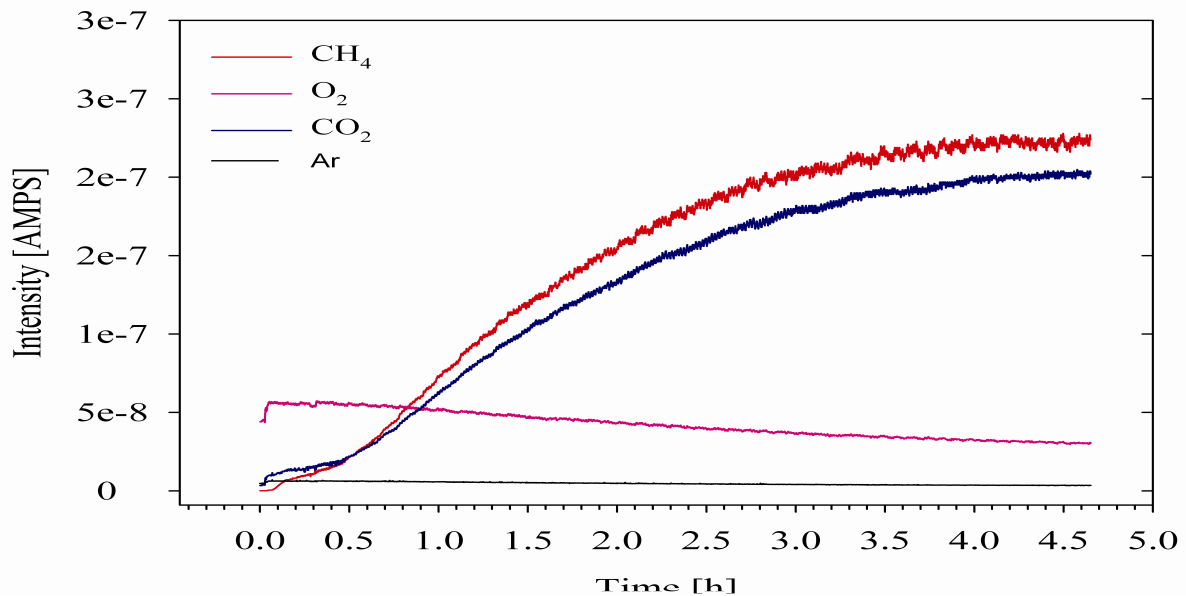
Fig. 3-6 *In situ benthic flux measurements of methane, carbon dioxide, oxygen and argon by the CTMIS coupled to the Inspectr200-200 in the Gdansk Bay (Baltic Sea).*

With this application, we investigate the gas fluxes across the sediment-water interface in the shallow water region of Gdansk Bay (Baltic Sea). In this area, advective transport of methane induced by submarine groundwater discharge is the main driver for high methane concentration in the bottom water (920 µmol L^{-1}). Benthic chamber measurements over a period of 5 hours discovered that CH_4 and CO_2 were enriched in the chamber, while the O_2 concentration decreased (Fig. 3-6). In this example, the methane concentration in the benthic chamber increased to about 238.8 µmolL^{-1} within 60 minutes and the calculated flux of methane amounted to 97400 $\pm$ 40 µmol m^2 d^{-1}, which is comparable to other regions with advective transport of methane occurrences (Lichtschlag et al. 2010; Boetius and Suess 2004).

Another type of benthic flux studies focuses on the diffusive methane fluxes from coastal sediments. In regions unaffected by advection, we can generally expect rather low methane fluxes and concentrations in the bottom water (Reeburgh and Heggie 1977). This is the case for most Baltic Sea regions (Gentz, unpublished data; Piker et al. 1998). In Himmerfjärden, a low-salinity estuarine system in the central Baltic Sea, online measurements by the CT-MIS coupled to the mass spectrometer show a

methane flux of 331.5 µmol m^2 d^{-1}. Without the CT-MIS, the enrichment of the methane concentration of 0.081 µmol L^{-1} within 60 min in the sampled water would be below the detection limit (> 100 nmol L^{-1}) of the gas analyzer. By using the CT-MIS, the enrichment of the methane concentration in the sampled water (0.081 µmol L^{-1} within 60 min) is five times higher than the lowered detection limit (16 nmol L^{-1}), which provides a statistical ensured flux measurement of methane also in regions were very low methane fluxes are expected.

3.6   Discussion

Membrane inlet systems have been widely used for the phase separation of gases from seawater or freshwater samples prior to gas analyses by mass spectrometers, IR sensors or solid state gas detectors. Even if various membrane materials with different characteristics in terms of water vapour permeation are applied, a significant amount of H_2O_v is introduced into the analyzer unit. This H_2O_v could downgrade the detection limits, induce water condensation within optical sections, or generates a drift of the signals. With respect to these issues, we consider the cryotrap membrane inlet system described and tested here to be an improvement with regard to the analysis of major- and trace gases.

For the online and onsite analysis of methane, applying the CT-MIS lowers the detection limit of the mass spectrometer significantly, which allows an improved computation of mass budgets and supports the localization of point sources like natural methane seeps or gas flares as well as anthropogenic gas leakages considerably. This can be evidenced by measurements obtained for a water depth of 24 m around a gas flare in the North Sea (Fig. 3-5 C). Considering the entire survey area of 78401 m², CH_4 concentrations of less 16 nmol L^{-1} were observed for an area of 2840 m² (3.6 %, black coded region in Fig. 3-5 C). For an area of 37827 m² (48.3 %, red coded region in Fig. 3-5 C), CH_4 concentrations were established between 16 and 100 nmol L^{-1}, whereas concentrations of more than 100 nmol L^{-1} were detected for an area of 37734 m² (48.1 %, white and green coded region in Fig. 3-5 C). Without applying the CT-MIS, CH_4 would be detected only within an area of

37734 m². Consequently, more survey time would be required to localize such point sources of methane release.

The present possibility to measure lower concentrations of down to 16 nmol L^{-1}, which are often observed in various aquatic environments, helps to guide the research vessel (in case of utilizing a towed system as shown in Fig. 3-5 A) or a Remotely Operated Vehicle (ROV) toward the direction of a gas discharge site. Furthermore, a considerable underestimation of mass budgets could be avoided if data from the extended concentration range (16 to 100 nmol L^{-1}) would be included to the calculations.

From an analytical point of view, the results demonstrate the benefits of the CT-MIS coupled to a gas analyzer. Considering the technical perspective, issues mentioned in the introduction have been tested in the field (e.g., robustness, energy consumption and service life time) as well as in the laboratory (e.g., temperature settings) and successfully meet the requirements for using the CT-MIS in harsh environments especially aboard research vessels as well as underwater applications. Therefore, the CT-MIS could be simply adapted to other membrane inlet gas analyzers (Boulart et al. 2010; Johnson et al. 2000) where the reduction of water vapour would improve the performance such as detection limits and lifetime of these analyzers significantly.

3.7   Acknowledgments

References: Chapter 3

Bell, R. J., R. T. Short, and R. H. Byrne. 2011. In situ determination of total dissolved inorganic carbon by underwater membrane introduction mass spectrometry. Limnol Oceanogr-Meth 9: 164-175 .

Bell, R. J., R. T. Short, F. H. W. Van Amerom, and R. H. Byrne. 2007. Calibration of an in situ membrane inlet mass spectrometer for measurements of dissolved gases and volatile organics in seawater. Environ Sci Technol 41: 8123-8128.

Boetius, A., and E. Suess. 2004. Hydrate Ridge: a natural laboratory for the study of microbial life fueled by methane from near-surface gas hydrates. Chem Geol 205: 291-310.

Boulart, C., D. P. Connelly, and M. C. Mowlem. 2010. Sensors and technologies for in situ dissolved methane measurements and their evaluation using Technology Readiness Levels. Trends in Analytical Chemistry 29: 186-195.

Boulart, C., M. C. Mowlem, D. P. Connelly, J. P. Dutasta, and C. R. German. 2008. A novel, low-cost, high performance dissolved methane sensor for aqueous environments. Opt Express 16: 12607-12617.

Butler, J. H., and J. W. Elkins. 1991. An Automated Technique for the Measurement of Dissolved N2o in Natural-Waters. Marine Chemistry 34: 47-61.

Camilli, R., B. Bingham, C. M. Reddy, R. K. Nelson, and A. N. Duryea. 2009. Method for rapid localization of seafloor petroleum contamination using concurrent mass spectrometry and acoustic positioning. Mar Pollut Bull 58: 1505-1513.

Camilli, R., and H. Hemond. 2002. NEREUS engineering concept for an underwater mass spectrometer. Trends in analytical chemistry, 23: 307-313.

Clayton, C. J., S. J. Hay, S. A. Baylis, and B. Dipper. 1997. Alteration of natural gas during leakage from a North Sea salt diapir field. Marine Geology 137: 69-80.

Damm, E., R. P. Kiene, J. Schwarz, E. Falck, and G. Dieckmann. 2008. Methane cycling in Arctic shelf water and its relationship with phytoplankton biomass and DMSP. Marine Chemistry 109: 45-59.

Desmarais, D. J. 1978. Variable-Temperature Cryogenic Trap for Separation of Gas-Mixtures. Anal Chem 50: 1405-1406.

Emerson, S., C. Stump, B. Johnson, and D. M. Karl. 2002. In situ determination of oxygen and nitrogen dynamics in the upper ocean. Deep-Sea Res Pt I 49: 941-952.

Felden, J., F. Wenzhofer, T. Feseker, and A. Boetius. 2010. Transport and consumption of oxygen and methane in different habitats of the Haakon Mosby Mud Volcano (HMMV). Limnology and Oceanography 55: 2366-2380.

Glud, R. N., J. K. Gundersen, N. P. Revsbech, and B. B. Jörgensen. 1994. Effects on the benthic diffusive boundary layer imposed by microelectrodes. American Society of Limnology and Oceanography.

Gueguen, C., and P. D. Tortell. 2008. High-resolution measurement of Southern Ocean CO2 and O-2/Ar by membrane inlet mass spectrometry. Marine Chemistry 108: 184-194.

Hovland, M., and A. G. Judd. 1988. Seabed Pockmarks and Seepages. Graham and Trotman, London,: 293pp.

Johnson, K. M., A. Kortzinger, L. Mintrop, J. C. Duinker, and D. W. R. Wallace. 1999. Coulometric total carbon dioxide analysis for marine studies: measurement and internal consistency of underway TCO2 concentrations. Marine Chemistry 67: 123-144.

Johnson, R. C., R. G. Cooks, T. M. Allen, M. E. Cisper, and P. H. Hemberger. 2000. Membrane introduction mass spectrometry: Trends and applications. Mass Spectrom Rev 19: 1-37.

Kampbell, D. H., J. T. Wilson, and S. A. Vandegrift. 1989. Dissolved-Oxygen and Methane in Water by a Gc Headspace Equilibration Technique. Int J Environ an Ch 36: 249-257.

Kolb, B., G. Zwick, and M. Auer. 1996. A water trap for static cryo-headspace gas chromatography. Hrc-J High Res Chrom 19: 37-42.

Leifer, I., and J. Boles. 2005a. Measurement of marine hydrocarbon seep flow through fractured rock and unconsolidated sediment. Mar Petrol Geol 22: 551-568.

---. 2005b. Turbine tent measurements of marine hydrocarbon seeps on subhourly timescales. J Geophys Res-Oceans 110: -.

Lichtschlag, A. and others 2010. Methane and sulfide fluxes in permanent anoxia: In situ studies at the Dvurechenskii mud volcano (Sorokin Trough, Black Sea). Geochim Cosmochim Ac 74: 5002-5018.

Lloyd, D.; Scott, R. I. Direct measurement of dissolved gases in microbiological systems using membrane inlet mass spectrometry. J. Microbiol. Methods. Vol. 1983, 1, 313–328.

Lloyd, D., K. Thomas, D. Price, B. Oneil, K. Oliver, and T. N. Williams. 1996. A membrane-inlet mass spectrometer miniprobe for the direct simultaneous measurement of multiple gas species with spatial resolution of 1 mm. Journal of Microbiological Methods 25: 145-151.

McCarthy, M. J., and W. S. Gardner. 2003. An application of membrane inlet mass spectrometry to measure denitrification in a recirculating mariculture system. Aquaculture 218: 341-355.

McGinnis, D. F., J. Greinert, Y. Artemov, S. E. Beaubien, and A. Wuest. 2006. Fate of rising methane bubbles in stratified waters: How much methane reaches the atmosphere? J Geophys Res-Oceans 111: -.

McGinnis, D. F. and others 2011. Discovery of a natural CO2 seep in the German North Sea: Implications for shallow dissolved gas and seep detection. Journal of geophysical research 116.

McMurtry, G. M., J. C. Wiltshire, and A. Bossuyt. 2005. A deep ocean mass spectrometer to monitor hydrocarbon seeps and pipelines. 24th International Conference on Offshore Mechanics and Arctic Engineering.

Melin, T., and R. Tautenbach. 2006. Membranverfahren, Grundlagen der Modul- und Anlagenauslegung Springer-Verlag

Mendes, M. A., R. S. Pimpim, T. Kotiaho, J. S. Barone, and M. N. Eberlin. 1996a. The construction of a membrane probe and its application towards the analysis of volatile organic compounds in water via the MIMS and MIMS/MS techniques. Quim Nova 19: 480-485.

Mendes, M. A., R. S. Pimpim, T. Kotiaho, and M. N. Eberlin. 1996b. A cryotrap membrane introduction mass spectrometry system for analysis of volatile organic compounds in water at the low parts-per-trillion level. Anal Chem 68: 3502-3506.

Milkov, A. V., 2000. Worldwide distribution of submarine mud volcanoes and associated gas hydrates. Marine Geology 167: 29-42.

Niemann, H. and others 2005. Methane emission and consumption at a North Sea gas seep (Tommeliten area). Biogeosciences 2: 335-351.

Peters, L. I., and D. Yakir. 2010. A rapid method for the sampling of atmospheric water vapour for isotopic analysis. Rapid Commun Mass Sp 24: 103-108.

Piker, L., R. Schmaljohann, and J. F. Imhoff. 1998. Dissimilatory sulfate reduction and methane production in Gotland Deep sediments (Baltic Sea) during a transition period from oxic to anoxic bottom water (1993-1996). Aquat Microb Ecol 14: 183-193.

Prien, R. D. 2007. The future of chemical in situ sensors. Marine Chemistry 107: 422-432.

Reeburgh, W. S., and D. T. Heggie. 1977. Microbial Methane Consumption Reactions and Their Effect on Methane Distributions in Freshwater and Marine Environments. Limnology and Oceanography 22: 1-9.

Rehder, G., R. S. Keir, E. Suess, and T. Pohlmann. 1998. The multiple sources and patterns of methane in North Sea waters. Aquat Geochem 4: 403-427.

Sahling, H. and others 2008. Pockmarks in the Northern Congo Fan area, SW Africa: Complex seafloor features shaped by fluid flow. Marine Geology 249: 206-225.

Saltzman, E. S., W. J. De Bruyn, M. J. Lawler, C. A. Marandino, and C. A. McCormick. 2009. A chemical ionization mass spectrometer for continuous underway shipboard analysis of dimethylsulfide in near-surface seawater. Ocean Sci 5: 537-546.

Sauter, E. J. and others 2006. Methane discharge from a deep-sea submarine mud volcano into the upper water column by gas hydrate-coated methane bubbles. Earth Planet Sc Lett 243: 354-365.

Sauter, E. J., M. Schlüter, and E. Suess. 2001. Organic carbon flux and remineralization in surface sediments from the northern North Atlantic derived from pore-water oxygen microprofiles. Deep Sea Research Part I: Oceanographic Research Papers 48: 529-553.

Schlüter, M., and T. Gentz. 2008. Application of Membrane Inlet Mass Spectrometry for Online and In Situ Analysis of Methane in Aquatic Environments. J Am Soc Mass Spectr 19: 1395-1402.

Schlüter, M., P. Linke, and E. Suess. 1998. Geochemistry of a sealed deep-sea borehole on the Cascadia Margin. Marine Geology 148: 9-20.

Schroot, B. M., G. T. Klaver, and R. T. E. Schuttenhelm. 2005. Surface and subsurface expressions of gas seepage to the seabed - examples from the Southern North Sea. Mar Petrol Geol 22: 499-515.

Schroot, B. M., and R. T. E. Schuttenhelm. 2003a. Expressions of shallow gas in the Netherlands North Sea. Neth J Geosci 82: 91-105.

---. 2003b. Shallow gas and gas seepage: expressions on seismic and other acoustic data from the Netherlands North Sea. J Geochem Explor 78-9: 305-309.

Short, R. T. and others 2001. Underwater mass spectrometers for in situ chemical analysis of the hydrosphere. J Am Soc Mass Spectr 12: 676-682.

Short, R. T., D. P. Fries, S. K. Toler, C. E. Lembke, and R. H. Byrne. 2006a. Development of an underwater mass spectrometry system for in-situ chemical analysis,. Meas. Sci. Technol. 10: 1195–1201.

Short, R. T., S. K. Toler, G. P. G. Kibelka, D. T. R. Roa, R. J. Bell, and R. H. Byrne. 2006b. Detection and quantification of chemical plumes using a portable underwater membrane introduction mass spectrometer. Trac-Trend Anal Chem 25: 637-646.

Simmonds, P. G. 1984. Analysis of Trace Halocarbons in Natural-Waters by Simplified Purge and Cryotrap Method. J Chromatogr 289: 117-127.

Suess, E. and others 1999. Gas hydrate destabilization: enhanced dewatering, benthic material turnover and large methane plumes at the Cascadia convergent margin. Earth Planet Sc Lett 170: 1-15.

Tortell, P. D. 2005. Dissolved gas measurements in oceanic waters made by membrane inlet mass spectrometry. Limnol Oceanogr-Meth 3: 24-37.

Tortell, P. D., and M. C. Long. 2009. Spatial and temporal variability of biogenic gases during the Southern Ocean spring bloom. Geophys Res Lett 36: -.

Van Der Laan-Luijkx, I. T., R. E. M. Neubert, S. Van Der Laan, and H. a. J. Meijer. 2010. Continuous measurements of atmospheric oxygen and carbon dioxide on a North Sea gas platform. Atmos Meas Tech 3: 113-125.

Von Deimling, J. S., G. Rehder, J. Greinert, D. F. McGinnnis, A. Boetius, and P. Linke. 2011. Quantification of seep-related methane gas emissions at Tommeliten, North Sea. Continental Shelf Research 31: 867-878.

Wankel, S. D. and others 2010. New constraints on methane fluxes and rates of anaerobic methane oxidation in a Gulf of Mexico brine pool via in situ mass spectrometry. Deep Sea Research Part II: Topical Studies in Oceanography 57: 2022-2029.

Wenner, P. G. and others 2004. Environmental chemical mapping using an underwater mass spectrometer. Trac-Trend Anal Chem 23: 288-295.

Wexler, A. 1977. Vapour-Pressure Formulation for Ice. J Res Nbs a Phys Ch 81: 5-20.

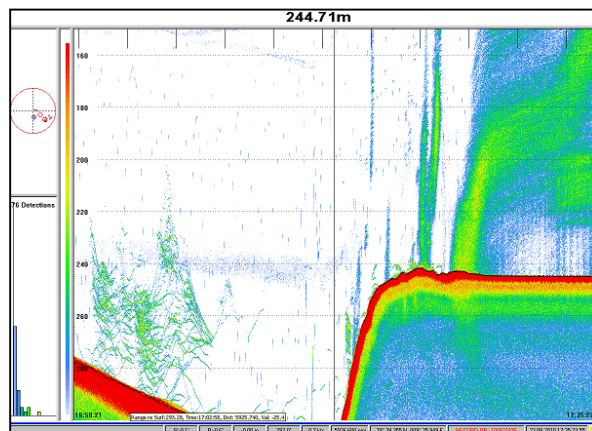# Chapter 4 – Manuscript II

~ Pathways of Methane ~

Manuscript submitted to "Continental Shelf Research"

Hydro acoustic image of gas bubbles in the water column

A water column study of methane around a seafloor gas ebullition area located at the West Spitsbergen margin.

Torben Gentz[1], Ellen Damm[1], Jens Schneider von Deimling[2], Susan Mau[1], Michael Schlüter[1]

[1]   Alfred Wegener Institute for Polar and Marine Research, Am Handelshafen 12, D-27570 Bremerhaven, Germany

[2]   Helmholtz Centre for Ocean Research (GEOMAR), Wischhofstr. 1-3, D-24148 Kiel, Germany

Keywords: Methane pathways; gas bubbles; underwater mass spectrometry; oxidation rates; West Spitsbergen continental margin, gas hydrate

4.1   Abstract

In the Arctic Seas, the West Spitsbergen continental margin is becoming a prominent methane seep area. In this area free gas formation and gas ebullition are currently under debate as a consequence of hydrate dissociation due to global warming. Recent studies revealed shallow gas accumulation and ebullition of methane into the water column at more than 250 sites in an area of 665 km². We conducted a detailed study of a subregion of this area, which covers an active gas ebullition area of 175 km^2 characterized by 10 gas flares reaching from the seafloor at ~ 245 m up to 50 m water depth to identify the fate of the released gas due to dissolution of methane from gas bubbles and subsequent mixing, transport and microbial oxidation.

The oceanographic data indicated a salinity-controlled pycnocline situated ~20 m above the seafloor. A high resolution sampling program at the pycnocline at the active gas ebullition flare area revealed, that the methane concentration gradient is strongly controlled by the pycnocline. While high methane concentrations of up to 524 nmol L^{-1} were measured below the pycnocline, low methane concentrations of less than 20 nmol L^{-1} were observed in the water column above. Variations in the $\delta^{13}C_{CH4}$ values point to a ^{13}C depleted methane source (~-60 ‰ VPDB) being mainly mixed with a background values of the ambient water (~-37.5 VPDB). A gas bubble dissolution model indicates that ~80 % of the methane released from gas bubbles into the ambient water takes place below the pycnocline. This dissolved methane will be laterally transported with the current northwards to greater depth and most likely microbial oxidized in between 50 – 100 days, since microbial CH$_4$ oxidation rates of 0.78 nmol d^{-1} were measured. Above the pycnocline, methane concentrations decrease to local background concentration of 10 nmol L^{-1}.

Our results suggest that the methane dissolved from gas bubbles is efficiently trapped below the pycnocline and, thus, limits the methane concentration in surface water and the air-sea exchange during summer stratification. During winter the lateral stratification breaks down and fractions of the bottom water enriched in methane may be vertically mixed and thus be potentially an additional source for atmospheric methane.

4.2   Introduction

Atmospheric methane (CH_4) is the most abundant organic compound in the atmosphere and is influencing the global climate. This greenhouse gas has a global warming potential, which is 20 - 40 times higher than carbon dioxide (CO_2) on a 100 year timescale, and the emissions constitute the second largest contribution to historical warming after CO_2 (Shindell et al. 2009). Present estimations, compiled in the IPCC report (2007), reveal an emission of 503 to 610 Tg CH_4 yr^{-1} entering the atmosphere. Geological sources, such as micro seepages, geothermal seeps, mud volcanoes or pockmarks have a emission potential of 40 to 60 Tg CH_4 yr^{-1} (Etiope 2004; Etiope and Klusman 2002; Kvenvolden and Rogers 2005). This includes the emission from seabed methane release in marine environments (Kvenvolden and Rogers 2005) and occur worldwide on continental margins, estuaries, and river deltas (Judd and Hovland 2007). Prominent locations are the Håkon Mosby Mud Volcano (Felden et al. 2010; Jerosch et al. 2007; Sauter et al. 2006), the Tommeliten field in the North Sea (Hovland and Sommerville 1985), the Santa Barbara Basin (Fischer 1978; Leifer and Clark 2002), the Black Sea (Limonov et al. 1997) as well as the West Spitsbergen continental margin (Hustoft et al. 2009; Knies et al. 2004; Mienert et al. 2005; Westbrook et al. 2008). The emission of CH_4 from marine seeps to the upper water column is estimated to be about 30 Tg CH_4 yr^{-1}, but only 10 Tg CH_4 yr^{-1} might reach the atmosphere (Kvenvolden and Rogers 2005). The remainder is dissolved and microbial oxidized to CO_2 in the water column (Kvenvolden and Rogers 2005). However, in shallow shelf areas like the North Sea, the release of CH_4 from the seafloor has a greater potential to enter the atmosphere (McGinnis et al. 2006) especially during the well mixed winter season (Schneider Von Deimling et al. 2011).

Due to ocean warming, increasing bottom water temperature could result in sub-sea thawing of permafrost (Shakhova et al. 2010) and destabilization of gas hydrates (Jung and Vogt 2004; Mienert et al. 2005) especially in the Nordic Seas and the Arctic. As a result, Buffett and Archer (2004) estimated an additional release of CH_4 up to tens of Tg yr^{-1} into the water column causing potentially ocean acidification (Biastoch et al. 2011). One of these affected areas could be the in this study investigated West Spitsbergen continental margin (Fig. 1). Previous

investigations in this area (e.g., Westbrook et al. 2009) showed a significant release of gas bubbles at more than 250 sites in a water depth between 150 to 400 m mostly aligned along a morphology lineation along the seafloor. The release of gas bubbles was detected within and outside the present upper limit of the gas hydrate stability zone (GHSZ), which was detected to be at ~ 400 m by geophysical studies (Hustoft et al. 2009; Knies et al. 2004; Rajan et al. 2012; Westbrook et al. 2009). This area is strongly affected by the northward-flowing West Spitsbergen current (Walczowski et al. 2005) which warmed up by 1 °C over the last 30 years (Schauer et al. 2004). According to Westbrook et al. (2009), the observed gas release might be a response to this recent warming and might have caused emission of about 0.027 Tg CH_4 yr^{-1}. However, it is questionable if the CH_4 reaches the atmosphere after gas bubble dissolution and microbial oxidation in the water column. Therefore, we conducted a study in an active gas ebullition area offshore Spitsbergen to investigate the potential pathways of gas seepage released methane. The mass transfer of CH_4 from rising gas bubbles into the ambient water column was calculated by a gas dissolution model (McGinnis et al. 2006) and the subsequent transport and microbial oxidation of the dissolved CH_4 were investigated by comparing hydroacoustic data with oceanographic and geochemical data.

4.3   Regional settings

4.3.1   Geology and seepage

The study area is located on the continental slope 22.5 km northwest off Prins Karls Forland (Spitsbergen) between Kongsfjorden and Isfjorden (Fig. 4-1). Previous investigations detected a prominent moraine system formed by glacial erosion or glaciotectonic detachment of larger blocks or sediments (Landvik et al. 2005). The investigated area with a mean water depth of 245 m is located close to the shelf edge with a steep slope located to the East and a less steep slope located to the North of the study area (Fig. 4-1). The gas hydrate stability zone tapers out at a sediment depth of about 400 m (Westbrook et al. 2009). The presence of shallow gas accumulations and pockmarks in this area was suggested by Rajan et al. (2012) who applied high-resolution mapping of the seafloor. The study area is the northernmost section of the region investigated by Rajan et al. (2012) and Westbrook et al. (2009), who both observed gas ebullitions into the water column by hydroacoustic. Highest methane concentration of 42 nmol L^{-1} was reported for a gas flare close to the seabed (~230 m water depth) according to Westbrook et al. (2009). Apart from the high methane concentrations close to the seafloor the observed background concentration of dissolved CH_4 in the mid and surface water is about 10 nmol L^{-1}. This is significantly exceeding the background values of most parts of the ocean, e.g. a background of 2.5 - 3.5 nmol L^{-1} was reported for Atlantic Ocean water (Rehder et al. 1999) and points to methane release from several inter-granular seepages or micro-seepages sites widely spread over the continental shelf (Damm et al. 2005).
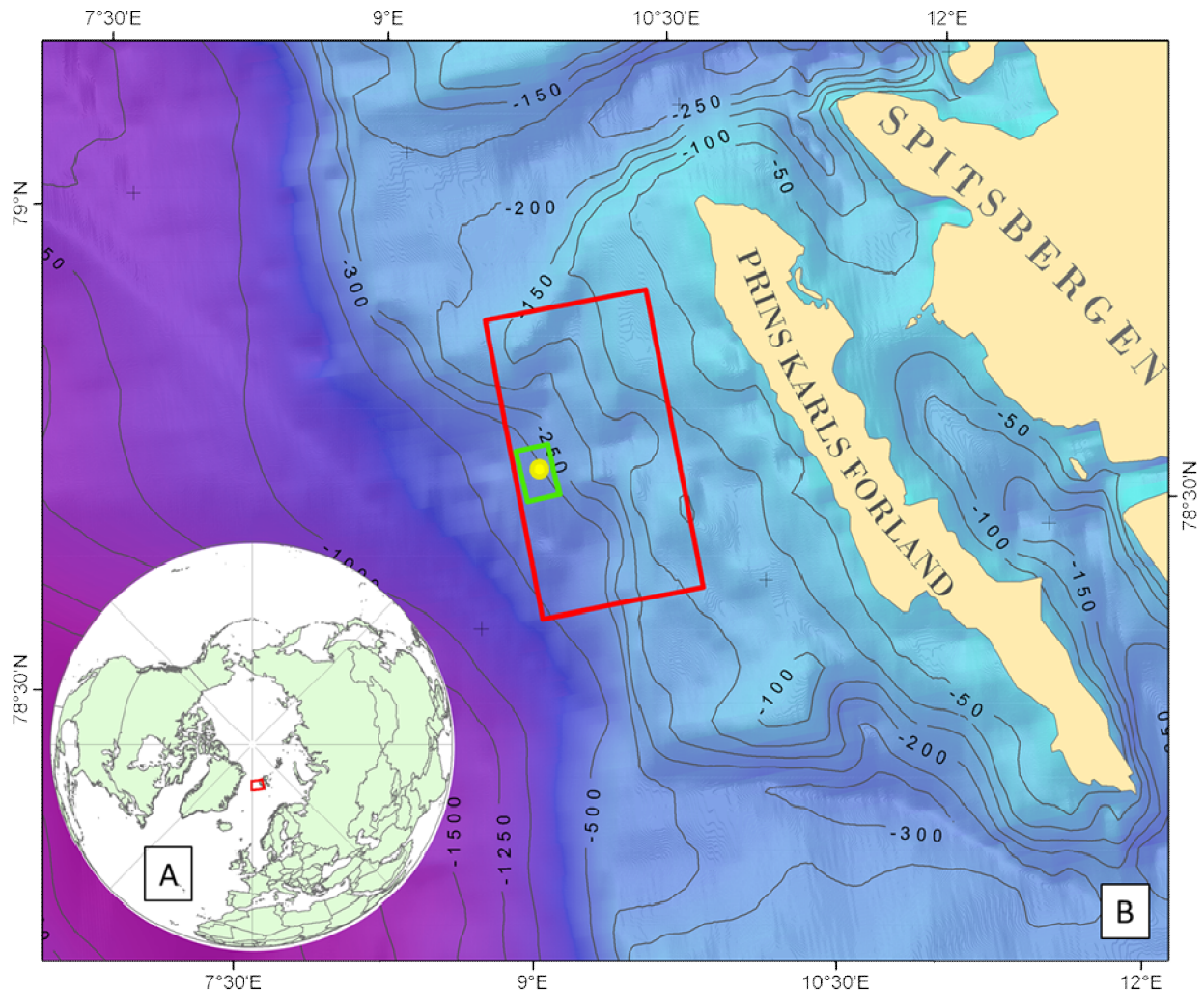
Fig. 4-1 *(A) Global view of the study area west of Spitsbergen. (B) The area investigated by Westbrook et al. (2009) is shown as red rectangle, the detailed study area (green rectangle) and the crossing point of the CTD-transects (yellow dot). Bathymetry is taken from the International Bathymetric Chart of the Arctic Ocean (IBCAO). The contour lines show the water depth and the light blue colored area indicates the shelf bank.*

4.3.2 Hydrography

The oceanographic conditions in the study area are controlled by the West Spitsbergen Current (WSC), which transports Atlantic Water (AW) northwards along the shelf edge (Schauer et al. 2004). The Coastal Current (CC) as an extension of the East Spitsbergen Current might introduce less saline water than the Atlantic Water into the study area (Saloranta and Svendsen 2001). In addition, seasonal events like formation and melting of sea ice or glaciers, river run off from Spitsbergen, fjord outflow, and special events like storm activities influence the hydrography of the study area causing strong seasonal variations. The WSC is stratified throughout the summer, but vigorous convection vertically mixes the AW within the WSC during winter (Cisewski et al. 2003).

4.4 Sampling and analytical procedures

During the expedition HE 333 in August 2010, the water column was investigated by hydroacoustic surveys, geochemical analysis of water samples, and by oceanographic data recording. In total, 175 km² (Fig. 4-1) were surveyed with a modern swath multibeam system (EM 710 by KONGSBERG MARITIM AS) and a split beam fish finder sonar (EK 60 by Simrad) to detect gas flares. In addition, 145 discrete water samples were collected using a CTD/Rosette sampler system at 22 stations and high resolution mapping of CH_4 was carried out with an underwater mass spectrometer (UWMS) in 10 m water depth.

4.4.1 CTD casts and water sampling

In total 13 vertical CTD-casts were deployed to collect water samples and oceanographic data by a system consisted of a rosette sampler hosting 12 10-L-Niskin bottles, a Seabird SBE 911 conductivity/temperature/depth (CTD) profiler, a Seabird SBE 43 oxygen (O_2) sensor, and a Benthos PSA-916 altimeter. A south - north (S – N) transect and an east - west (E – W) transect was sampled crossing at a point, where most gas flares was observed (Fig. 4-1). Additional 9 CTD casts were towed 2 m, 10 m, and 20 m ($\pm$ 1 m) above the seafloor to obtain more water samples and oceanographic data at larger depths. The system was adjusted via the

altimeter to a defined depth above the seafloor, then water samples were collected by drifting in the same water depth along transects. To flush the Rosette water sampler, the device was heaved and lowered before each sampling.

4.4.2 Water measurements

4.4.2.1 Dissolved CH_4 concentration

A novel underwater membrane inlet mass spectrometer (UWMS) was applied for on-board measurements of dissolved gases as well as high resolution mapping of CH_4 concentrations at 10 m water depth (Gentz and Schlüter 2012). The UWMS allows a high frequency sampling frequency (every 2 s) and thus high spatial coverage to detect increased methane concentrations. Furthermore, standard gas extraction and analysis by gas chromatography have been performed on board.

Water samples were taken immediately from the Niskin bottles and analysed by the UWMS to obtain simultaneous measurement of dissolved CH_4, nitrogen (N_2), O_2, and argon (Ar). The mass spectrometer (Bell et al. 2007; Short et al. 2001; Short et al. 1999) consists of a membrane inlet system, a quadrupole mass analyzer, a turbo pump and a new designed cryotrap (Gentz and Schlüter 2012) which lowers the detection limit of CH_4 from more than 100 nmol L^{-1} down to 16 nmol L^{-1} (Schlüter and Gentz 2008). During the operation of the UWMS, water is continuously pumped (3 ml min^{-1}) via a peristaltic pump (KC Denmark) to the heated (50 °C) membrane inlet system (MIS), where gas permeation takes place. The benefit of the instrument is that the samples can be measured directly without any sample preparation within less than 2 min. Due to the fast data availability of the dissolved methane concentrations, cruise and mission planning can be optimized on board in short time.

Discrete water samples collected by the Rosette water sampler were analysed for CH_4 concentrations, $\delta^{13}C_{CH4}$ values, and microbial CH_4 oxidation rates. CH_4 concentrations were analysed by mass spectrometer and gas chromatography (Kampbell et al. 1989). For gas chromatography measurements, the water samples were taken immediately from the Niskin bottles and transferred into 20 ml glass vials,

capped with a Teflon septum, and crimped gas tight. A head space of 5 ml volume was introduced by inserting Ar gas. After 5 hours of equilibration, the gas concentration in the head space was analysed by using the gas chromatograph TraceGC (Thermo Finnigan; Waltham, USA), equipped with a flame-ionization detector and a Porapak Q column. The GC oven was operated isothermally at 100 °C and the temperature at the sample inlet was 300 °C. Two standard gases (10 ppm and 1000 ppm) were used for the calibration. Based on the CH_4 concentration in the head space and the CH_4 concentration in the aqueous phase, which was calculated using the Bunsen coefficient (Wiesenburg and Guinasso 1979), the CH_4 concentration in the water sample was derived. The overall error of the method was about 5%.

A detailed cross validation of the methane concentrations derived by the GC and UWMS was done by Schlüter and Gentz (2008). The results reveal a close correlation of both analysing techniques which was verified in this study.

4.4.2.2 *Stable carbon isotopic ratio*

For measurements of the carbon isotopic ratio of CH_4, the water samples were taken immediately from the Niskin bottles. The dissolved gas was extracted from the water samples by vacuum-ultrasonic treatment (Schmitt et al. 1991). This method achieved 63% recovery of the total dissolved CH_4 (Lammers and Suess 1994). The $\delta\,^{13}C_{CH4}$ values were determined by a Delta XP plus Finnigan mass spectrometer. The extracted gas was purged and trapped with PreCon equipment (Finnigan) to pre-concentrate the sample. All isotopic ratios were given in a δ-notation relative to the Vienna Pee Dee Belemnite (VPDB) standard (Craig 1957). Depending on the CH_4 concentration, the reproducibility derived from duplicates was 0.5 - 1 ‰ VPDB.

4.4.2.3 CH_4 *oxidation rate*

At the station where the S - N and E - W transects cross (CTD 34, 78°39.14 N and 9°25.93 E, yellow dot in Fig. 4-1) additional water samples were taken for CH_4 oxidation rate measurements throughout the water column. All samples were collected in 100 ml crimp-top sample bottles, which were flushed with two volumes of water and filled completely to exclude bubbles. At each chosen water depth, two

samples were taken and at every other water depth, an additional control sample was collected. Control samples were treated by injecting saturated mercury chloride (HgCl$_2$) to stop metabolic processes before tracer injection. 50 µL of [^{3}H]-CH$_4$ (ARC Inc., 0.37 – 0.74 TBq mmol^{-1}) was injected in each sample as described in Valentine et al. (2001) raising the ambient CH$_4$ concentrations by 1 – 2 nmol L^{-1}. The samples were subsequently shaken for ~10 min on an orbital shaker and incubated in the dark at 2 °C. Incubations were stopped after 3 days, a 1 mL aliquot of each sample was taken and mixed with 5 ml Ultima Gold scintillation cocktail for analysis in a liquid scintillation counter (Single Sample LSC, Betascout Hidex) on board to determine the total radioactivity injected. Then, the sample was sparged for ≥ 30 min with N$_2$ gas to remove remaining [^{3}H]-CH$_4$. Samples were capped again and stored at 4 °C until further analysis. The residual radioactivity of [^{3}H]-H$_2$O was measured in the laboratory (Packard Tri-Carb LSC). All measurements were corrected for quench effects and for differences associated with the different counters used. From the corrected value, the amount of ^{3}H that remained in the water in control experiments (0.2 $\pm$ 0.1 %) was subtracted. 90% of biological replicate samples differed by < 30%. CH$_4$ oxidation rates (r_{OX}) were calculated assuming first order kinetics as described in Valentine et al. (2001).

$$r_{OX} = k' [CH_4] \qquad (1)$$

where k' is the effective first order rate constant calculated as the fraction of labeled CH$_4$ oxidized per unit time and [CH$_4$] is the ambient CH$_4$ concentration.

4.4.3 Hydroacoustic data acquisition

An EM 710 multibeam echo sounder (70-100 kHz) from KONGSBERG MARITIM AS was applied to acquire the bathymetry in high resolution (1 x 2 °). Surveys were run with a maximum swath angle of 130° and a maximum ping rate of 30 Hz at 4 knots ship speed. A fish finder sonar system (Simrad EK60) operated at 38 kHz was used to detect and map the horizontal and vertical distribution of gas flares in the water column. For unambiguous identifications of gas vents the protocol suggested in Judd et al. (1997) was applied.

4.4.4 Bubble gas exchange modelling

The gas bubble dissolution model by McGinnis et al. (2006) optimized by McGinnis (personal communication) for the regional settings was applied to estimate the maximum height of ascending bubbles and the transfer of released methane from the gas bubble into the water column. Model simulations were compared to the acoustic images of gas flares and the discrete dissolved CH_4 concentrations of water samples collected using CTD-casts.

4.5 Results

4.5.1 Flare imaging

The flare imaging was conducted to locate active gas bubble ebullition sites in the study area, thus, supporting the geochemical sampling of CH_4 anomalies in the water column in close vicinity to the seeps.

At least 4 transects show acoustic evidence for gas release in the study area (Fig. 4-2 A). In S – N direction, 10 gas flares were observed in water depths of 242 – 258 m along a distance of 11.5 km (Fig. 4-2 B, table 1). All three transects in E - W direction (Fig. 4-2 A) confirms that most of the gas flares are lined up in S – N direction. The flare backscatter intensities peak around 50 m rise height and decay above. This indicates the minimum measured rise height was 50 m and the maximum measured rise height was up to 200 m (Fig. 4-2 B). These observations of the gas flare locations as well as the maximum rise heights match with the observations by Westbrook et al. (2009). Even though the majority of the flares presented in Fig. 4-2 only rise until 150 m water depth, the bulk bubble rise height might be even higher considering beam geometry and sampling bias suggested in Schneider von Deimling et al. (2011).

From the tilt of the plume in the S - N transect together with an estimated bulk bubble rise velocity of 0.08 - 0.25 m s^{-1} we estimated a water mass current of 0.3 to 0.5 m s^{-1} in northerly direction resulting in a residence time of the bottom water at the S – N transect between 0.27 - 0.44 d.
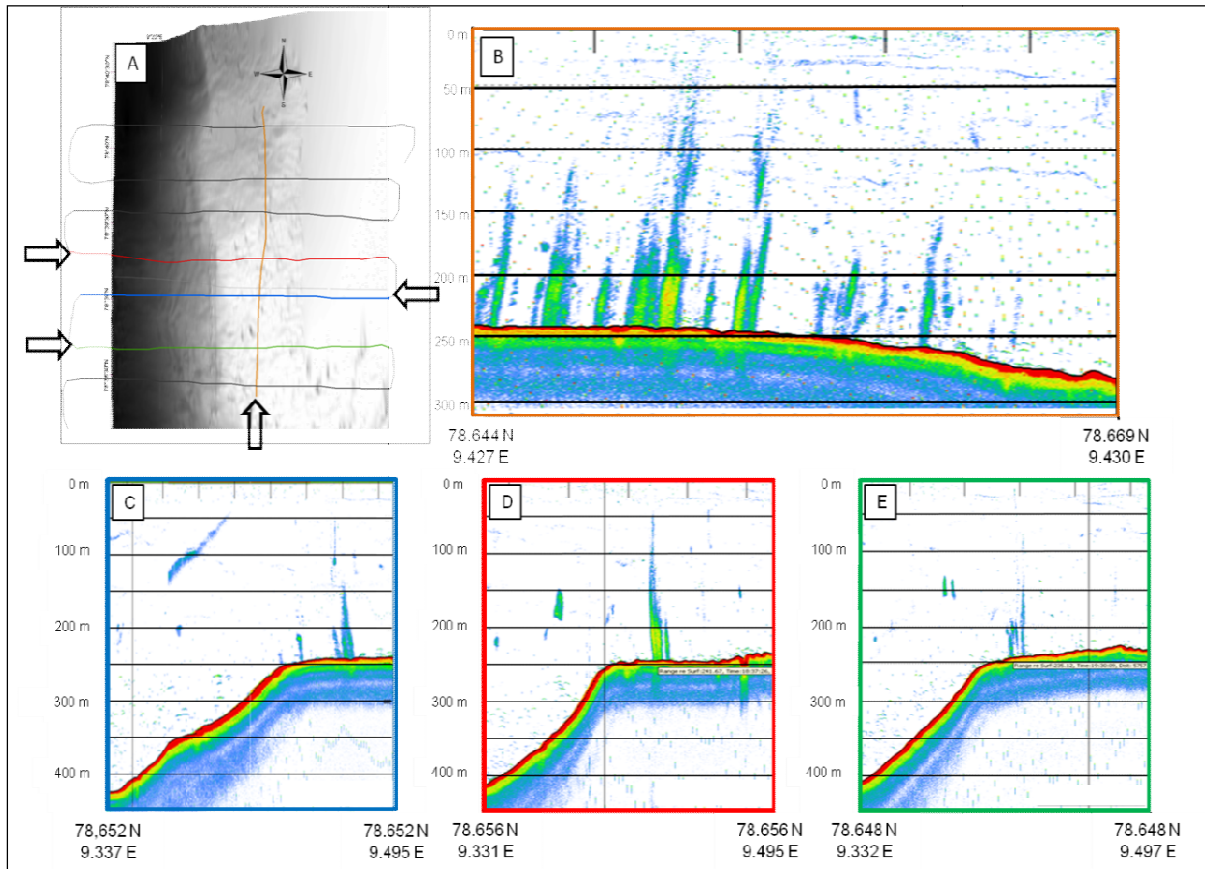
Fig. 4-2 *(A) Transect lines of the flare imaging surveys in the study area shown in Fig. 4-1 (green rectangle). Start point and direction of each transect is indicated by arrows. (B) Flare images of the gas flare transect 1 in S – N direction (orange line in A) and transects in E – W direction (C, D and E).*

Depth [m]	Latitude [DD]	Longitude [DD]
258	78.661 N	9.437 E
248	78.657 N	9.434 E
246	78.654 N	9.432 E
243	78.654 N	9.433 E
242	78.653 N	9.433 E
242	78.651 N	9.432 E
243	78.650 N	9.431 E
242	78.649 N	9.431 E
242	78.647 N	9.432 E
249	78.645 N	9.432 E

Table 4-1 *Location and water depth of the observed flares with an estimated error of ± 0.003 N and ± 0.01 E*

4.5.2 Water masses in the study area

The CTD data of 13 vertical profiles and 9 horizontal transects collected on two consecutive days in August 2010 illustrate the oceanographic conditions in the study area during the survey (Fig. 4-3). The water mass classification described by Slubowska-Wodengen et al. (2007) was applied to identify 3 distinct layers. A surface layer (0 – 40 m) herein later on referred to as Layer I consisted of fresh Polar Water (PW, Salinity (S) < 34.4). Layer II below (40 - 225 m) displays a mixture of subsurface, dense shelf water (ASW, 34.4 ≤ S ≤ 34.9), Lower Arctic Intermediate Water (LAIW, S> 34.1, T> 3 °C), and shallow Atlantic Water (AWs, S> 34.90, T> 3.6 °C).
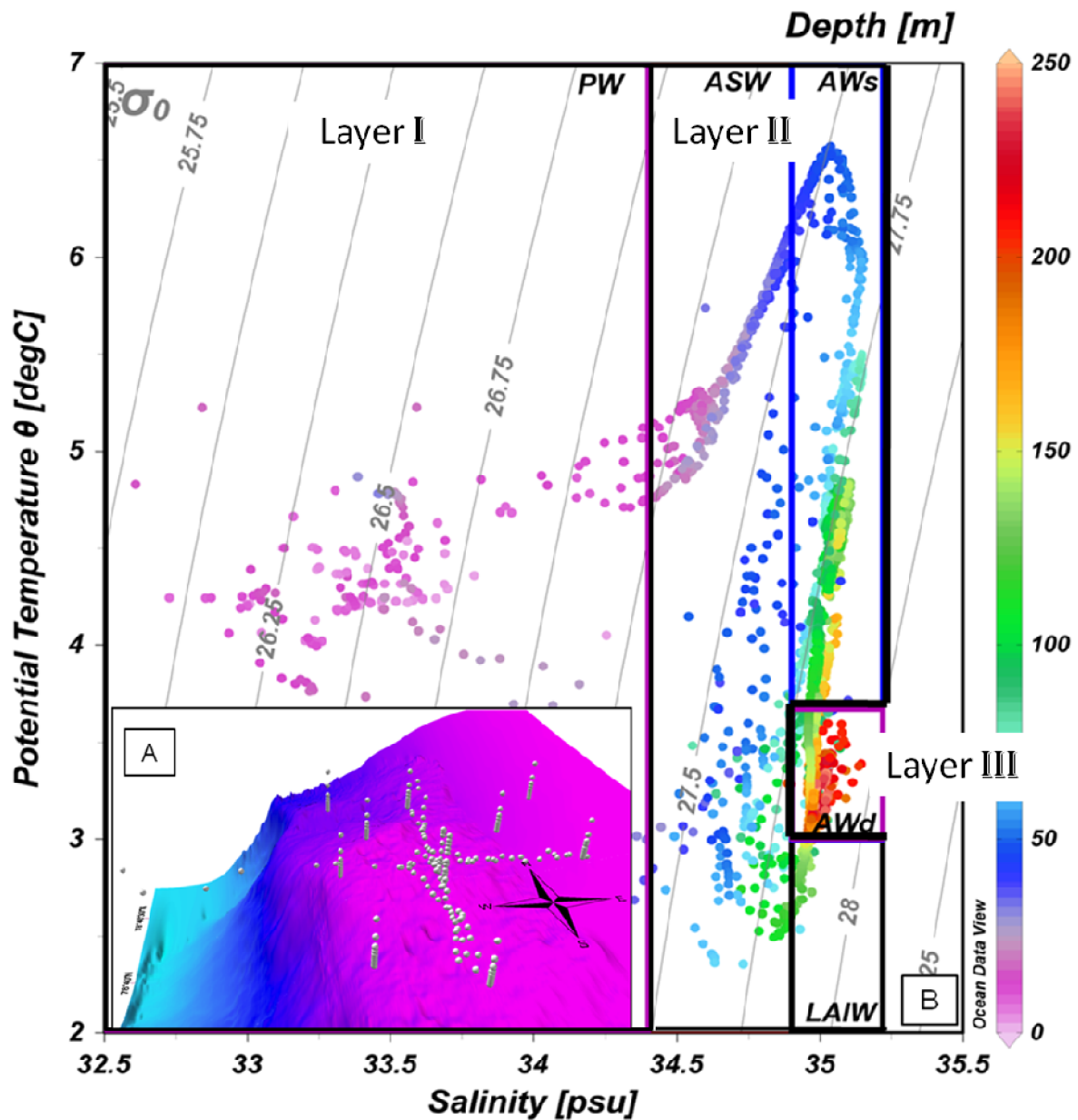
Fig. 4-3 *(A) 3D view of the bathymetry showing vertical and horizontal CTD sampling positions at the shelf bank close to the shelf edge. (B) Potential temperature vs. salinity (T / S) plot based on all CTD measurements collected in the study area for identification of water masses according to the classification of the water masses by Slubowska-Wodengen et al, (2007). The color of the dots indicates the water depths. Layer I (surface layer) consists of Polar water (PW). Layer II is a mixture of Arctic surface water (ASW), surface Atlantic Water (AWs), and lower Arctic Intermediate Water (LAIW). Layer III, the lowermost water mass, consists of deep Atlantic water (AWd). Graphic created by Ocean Data View (R.Schlitzer, Ocean Data View, 2011, http://odv.awi.de)*

Layer III (AWd, S> 34.90, T< 3.6 °C) comprises the water from the seafloor to 20 m above the seafloor (Figs. 4-4 and 4-5). This layer is characterized by a maximum salinity of 35.02, an internal potential density of 27.885 kg m^{-3}, a minimum temperature of 3.16 °C, and O$_2$ concentration of up to 6.60 ml L^{-1} (Figs. 4-4 and 4-5).
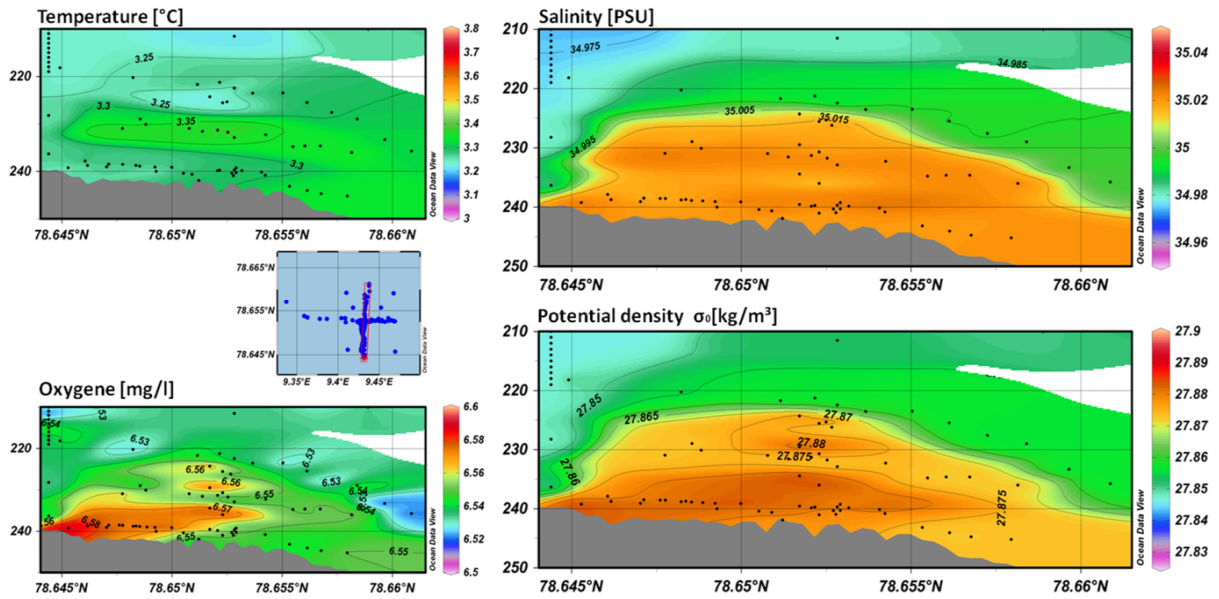
Fig. 4-4 *Oxygen concentrations, salinity, temperature, and the potential density indicate the extent of layer III, i.e., deeper Atlantic water (AWd), in S - N direction.*
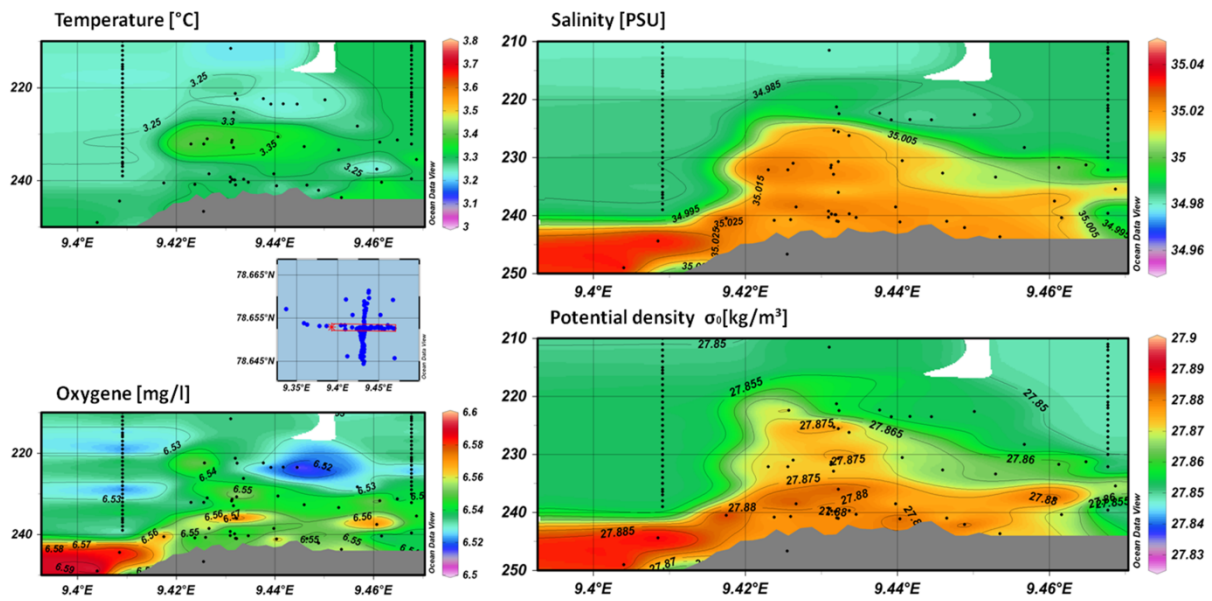
Fig. 4-5 *Oxygen concentrations, salinity, temperature, and the potential density indicate the extent of layer III, i.e., deeper Atlantic water, in E – W direction.*

4.5.3 CH$_4$ concentrations, microbial CH$_4$ oxidation rates, and stable carbon isotopic ratios

4.5.3.1 Vertical sampling of the water column

Water samples for CH$_4$ concentrations, δ^{13}C values, and CH$_4$ oxidation rate measurements were collected at station 34 (78°39.14 N and 9°25.93 E, Fig. 4-6) situated at the same location, where Westbrook et al. (2009) previously sampled water within a gas flare for methane analysis. The CH$_4$ concentration decreases from 48 nmol L^{-1} close to the seafloor to local background concentration of ~ 10 nmol L^{-1} (Damm et al. 2005) at 175 m water depth and remains at this concentration level throughout the water column. This methane concentration profile is in similarity to the observations by Westbook et al. (2009). The methane in Layer III is compared to the methane in Layer I and II depleted in ^{13}C (Fig. 4-6 A), nevertheless, the variation is in larger range (Fig. 4-6 A). Microbial CH$_4$ oxidation was enhanced in Layer III compared to the other layers above (Fig. 4-6 B). CH$_4$ oxidation rates of 0.77 ± 0.2 nmol L^{-1} d^{-1} corresponding to elevated CH$_4$ concentrations of 42.3 ± 2 nmol L^{-1} (Fig. 4-6 A) were measured in Layer III.

In Layer I and Layer II, CH_4 oxidation rates were < 0.22 nmol $L^{-1} d^{-1}$ corresponding to CH_4 concentrations of < 25.2 nmol L^{-1}. This results in a much faster turnover time of the methane in the deep Layer III if compared to much longer turnover times in Layer II and Layer I (Fig. 4-6 B).

In a water depth of 10 m, above the gas flares, the UWMS was deployed to measure dissolved CH_4 concentrations with high spatial resolution. These continuous measurements support, that CH_4 concentrations remain below the detection limit of 16 nmol L^{-1}. This underlines that no highly enhanced methane concentration due to the gas ebullition could be observed at the sea surface.
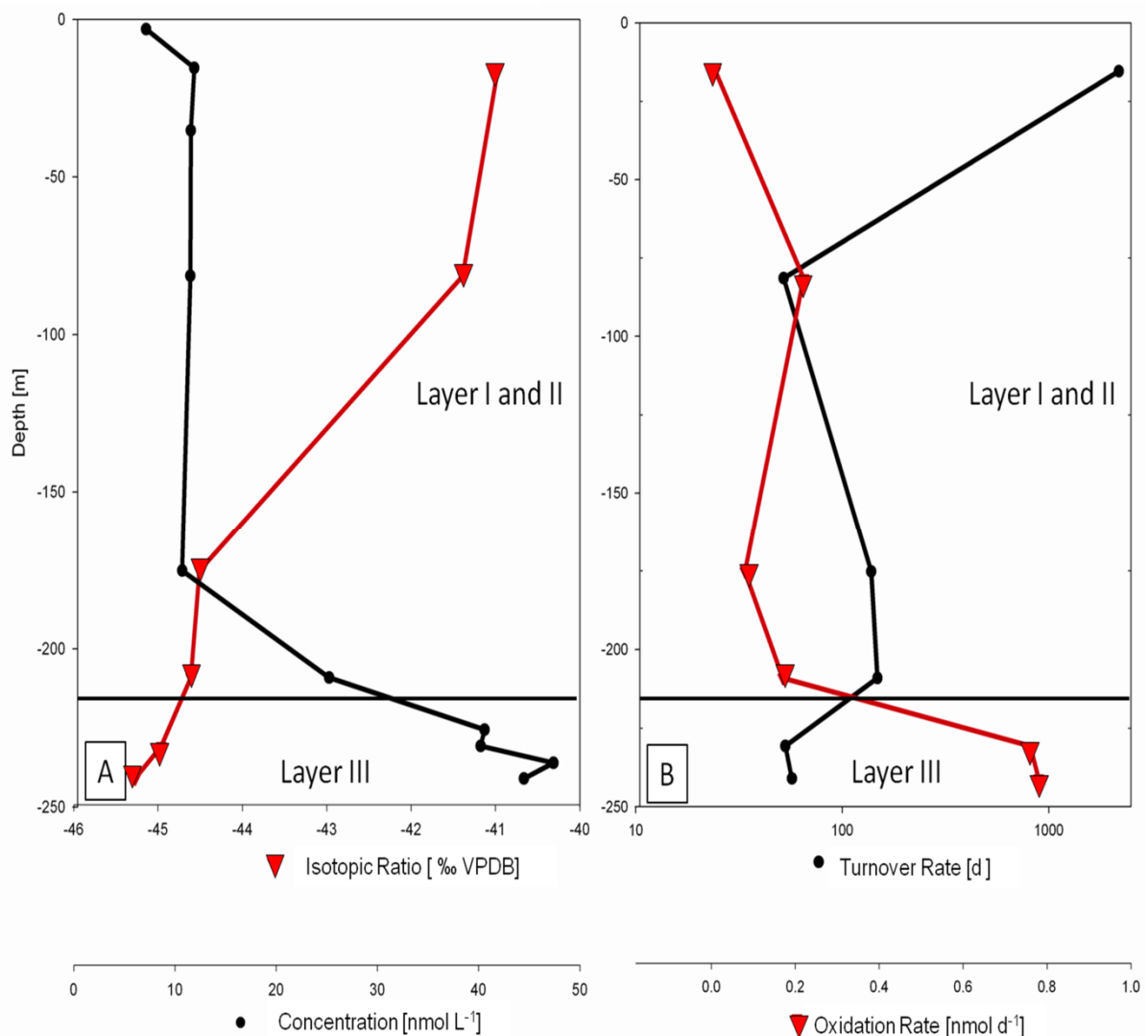
Fig. 4-6 *Profiles of station 34 (A) CH₄ concentration (black dots) and isotopic ratio (red triangles). (B) microbial CH₄ oxidation rates (red triangles) and turnover times (black dots).*

4.5.3.2 Detailed sampling of the dissolved CH_4 concentrations in the bottom water (Layer III) and stable carbon isotopic ratios.

Besides the vertical distribution of CH_4 in the water column, a spatially high resolution survey of dissolved CH_4 concentrations in 2 m, 10 m, 20 m above the seafloor was conducted crossing the gas flares shown in figure 4-2 C,D,E, and figure 4-7 A. The CH_4 concentrations range between 15 to 524 nmol L^{-1} (Fig. 4-7). Highest concentrations of 346 and 524 nmol L^{-1} were observed 2 m above the seafloor (green and blue dot in Fig. 4-7 B); the average CH_4 concentration at this depth is 70 nmol L^{-1}, which is the highest average in the entire water column. 10 m above the seafloor, the highest CH_4 concentration is 140 nmol L^{-1} while the average concentration decreased to 40 nmol L^{-1}. The CH_4 concentrations at 20 m above the seafloor are less than 30 nmol L^{-1} except of one sample with 50 nmol L^{-1}. The average concentration is 12 nmol L^{-1}, which is close to the background concentration of CH_4 in the study area (Fig. 4-7 D).
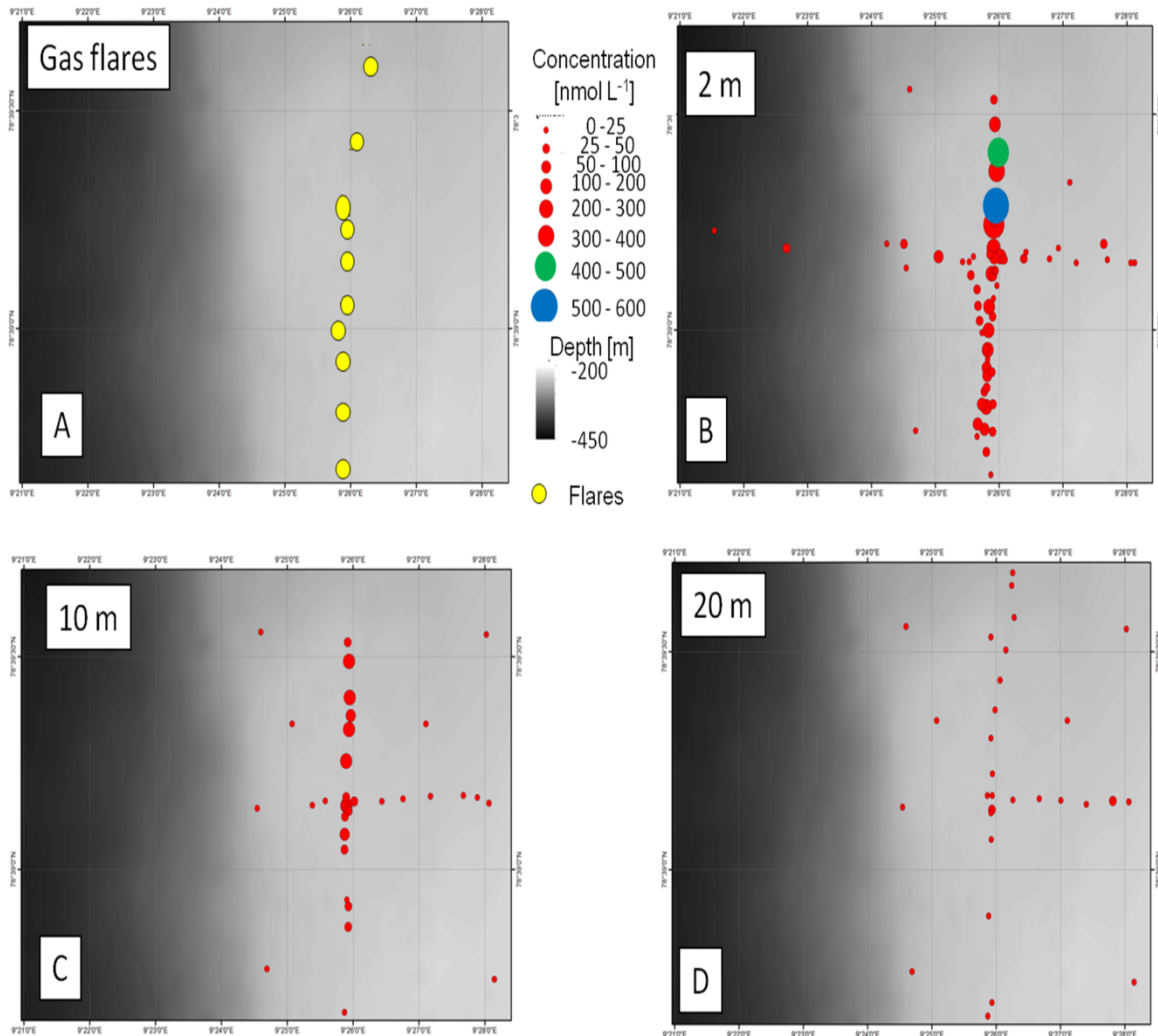
Fig. 4-7 *Positions of the observed gasflares (A) and* CH$_4$ *concentrations in 2 m (B), 10 m (C) and 20 m (D) above the seafloor.*

The $\delta^{13}C_{CH4}$ values of all samples of the entire water column range between -37.5 and -61.6 ‰ VPDB (Figs. 4-8 A, B). These results were compared to the measured inverse CH$_4$ concentration of the same samples (Fig. 4-8 A). This Keeling plot point out that increasing depletion in $\delta^{13}C$ is related to increasing CH$_4$ concentration (Fig. 4-8 A). Additionally, the $\delta^{13}C_{CH4}$ values in Layer II and Layer I range just in between -39.71 to -43.55 ‰ VPDB (red dots in Fig. 4-8 A), while the $\delta^{13}C_{CH4}$ values in Layer III varies in a wider range of -37.5 and -61.6 ‰ VPDB (black dots in Fig. 4-8 A). According to Faure (1986) the slopes of the linear regression curves (Fig. 4-8 A) indicate that the CH$_4$ in Layer III is a mixture of two end members, while in Layer II and I only one source could be identified.

In Layer III ^{13}C depleted C-CH$_4$ was found mainly along the S – N transect with $\delta^{13}C_{CH4}$ values from -61.6 to -52.6 ‰ VPDB (mean – 59.5 ‰ VPDB). In contrast, more ^{13}C enriched C-CH$_4$ was found along the E - W transect where the $\delta^{13}C_{CH4}$ values range between -37.5 and -52.9 ‰ VPDB (mean - 42.4 ‰ VPDB; Fig. 4-8 B). In S – N direction sampling was done in line with the gas flares and water current direction. This reveals in increasing CH$_4$ concentrations from 48 to 346 nmol L^{-1}. In E – W direction the CH$_4$ concentrations of 16.4 and 39.4 nmol L^{-1} and the $\delta^{13}C_{CH4}$ values near background values show less influence of the dissolved methane distribution at the gas flares if compared to the S – N direction. In addition to spatial variations, both, CH$_4$ concentration and $\delta^{13}C_{CH4}$ values, show temporal fluctuations. In the crossing zone of both transects sampling was carried out in Layer III three times within 24 hours (red circle in Fig. 4-8 B). Values shift from -38 ‰ VPDB and 139 nmol L^{-1} at the first measurement (21.08.2010 18:00) to -57 ‰ VPDB and 109 nmol L^{-1} at the second measurement (22.08.2010 12:32) to -53 ‰ VPDB and 64 nmol L^{-1} (22.08.2010 14:13) at the third measurement.
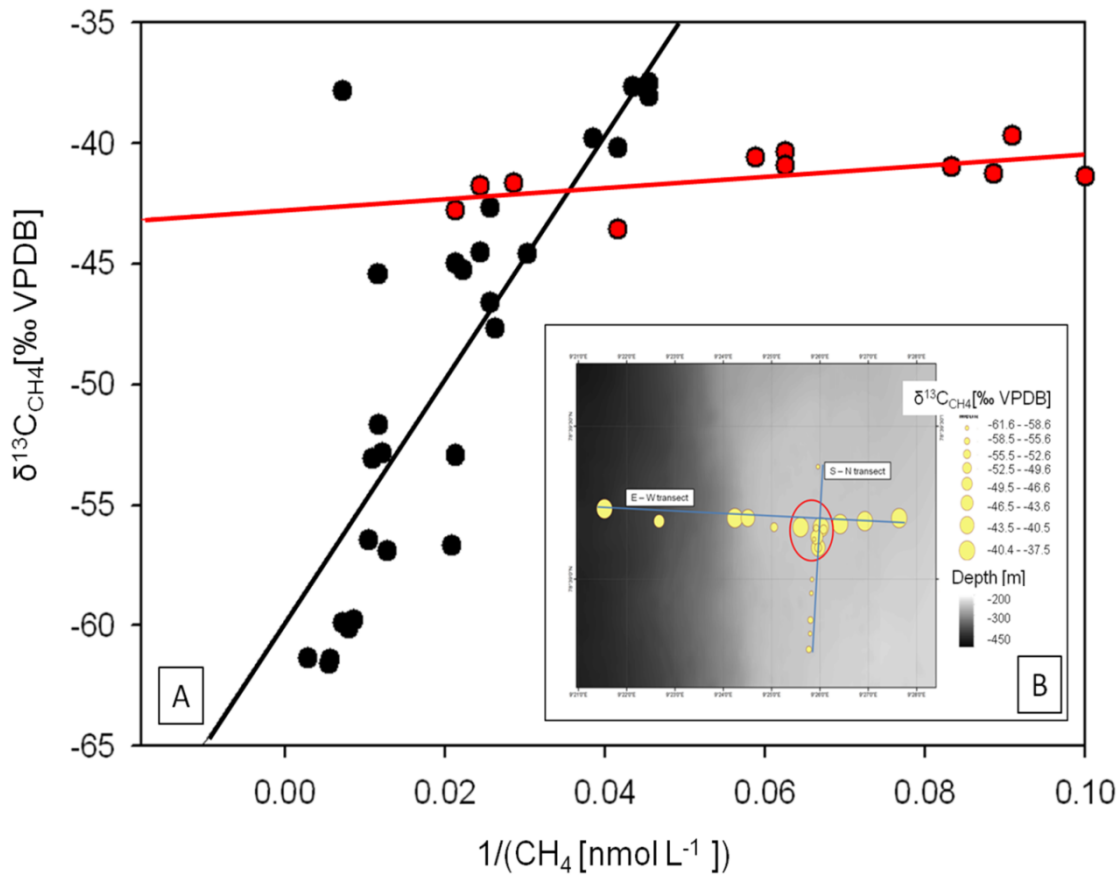
Fig. 4-8 *(A) Inverse CH$_4$ concentration versus $\delta^{13}C_{CH4}$ values (Keeling plot). Layer III is presented by black dots and Layer II and I by red dots. (B) Distribution of $\delta^{13}C_{CH4}$ 2 m above the seafloor including the transect lines. The red circle indicates the crossing zone of the two transects.*

4.6 **Discussion**

4.6.1 Gas ebullition as the source for dissolved CH$_4$ in the water column

In the study area we consider the release and the rise of methane loaded gas bubbles from the seafloor as the main source for dissolved CH$_4$ in the water column. Initially, CH$_4$ loaded gas bubbles are supersaturated compared to the ambient water composition, and consequently CH$_4$ is transported out of the bubble until the dynamical equilibrium is reached. Simultaneously, major gases like N$_2$, O$_2$ or CO$_2$ dissolved in the seawater are supersaturated with respect to the initial composition of the gas bubble, which causes a mass transfer of these gases into the gas bubble.

These processes were modeled by e.g., Leifer and Judd, (2002) and McGinnis et al., (2006) to estimate the decrease in bubble size and change of gas composition during the ascent of a CH_4 loaded gas bubble from the seabed towards the sea surface.

As an example we considered the relation between the dissolution of the gas bubbles and their change in gas composition during the rise derived by the use of graphical user interface SIBGui (Greinert and McGinnis 2009) with the highest observed gas bubble rise heights by hydroacoustic (Fig. 4-9 B). Input parameters of the SIBGui (optimized by Dan McGinnis for the study area) were initial bubble size, initial CH_4 fraction in the gas bubble as well as salinity, temperature, O_2, and CH_4 concentration in the water column. The parameters were derived from CTD cast 34 which is located next to a gas flare in the study area and we assumed that the initial gas bubbles purely consist of CH_4.
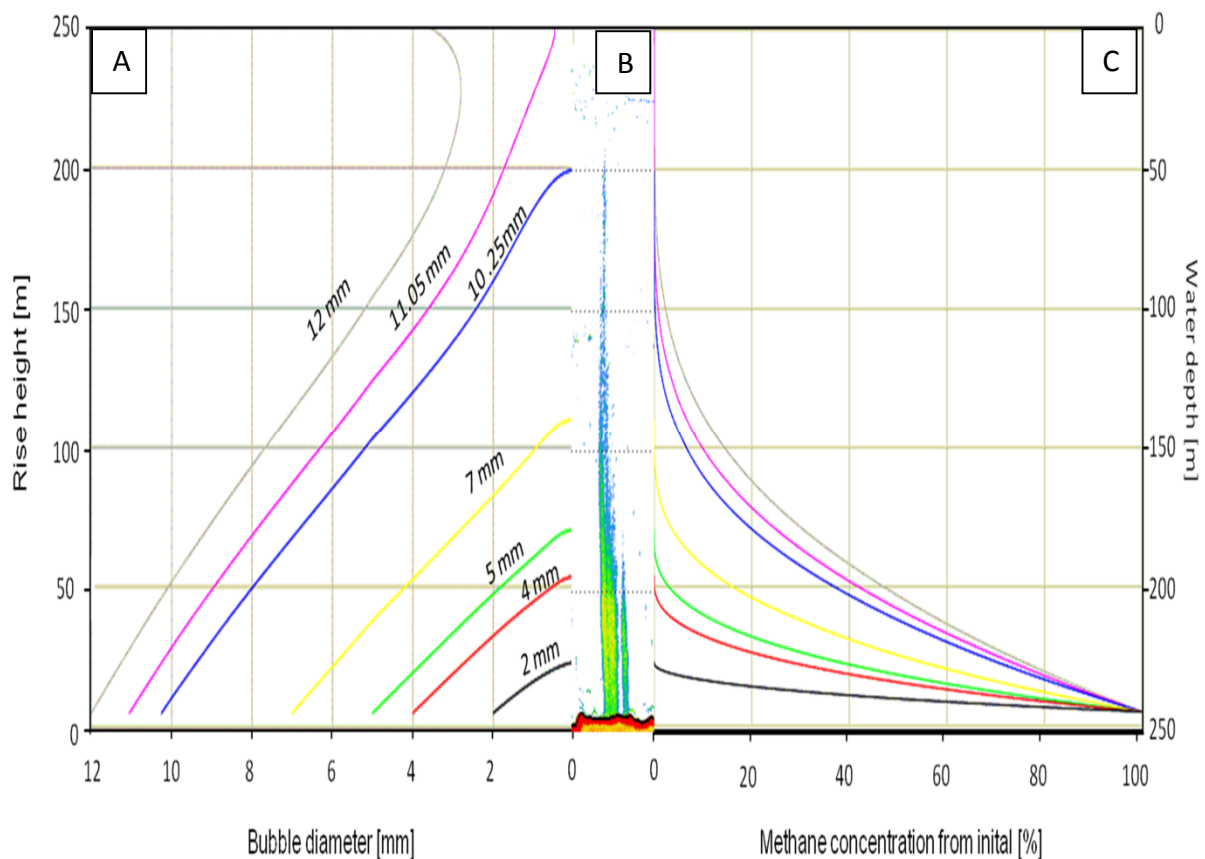
Fig. 4-9 *Decrease of the bubble diameter during the ascend from the seafloor for initial bubbles sizes of 2 mm to 12 mm (A) compared with the hydroacoustic image of the highest detected gas flare (B). Decrease of the initial CH_4 concentration in the bubbles during their rise in the water column (C).*

The calculated initial bubble diameter to reach the water surface would be larger than 11.05 mm. Considering the maximum acoustically derived rise height of 200 m in the water column (Fig. 4-9 B) an initial bubble diameter of at least 10.25 mm (Fig. 4-9 A) would be required. For this case, 99.99% of the methane in the gas bubble would be dissolved below 150 m. This suggests that no CH_4 could be transferred directly into the atmosphere via bubble transport in the study area. In the study area, a 5 mm bubble would rise up 69.5 m (Fig. 4-9 A) which is in order to the observed flare backscatter intensities of the gas flares. Nevertheless, the dissolution of the CH_4 takes place so quickly that, after rise of 20 m, only ~20 % of the initial CH_4 is left in the bubble (Fig. 4-9 A).

Given the vertical dissolved CH_4 concentrations distribution which strongly correlates with the pycnocline (Fig. 10) we suggest that the elevated methane concentrations in the deep water derive from dissolving gas bubbles smaller than 5 mm. Therefore, we assume that ~80 % of the seabed released CH_4 via gas bubble is dissolved below the pycnocline in Layer III. Nevertheless, the impact of dissolved fluid flow and/or diffusive methane source strength remains to be investigated.

4.6.2 Pathways and origin of CH_4 in the water column

Flare imaging and model results indicate that hardly any CH_4 reaches the atmosphere via the transport of gas bubbles. Hence, the majority of the CH_4 is dissolved in the ambient water. In the bottom water, CH_4 concentrations decrease by 93 % within 6 m vertical distance, from 142 nmol L^{-1} at 15 m above the seafloor to 10 nmol L^{-1} at 21 m above the seafloor (Fig. 4-10). Such a large decrease in CH_4 concentration cannot be explained by bubble dissolution (see model results above). Already 21 m above the seafloor the CH_4 concentrations are as low as the local background concentration hinting to a restricted vertical transport.

Pycnoclines have been observed before to limit the vertical transport of dissolved CH_4 and favor the lateral transport in the same density layer (Damm et al. 2005; Schmale et al. 2010). In the study area, a salinity gradient generates a density gradient at ~20 m above the seafloor. As a consequence CH_4 is dominantly enriched in Layer III.

Therefore, exclusively in Layer III CH_4 concentrations higher than 50 nmol L^{-1} were detected. AWd, the water mass that defines Layer III, extend from the seafloor up to 20 m above the seafloor and was found along the transects in E – W and S - N direction (Fig. 4-3, Fig. 4-10). This water masses is part of the West Spitsbergen current (WSC) which flows northward east of the shelf edge and we assume that a part of this water mass is intruded onto the shelf bank by eddy overturning (Tverberg and Nost 2009).
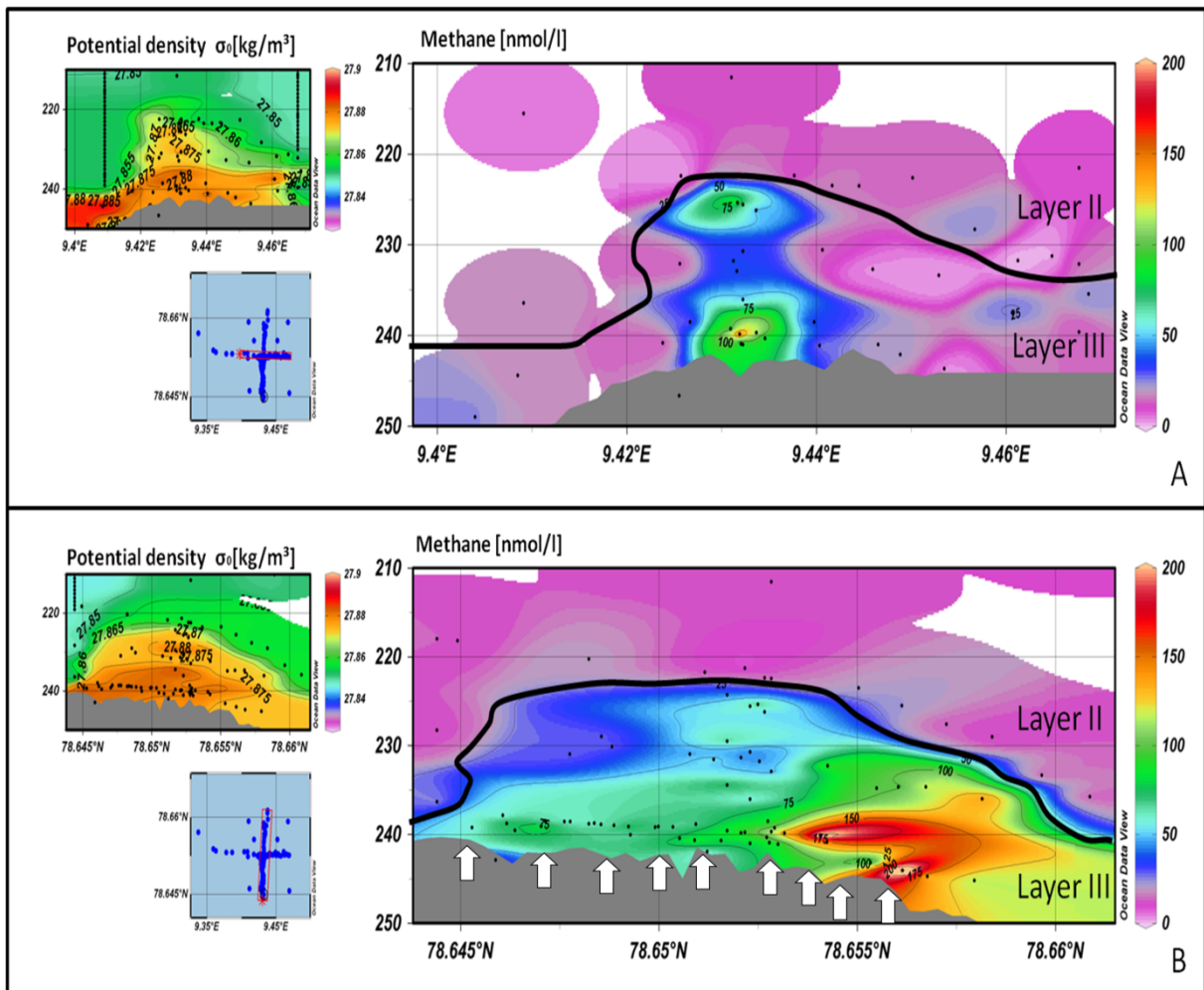
Fig. 4-10 *Dissolved* CH_4 *in the lower water column indicate the dominance of lateral transport. The pycnocline is indicated though black lines. (A) E – W transect, the plumes spreads inside Layer III in flow direction. A strong concentration gradient is seen between Layer III and II. (B) S – N transect – vertical spreading of the plume appears restricted. White arrows in (B) indicate the position of the observed gas flares.*

According to the flow directions of the WSC (Piechura et al. 2001; Walczowski et al. 2005) and the ESC (Saloranta and Svendsen 2001), the CH_4 enriched Layer III flows northward on the shelf bank alongside the shelf edge before down-welling to greater water depths. In S – N direction the vertical restriction of Layer III is confirmed by oceanographic changes (Fig. 4-4): increase in temperature (~0.13 °C) and a decrease in salinity (S ~0.1).

In addition, the extent of the CH_4 plume in northern direction matches with the current direction (Fig. 4-10 B). The CH_4 plume (concentrations > 25 nmol L^{-1}) is restricted in E – W direction to the area where gas release is observed (Fig. 4-10 A). The E - W extent of the plume is much smaller than the extent of Layer III in E – W direction (Fig. 4-10 A). These results indicate that mixing in E – W direction is limited due to the rapid transport by the WSC to the N direction.

The assumption of the rapid transport is supported by $\delta^{13}C_{CH4}$ measurements, which are commonly used to describe the potential fate of CH_4 due to mixing with background CH_4 or microbial oxidation of CH_4 in the water column. We assume that the variations in isotopic composition (up to 19 ‰ VPDB in small area) in the water column do not reflect any isotopic fractionation which occurs in the water column when CH_4 is oxidized, (Fig 4-6 A) which might be most likely due to the short residence time of the water above the seafloor (max. 0.44 d). Therefore, by the interpretation of the Keeling plot (Fig. 4-8), we suggest that the isotopic heterogeneous CH_4 by time and region is related to mixing. The regression line in the Keeling Plot (Fig. 4-8) points to a mixing of CH_4 released from the gas bubbles with $\delta^{13}C_{CH4}$ values of around – 60 ‰ VPDB and background CH_4 of the inflowing water mass with $\delta^{13}C_{CH4}$ values of around – 40 ‰ VPDB. Nevertheless, a mixture of different gas types i.e. thermogenic and biogenic source types are likely (Knies et al. 2004), however, the isotopic signature of CH_4 detected in the water column can not contribute to resolve this question.

Although microbial oxidation does occur, the oxidation rate in Layer III (0.78 ± 0.22 nmol L^{-1} d^{-1}) is 3 times higher compared to Layer II (< 0.22 nmol L^{-1} d^{-1}) only a small fraction of the CH_4 is oxidized in the study area. If we consider the average concentration of 48.8 nmol L^{-1} in Layer III and a residence time of the water mass below 0.44 d, 99.3% of the CH_4 will be lateral transported out of the study area. If the advective transport is neglected, all methane in the surveyed box defined by the S - N and E - W transects would be microbially oxidized in 50 - 100 d. This is comparable to microbial oxidation in the Coal Oil Point plume (Mau et al. 2012) and the rapid consumption of the methane after the Gulf of Mexico oil spill (Kessler et al. 2011).

However, due to restricted vertical transport and the short residence time of the water mass of Layer III above the gas ebullition area, most of the stripped CH_4 is rapidly transported northward away from the study site within the bottom water and presumably microbially oxidized along its path. Nevertheless, the local CH_4 background concentration of ~10 nmol L^{-1} in Layer II (Damm et al. 2005; Westbrook et al. 2009) is compared to the ocean background concentration (Rehder et al. 1999) considerably enriched. We assume that the CH_4 in Layer II is a mixture of CH_4 originating from dissolution of rising gas bubbles and surface water enriched in CH_4 from several other sources like inter-granular seepages or micro-seepages occurring widely spread over the shelf (Damm et al. 2005). This assumption is supported by observations of enhanced CH_4 concentrations close to the pycnocline and in the gas flare (25 nmol L^{-1}, Fig. 4-10). The dissolved CH_4 appears to be significantly diluted as the isotopic signature of the CH_4 released from the seafloor (– 60 ‰ VPDB) is not identifiable anymore (- 39.71 to -43.55 ‰ VPDB, red dots in Fig 4-8 A). Using the mean atmospheric methane concentration of June 2005 in this area of 1.903 ppm (Ocean Station ZEP: http://www.esrl.noaa.gov/gmd/ccgg/iadv/, at 78.91N, 11.89 E) and the ambient values measured by CTD 34, the equilibrium methane concentration at the sea surface is 3.1 nmol L-1 according to Wiesenburg and Guinasso (1979). Consequently, the measured surface methane concentrations (Layer I) between 7.15 - 11.3 nmol L^{-1} indicate a saturation of 230 – 360 %. Nevertheless, the amount of seafloor-released CH_4 in the water column as well as the atmospheric efflux could not been estimated and need to be verified by future works.

4.7   Summary and conclusions

Hydroacoustic flare imaging measurements revealed 10 active gas flares confirming previous measurements and indicating the continuity of these gas flares. This is in accordance with studies by Westbrook et al. (2009). It is important to consider, that the amount of gas ebullition into the water column often varies with time. Several of the most intensively studied gas seeps (Greinert 2008; Leifer and Boles 2005; Schneider Von Deimling et al. 2010) exhibited a pulsating behavior, with periods of activity of several minutes or vigorous ebullitions. Therefore, long-term measurements are necessary to quantitative the amount of CH_4 emissions from this gas ebullition area.

Nevertheless, in close vicinity of these active seeps, a distinct plume of strongly elevated methane concentration (up to 540 nmol L^{-1}) was identified by our high tempo-spatial measurements. The data revealed a strong decrease of methane concentrations within 20 meters above the seafloor which indicates a fast dissolution of gas bubbles.

Even though some gas flares were observed rising up to 50 m water depth in this region, the dissolved methane plume appears to be trapped by a pycnocline 20 m above the seafloor hindering the vertical transport and favoring the horizontal transport. Microbial methane oxidation rate measurements indicate elevated rates in the water 20 m above seafloor compared to the upper water column, which suggests ongoing microbial oxidation while the CH_4 load is transported with the current to greater water depth. These results indicate that bubble transport can be excluded as a direct pathway of seafloor-released CH_4 to the atmosphere in the study area during the time of measurement.

However, during winter ice formation and resulting brine release leads to convective mixing down to the seafloor (supported by unpublished long term observations by A. Beszczynska-Möller). Summer stratification breaks down and vertical transport of CH_4 from Layer III is not limited anymore and can reach the sea surface. This seasonality of potential methane pathways is limited to high latitude regions and has been so far not considered in any budgets calculations such as the source calculation of atmospheric methane in higher latitudes by Fisher et al. (2011).

4.8   Acknowledgement

References: Chapter 4

Bell, R. J., R. T. Short, F. H. W. V. Amerom, and R. H. Byrne. 2007. Calibration of an In Situ Membrane Inlet Mass Spectrometer for Measurements of Dissolved Gases and Volatile Organics in Seawater. Environ. Sci. Technol. 41: 8123–8128.

Biastoch, A. and others 2011. Rising Arctic Ocean temperatures cause gas hydrate destabilization and ocean acidification. Geophys Res Lett 38.

Buffett, B., and D. Archer. 2004. Global inventory of methane clathrate: sensitivity to changes in the deep ocean. Earth Planet Sc Lett 227: 185-199.

Cisewski, B., G. Budeus, and G. Krause. 2003. Absolute transport estimates of total and individual water masses in the northern Greenland Sea derived from hydrographic and acoustic Doppler current profiler measurements. J Geophys Res-Oceans 108.

Craig, H. 1957. Isotopic standards for carbon and oxygen and correction factors for mass-spectrometric analysis of carbon dioxide. Geochim Cosmochim Ac 12: 133-149.

Damm, E., A. Mackensen, G. Budéus, E. Faber, and C. Hanfland. 2005. Pathways of methane in seawater: Plume spreading in an Arctic shelf environment (SW-Spitsbergen). Continental Shelf Research 25: 1453-1472.

Etiope, G. 2004. New directions: GEM - Geologic emissions of methane, the missing source in the atmospheric methane budget. Atmos Environ 38: 3099-3100.

Etiope, G., and R. W. Klusman. 2002. Geologic emissions of methane to the atmosphere. Chemosphere 49: 777-789.

Faure, G. 1986. Principles of isotope geochemistry. John Wiley and Sons. chapters 6: 8.

Felden, J., F. Wenzhofer, T. Feseker, and A. Boetius. 2010. Transport and consumption of oxygen and methane in different habitats of the Hakon Mosby Mud Volcano (HMMV). Limnology and Oceanography 55: 2366-2380.

Fischer, P. J. 1978. Natural gas and oil seeps,Santa Barbara Basin, California.

Fisher, R. E. and others 2011. Arctic methane sources: Isotopic evidence for atmospheric inputs. Geophys Res Lett 38.

Gentz, T., and M. Schlüter. 2012. Underwater cryotrap-membrane inlet system (CT-MIS) for improved in situ analysis of gases. Limnol. Oceanogr. Methods 10: 317-328

Greinert, J. 2008. Monitoring temporal variability of bubble release at seeps: The hydroacoustic swath system GasQuant. J Geophys Res-Oceans 113.

Greinert, J., and D. F. McGinnis. 2009. Single bubble dissolution model – The graphical user interface SiBu-GUI. Environmental Modelling & Software 24: 1012-1013.

Hovland, M., and J. H. Sommerville. 1985. Characteristics of two natural gas seepages in the North Sea. Mar Petrol Geol 2: 319-326.

Hustoft, S., B. Dugan, and J. Mienert. 2009. Effects of rapid sedimentation on developing the Nyegga pockmark field: Constraints from hydrological modeling and 3-D seismic data, offshore mid-Norway. Geochem Geophy Geosy 10.

Intergovernmental Panel on Climate Change (2007) IPCC fourth assessment report (AR4). Working Group 1, The Physical Science Basis

Jerosch, K., M. Schluter, J. P. Foucher, A. G. Allais, M. Klages, and C. Edy. 2007. Spatial distribution of mud flows, chemoautotrophic communities, and biogeochemical habitats at Hakon Mosby Mud Volcano. Marine Geology 243: 1-17.

Judd, A., G. Davies, J. Wilson, R. Holmes, G. Baron, and I. Bryden. 1997. Contributions to atmospheric methane by natural seepages on the UK continental shelf. Marine Geology 137: 165-189.

Judd, A. G., and M. Hovland. 2007. Seabed Fluid flow: The impact on Geology, Biology and the Marine Environment.

Jung, W. Y., and P. R. Vogt. 2004. Effects of bottom water warming and sea level rise on Holocene hydrate dissociation and mass wasting along the Norwegian-Barents Continental Margin. J Geophys Res-Sol Ea 109.

Kampbell, D. H., J. T. Wilson, and S. A. Vandegrift. 1989. Dissolved-Oxygen and Methane in Water by a Gc Headspace Equilibration Technique. Int J Environ an Ch 36: 249-257.

Kessler, J. D. and others 2011. A Persistent Oxygen Anomaly Reveals the Fate of Spilled Methane in the Deep Gulf of Mexico. Science 331: 312-315.

Knies, J., E. Damm, J. Gutt, U. Mann, and L. Pinturier. 2004. Near-surface hydrocarbon anomalies in shelf sediments off Spitsbergen: Evidences for past seepages. Geochem Geophy Geosy 5.

Kvenvolden, K. A., and B. W. Rogers. 2005. Gaia's breath - global methane exhalations. Mar Petrol Geol 22: 579-590.

Lammers, S., and E. Suess. 1994. An improved head-space analysis method for methane in seawater. Marine Chemistry 47: 115-125.

Landvik, J. Y. and others 2005. Rethinking Late Weichselian ice-sheet dynamics in coastal NW Svalbard. Boreas 34: 7-24.

Leifer, I., and J. Boles. 2005. Measurement of marine hydrocarbon seep flow through fractured rock and unconsolidated sediment. Mar Petrol Geol 22: 551-568.

Leifer, I., and J. Clark. 2002. Modeling trace gases in hydrocarbon seep bubbles. Application to marine hydrocarbon seeps in the Santa Barbara Channel. Geol Geofiz 43: 613-621.

Leifer, I., and A. G. Judd. 2002. Oceanic methane layers: the hydrocarbon seep bubble deposition hypothesis. Terra Nova 14: 417-424.

Limonov, A. F., T. C. E. Van Weering, N. H. Kenyon, M. K. Ivanov, and L. B. Meisner. 1997. Seabed morphology and gas venting in the Black Sea mudvolcano area: Observations with the MAK-1 deep-tow sidescan sonar and bottom profiler. Marine Geology 137: 121-136.

Mau, S., M. B. Heintz, and D. L. Valentine. 2012. Quantification of CH4 loss and transport in dissolved plumes of the Santa Barbara Channel, California. Continental Shelf Research 32: 110-120.

McGinnis, D. F., J. Greinert, Y. Artemov, S. E. Beaubien, and A. Wuest. 2006. Fate of rising methane bubbles in stratified waters: How much methane reaches the atmosphere? J Geophys Res-Oceans 111: -.

Mienert, J., M. Vanneste, S. Bunz, K. Andreassen, H. Haflidason, and H. P. Sejrup. 2005. Ocean warming and gas hydrate stability on the mid-Norwegian margin at the Storegga Slide. Mar Petrol Geol 22: 233-244.

Piechura, J., A. Beszczynska-Moller, and R. Osinski. 2001. Volume, heat and salt transport by the West Spitsbergen Current. Polar Res 20: 233-240.

Rajan, A., J. Mienert, and S. Bünz. 2012. Acoustic evidence for a gas migration and release system in Arctic glaciated continental margins offshore NW-Svalbard. Mar Petrol Geol 32: 36-49.

Rehder, G., R. S. Keir, E. Suess, and M. Rhein. 1999. Methane in the northern Atlantic controlled by microbial oxidation and atmospheric history. Geophys Res Lett 26: 587-590.

Saloranta, T. M., and H. Svendsen. 2001. Across the Arctic front west of Spitsbergen: high-resolution CTD sections from 1998-2000. Polar Res 20: 177-184.

Sauter, E. J. and others 2006. Methane discharge from a deep-sea submarine mud volcano into the upper water column by gas hydrate-coated methane bubbles. Earth Planet Sc Lett 243: 354-365.

Schauer, U., E. Fahrbach, S. Osterhus, and G. Rohardt. 2004. Arctic warming through the Fram Strait: Oceanic heat transport from 3 years of measurements. J Geophys Res-Oceans 109.

Schlüter, M., and T. Gentz. 2008. Application of Membrane Inlet Mass Spectrometry for Online and In Situ Analysis of Methane in Aquatic Environments. J Am Soc Mass Spectr 19: 1395-1402.

Schmale, O., S. E. Beaubien, G. Rehder, J. Greinert, and S. Lombardi. 2010. Gas seepage in the Dnepr paleo-delta area (NW-Black Sea) and its regional impact on the water column methane cycle. J Marine Syst 80: 90-100.

Schmitt, M., E. Faber, R. Botz, and P. Stoffers. 1991. Extraction of methane from seawater using ultrasonic vacuum degassing. Anal Chem 63: 529-532.

Schneider Von Deimling, J., J. Greinert, N. R. Chapman, W. Rabbel, and P. Linke. 2010. Acoustic imaging of natural gas seepage in the North Sea: Sensing bubbles controlled by variable currents. Limnol Oceanogr-Meth 8: 155-171.

Schneider Von Deimling, J. S., G. Rehder, J. Greinert, D. F. Mcginnnis, A. Boetius, and P. Linke. 2011. Quantification of seep-related methane gas emissions at Tommeliten, North Sea. Continental Shelf Research 31: 867-878.

Shakhova, N., I. Semiletov, A. Salyuk, V. Yusupov, D. Kosmach, and Ö. Gustafsson. 2010. Extensive Methane Venting to the Atmosphere from Sediments of the East Siberian Arctic Shelf. Science 327: 1246-1250.

Shindell, D. T., G. Faluvegi, D. M. Koch, G. A. Schmidt, N. Unger, and S. E. Bauer. 2009. Improved Attribution of Climate Forcing to Emissions. Science 326: 716-718.

Short, R. T. and others 2001. Underwater mass spectrometers for in situ chemical analysis of the hydrosphere. J Am Soc Mass Spectr 12: 676-682.

Short, R. T., D. P. Fries, S. K. Toler, C. E. Lembke, and R. H. Byrne. 1999. Development of an underwater mass-spectrometry system for in situ chemical analysis. Meas Sci Technol 10: 1195-1201.

Slubowska-Wodengen, M., T. L. Rasmussen, N. Koc, D. Klitgaard-Kristensen, F. Nilsen, and A. Solheim. 2007. Advection of Atlantic Water to the western and northern Svalbard shelf since 17,500 cal yr BP. Quaternary Sci Rev 26: 463-478.

Tverberg, V., and O. A. Nost. 2009. Eddy overturning across a shelf edge front: Kongsfjorden, west Spitsbergen. J Geophys Res-Oceans 114.

Valentine, D. L., D. C. Blanton, W. S. Reeburgh, and M. Kastner. 2001. Water column methane oxidation adjacent to an area of active hydrate dissociation, Eel River Basin. Geochim Cosmochim Ac 65: 2633-2640.

Walczowski, W., J. Piechura, R. Osinski, and P. Wieczorek. 2005. The West Spitsbergen Current volume and heat transport from synoptic observations in summer. Deep-Sea Res Pt I 52: 1374-1391.

Westbrook, G. K. and others 2008. Estimation of gas hydrate concentration from multi-component seismic data at sites on the continental margins of NW Svalbard and the Storegga region of Norway. Mar Petrol Geol 25: 744-758.

---. 2009. Escape of methane gas from the seabed along the West Spitsbergen continental margin. Geophys Res Lett 36: -.

Wiesenburg, D. A., and N. L. Guinasso. 1979. Equilibrium Solubilities of Methane, Carbon-Monoxide, and Hydrogen in Water and Sea-Water. J Chem Eng Data 24: 356-360.

Chapter 5 – Manuscript III

~ High resolution detection, mapping and quantification ~

of methane in gas ebullition areas.

Manuscript in preparation for

"Earth and Planetary Science"

Recovery of the in situ mass spectrometer (HE362).

High resolution determination and inventory calculation of methane in the water column at a gas seepage area in the North Sea via *in situ* mass spectrometry.

Torben Gentz, Sören Krägewski, Roi Martinez, Michael Schlüter,

Alfred Wegener Institute for Polar and Marine Research, Am Handelshafen 12, D-27570 Bremerhaven Germany

5.1   Abstract

A high resolution determination, mapping and quantification of climate relevant methane released from submarine geological sources is required to estimate their potential contribution to its atmospheric budget. Several marine geological sources like cold streams, coastal anoxic sediments or mud volcanoes are recognized as significant, unfortunately, most submarine sources remain poorly quantified. In our shallow study area (~41 m water depth) in the Netherlands economic zone of the southern North Sea recent seismic studies revealed the occurrence of shallow gas accumulation, gas chimneys and subsequent seabed methane release into the water column. Nevertheless, very little is known about the fate of the released methane.

While conventional methods hardly reach the spatial and temporal resolution necessary for a detailed inventory calculation of the dissolved CH_4 above gas ebullition, we applied a novel underwater mass spectrometer. Due to the *in situ* use, the technique is unaffected by potential sampling artifacts and reveals an up to 750 times higher sampling frequency compared to conventional methods. During three deployments in an area of 400 x 410 m we measured ~11900 samples which lead to detail mapping and 3-D visualization of the dissolved CH_4 concentration in the water column above the gas seep. Combined by other techniques like multibeam and video observation, discrete water and gas bubble sampling, as well as hydroacoustics and oceanographic data we described and calculated the amount of seabed released methane; the CH_4 inventory in the water column and subsequent the potential methane release into the atmosphere.

With the aid of multibeam, anomalies (up to 2.5 m) in the bathymetry are determined at the same position where gas ebullition through the entire water column to the sea surface was observed via hydroacoustic. Based on the video taken from the sediment 113 active CH_4 streams with a total amount of seabed methane release of 35.3 $\pm$ 17.65 t CH_4 yr^{-1} were detected in an "affected" area of 3800 m² in size. By the Inspectr200-200 highest dissolved CH_4 concentrations (~3.5 µmol L^{-1}) were measured near the seabed in the gas seep area and the inventory in the water column is calculated to ~6.4*10^5 µmol with an air sea exchange flux of up to ~210 $\pm$ 63 µmol m^{-2} d^{-1}. As the observed pycnocline in 29 m water depth limits the vertical transport of dissolved CH_4 we divided the inventory in bottom water below and mixed water layer above the pycnocline. Therefore, we consider a indirect CH_4 transport of ~40 % of the total seabed released methane through dissolution of gas bubbles in the mixed water layer. Additionally to this amount we indicated direct methane transfer via gas bubbles ~25 %, which emphasize that ~65 % (23 $\pm$ 11.5 t CH_4 yr^{-1}) of the entire CH_4 emission potentially contributing to the atmospheric CH_4 budget, which is far above most studied gas seepages.

5.2   Introduction

The greenhouse gas methane (CH_4) has a global warming potential which is at least 20 - 40 times higher than carbon dioxide (CO_2) (Khalil and Moraes 1995) on a 100 year timescale. Thus, constraining the sources and sinks of CH_4 is important to improve climate predictions. Submarine geological sources like seeps, mud volcanoes or pockmarks observed along the coastal margins (Hovland and Judd 1988; Milkov 2000) are examples for the release of gases into the marine environment by rising gas bubbles or dissolved in pore water, but not yet considered in the IPCC report (Etiope and Favali 2004; Etiope and Klusman 2002; Kvenvolden and Rogers 2005). The total emission of submarine CH_4 into the upper water column from marine seeps (e.g., Håkon Mosby Mud Volcano, Tommeliten field, Santa Barbara Basin, Black Sea, West Svalbard continental margin) is roughly estimated to amount up to 30 Tg CH_4 yr^{-1} (Kvenvolden and Rogers 2005). Due to ocean warming especially in the Nordic Seas and the Arctic, increasing bottom water temperature could result in sub-sea thawing of permafrost (Shakhova et al. 2010) and destabilization of gas hydrates (Jung and Vogt 2004; Mienert et al. 2005). As a result, it could be estimated that an additional release of CH_4, amounting to up to tens of Tg yr^{-}, gets released into the water column (Buffett and Archer 2004). In shallow water, such as shelf areas like the North Sea, the release of CH_4 from the seabed in form of diffusive flux or gas bubbles has a higher potential to enter the atmosphere (McGinnis et al. 2006; Reshetnikov et al. 2000). Initially, CH_4 loaded gas bubbles are supersaturated compared to the ambient water composition, and consequently CH_4 is dissolved into ambient water until the equilibrium is reached. These processes were modeled by e.g., Leifer and Judd, (2002), McGinnis et al., (2006). Therefore, beside diffuse flux two potential pathways in these environments are (A) direct via rising bubbles or (B) indirect via vertical transport of the dissolved CH_4 in the water column.

Nevertheless, in the known seepage areas only a small amount reaches the atmosphere. For example, Schneider von Deimling et al., (2011) estimated that ~4% of the CH_4 initially released at the seafloor in the Tommeliten field is transported to the atmosphere whereas the remaining CH_4 fraction is horizontal transported and /or microbial oxidized.

For investigation of the dissolved CH_4 concentrations in these study areas, conventional techniques like water sampling by e.g., rosette water sampler, phase separation by head space technique and subsequent analyses onboard the vessel or in the laboratory onshore by gas chromatography are well established (Kampbell et al. 1989; Lammers and Suess 1994) and provide very accurate data. Nevertheless, this method is affected by degassing due to pressure decreasing and temperature increasing as well as dissolving of potentially trapped gas bubbles during the retrieval of the water sample to the sea surface (Leifer and Judd 2002; Schlüter et al. 1998). However, this method is also rather time consuming, which limits the number of sampling sites and therefore the spatial and temporal resolution. Especially in gas ebullition areas where the spatial extent of discharge sites is highly variable (mostly a few square meters) and may change over time, the resolution of the established methods as well as the spatial accuracy during sampling is sufficient to describe i.e. flux rates like Solomon et al. (2009) but two or three-dimensional descriptions of the concentration fields of trace gases like CH_4 in the water column could hardly reached.

For this purpose, specific membrane inlet systems and underwater mass spectrometer (UWMS) like the Inspectr200-200, the THETYS or the NEREUS (Bell et al. 2007; Camilli and Hemond 2004; Hemond and Camilli 2002; Kibelka et al. 2004; Short et al. 1999; Wenner et al. 2004) were designed. Compared to conventional techniques, the novel *in situ*, online and real time gas analysis in high frequency by UWMS is unaffected by the aspects mentioned before and supports detailed chemical mapping of discharge sites due to the fast response time (~20 s) and high sampling rate (<3 s for each scan).

Therefore, the application of UWMSs opens new research fields to calculate inventories, evaluate the fate of gases as well as estimating the air-sea exchange of trace gases in gas seep areas.

Here, we present first results of a detailed CH_4 plume distribution and inventory calculation in the water column from a multi-method approach obtained at a gas seep area first indicated by Schroot et al., (2003a), in the southern North Sea. A novel underwater mass spectrometer (Inspectr200-200) (Bell et al. 2007; Short et al. 2001; Short et al. 1999; Wenner et al. 2004), which we partly redesigned (Gentz and Schlüter 2012), was used to quantify CH_4 in the dissolved phase of the water column in high resolution. Through video observation of the seabed, we determined the amount and locations of gas streams and the seabed area affected by gas ebullition. Additionally, analyses of CH_4 (concentration and isotopic ratio) as well as hydrographic and geochemical data were taken by CTD coupled with a rosette water sampler system. Based on the coinciding results of our CH_4 measurements, the hydroacoustic-, the oceanographic- and video observation, we propose that CH_4 flux to the atmosphere occurs directly via bubbles and indirect via dissolved CH_4, which is being released from the bubbles during their ascent in the water column.

The data presented here shows the necessity of these new techniques for improving inventory calculations at gas seeps areas and their contribution to the atmospheric CH_4 budget.

5.3   Regional setting

The study area is located on the European shelf in the Netherland part of the Southern Central North Sea, very close to the German border (Fig. 5-1). The area is characterized by strong seasonal forcing and shallow water depths of 30 - 45 m. On top of a Permian Zechstein salt dome, source rocks of hydrocarbons are observed. The area is typically a gas basin, with mainly Carboniferous source rocks and a number of oil and condensate fields holding hydrocarbons from Jurassic source rocks were observed (Schroot et al. 2005). In our detailed study area (55.306°N, 4.091°E; Fig. 5-1) of 140.000 m² in license block B13, seismic studies from Schroot et al., (2005) show shallow gas fields, with reservoirs of Pliocene to Pleistocene age at depths of 600–700 m. Geochemical analyses of the gas reservoir in depths of 600 m by Schroot et al., (2005) show a $\delta^{13}C_{CH4}$ value of -70.3 ‰ VPDB, and a CH_4 ratio of 99.6 % which indicates to a biogenic source. The sedimentary postdates the Mid-Miocene unconformity, a surface which is buried at a depth of 1000 to 1500 m depth (Schroot et al. 2005; Schroot and Schuttenhelm 2003a; Schroot and Schuttenhelm 2003b). The gas reservoir is leaking via a gas chimney and subsequent gas saturation of the near surface environment is observed (Kuhlmann and Wong 2008; Schroot et al. 2005). According to the classification by the GORE™ Survey for Exploration, the $\delta^{13}C_{CH4}$ values of samples taken by Schroot et al., (2005) in sediment depths of 3.5 m belong to cluster A, which represents biogenic CH_4 with light thermogenic influence, and cluster B, which represents biogenic CH_4 with altered light thermogenic influence. The $\delta^{13}C_{CH4}$ values are verified during the cruise He362. The bathymetry of the study area in block B13 is flat with a mean depth of 41 m. With the aid of hydroacoustics, active gas seeps were observed in 2005 (Schroot et al. 2005), 2010 (HE337) and 2011 (HE362). In 2011, two 2.5 m-wide depressions of 1.3 m depth and several sediment hummocks of up to 2.2 m in height occur in the gas release area. Via video observation, 113 gas streams are observed in the study area. A detailed description of the seafloor observation is given in the result part (Fig. 5-3).
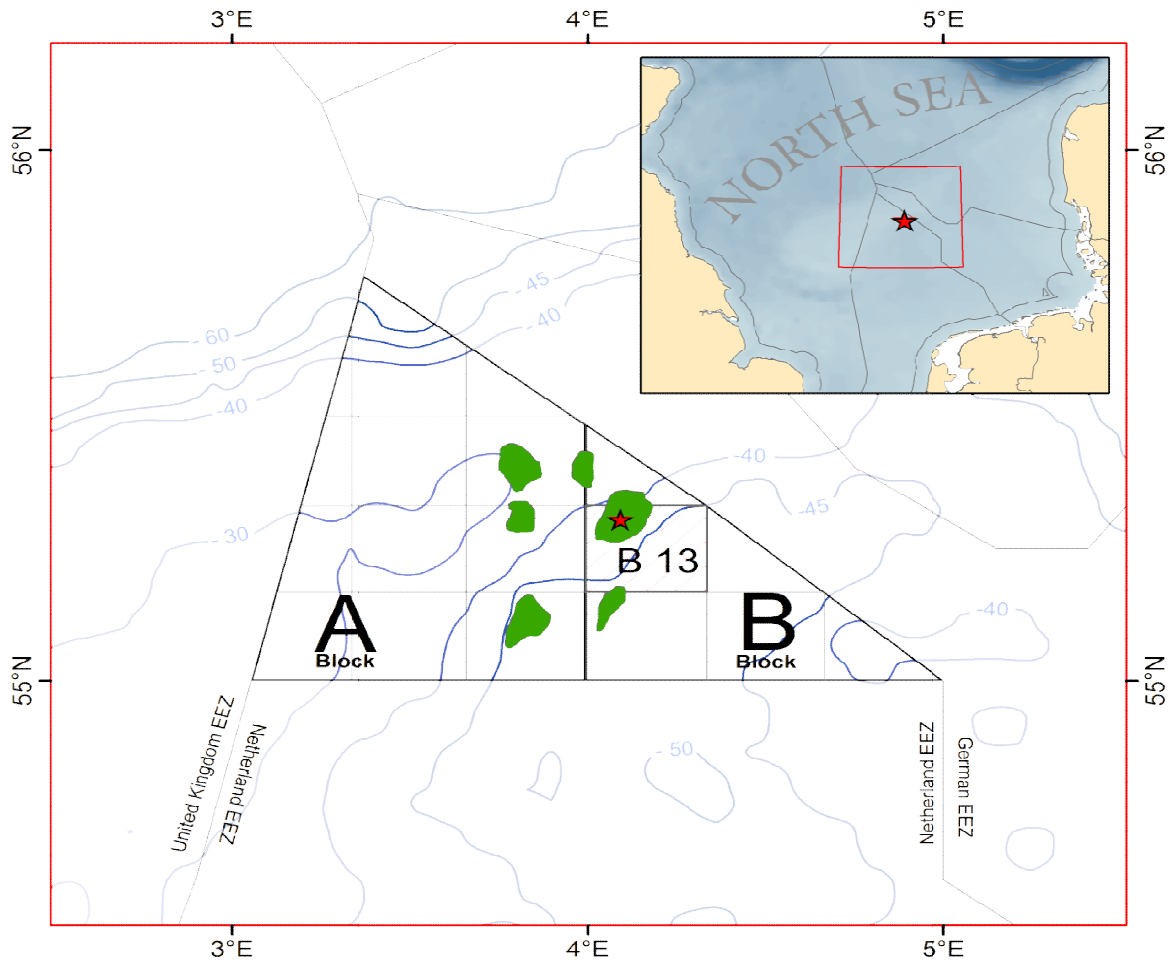
Fig. 5-1 *The study area (red star) in license block B 13 is located in the southern North Sea at the border between Germany and the Netherlands. Green areas indicate shallow Plio-Pleistocene gas fields in 600 m depth modified after Schroot et al., 2005 in the economic zone of the Netherlands. Contour lines indicate the water depth.*

The hydrographic settings in this area are strongly affected by tides and seasonal variations, which occur in the entire central and southern North Sea. The hydrographic conditions in the study area in August 2011 are shown in figure 5-5. Ten CTDs were conducted within the main gas ebullition area (~3800 m²), as well as four in the surrounding area. All profiles show similar water column settings when compared. At 27 – 33 m water depth, a distinct pycnocline with strong temperature gradients of ~3 °C as well as potential salinity gradients of ~0.7 kg m^{-3} is observed. Referring to Goedecke et al., (1967) and Tomczak et al., (1963), this water column is

stratified until October. Water cooling in October and increasing wind speed cause the water column to destabilize and eventually mixing. Due to storms, the water column is homogeneous in December and the maximum vertical mixing is reached. In May, warming in connection with decreasing storm activity decreases the extent of vertical mixing and results in the establishment of a strong pycnocline.

5.4   Methods and materials

During the expeditions HE337 (28.09.2010 – 29.09.2010) and HE362 (10.08.2011 – 14.08.2011), we performed hydroacoustic surveys and obtained geochemical as well as geophysical data recording of the water column. We examined a very detailed area of 0.142 km² in size via high-resolution bathymetry by multibeam survey as well as performing gas flare detection via a split beam fish finder sonar system.

To measure the dissolved CH_4 concentration in high-resolution, we used an underwater mass spectrometer (Inspectr200-200) combined with a video observing system (ISITEC®) to visualize the gas bubbles in the entire water column. During the mass spectrometer operations an ADCP was deployed in the same frame to measure the water current.

Additionally, 14 vertical CTD profiles were performed while collecting 154 discrete water samples and two multiple sediment corer to sample the seabed sediments.

5.4.1 High-resolution mapping of dissolve gases in the water column
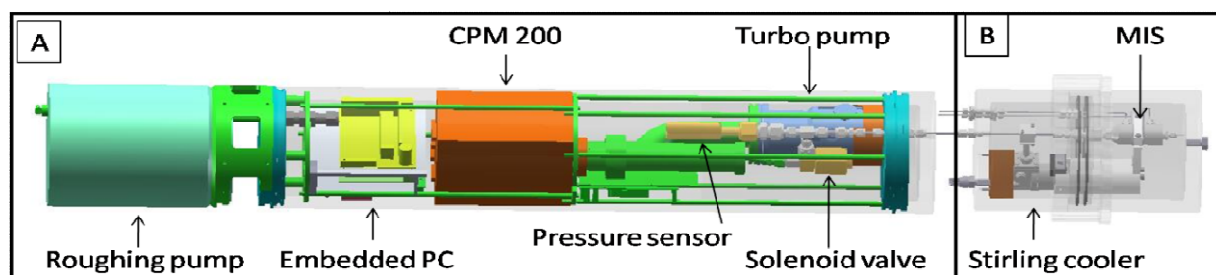
Fig. 5-2 Schematic drawing of the redesigned underwater mass spectrometer. (A) Housing of the sensor unit including the spare parts for the recording and analyzing of the gases as well as the pumps to get high vacuum. (B) Housing of the sample inlet. The main components are the Ricor™ cooler (K508) and the membrane inlet system.

A novel membrane inlet mass spectrometer (Inspectr200-200) was used to measure the dissolved CH_4 concentration in the study area. The mass spectrometer was designed for underwater applications (Bell et al. 2007; Schlüter and Gentz 2008; Short et al. 2001) and partly redesigned (Gentz and Schlüter 2012) to suit our applications. During HE362, the instrument was used underwater in defined depths (8m, 14m, 18m, 24m, 31m, and close to the seafloor) with an operating time of about 11 h, which revealed more than 11900 data records.

To separate the water sample unit from the sensor unit, the underwater mass spectrometer is divided in two pressure housings. The housing of the sensor unit (Fig. 5-2 A) contains an Inficon™ quadrupole mass spectrometer (Transpector CPM 200), a Varian™ turbo pump, a roughing pump, a pressure sensor (PSG502, Inficon™), a solenoid valve (EVI 005 M, Pfeiffer vacuum™) as well as an embedded PC and a micro-controller. The housing of the sample inlet (Fig. 5-2 B) contains a sample inlet and outlet, a membrane inlet system (MIS), as well as a stirling cooler (K508, Ricor™) to improve the detection limit for all gases and to secure the mass spectrometer against a potential water inflow by rupture of the membrane (Gentz and Schlüter 2012). The housings are connected via the vacuum line ($^1/_8$" capillary) and the connector for power supply.

During the operation of Inspectr200-200 water is constantly pumped at a flow rate of 3 ml min^{-1} by an external peristaltic pump from the outside into the pressure housing of the sample inlet, through the membrane inlet system (MIS), where gas permeation takes place, and back into the water column. The MIS includes a heater and a thermocouple to operate the membrane inlet system at a constant temperature of 50 °C. To avoid the collapse of the membrane tube made of polydimethylsiloxane (PDMS) under hydrostatic pressures of up to 2000 kPa (equivalent to ca. 200 m water depths) the membrane is supported on the inside by a stainless steel spring. Through the turbo pump, the pressure inside the PDMS membrane is held at less than 10^{-5} Torr. Gases permeating through the PDMS membrane are detected by the Inficon CPM 200 residual gas analyser in the sensor housing. According to Lloyd and Scott (1983), CH_4, N_2, O_2, Ar and CO_2 could be quantified by the ion current

detected at m/z ratios of 15, 28, 32, 40 and 44, respectively. Each 3 seconds a full data set of all gases is recorded. By cooling the capillary, which connects the two housings with the cryotrap, we were able to reduce the water vapour in the analytical line by more than 98%, which improves the signal quality and the detection limit of major and trace gases considerably (Gentz and Schlüter 2012; Schlüter and Gentz 2008). Therefore, the detection limit of the trace gas CH_4 was lowered from > 100 to 16 nmol L^{-1}.

5.4.2 Acoustic data acquisition

An EM 710 (90 kHz) multibeam echo sounder from KONGSBERG MARITIM AS was used at HE333 to acquire the bathymetry in a resolution of 1x2°. Surveys were run with a maximum swath angle of 130° at 4 knots ships speed.

A multi-frequency fish finder sonar system (Simrad EK60) was used to detect and map the horizontal and vertical distribution of gas flares in the water column. For unambiguous identifications of gas streams, a strict protocol is required to avoid misinterpretations often caused by fish. For this reason, the following criteria from Judd et al., (1997), are applied: Echo patterns identified as gas flares have to touch the seafloor, which is considered to be the origin of gas ebullition; the vertical to horizontal dimension ratio of the echo pattern must be greater than two; and isolated flares are only included if detected at least twice at the same location.

5.4.3 Bubble gas exchange modeling

A gas bubble dissolution model by McGinnis et al., (2006) was used to estimate the amount of CH_4 in the gas bubbles, the dissolution of CH_4 from gas bubbles into water column and the direct CH_4 transfer via gas bubbles to the atmosphere.

5.4.4 Hydrography and discrete water sampling

In order to conduct studies of the water column, we used a Seabird SBE 911 conductivity temperature depth (CTD) profiler supplemented by an Seabird SBE 43 oxygen sensor, a Benthos PSA-916 altimeter and a rosette water sampler with 12-10 L Niskin bottles.

In total, 14 vertical CTD-profiles with a down-cast speed of 0.5 m s^{-1} and up to 12 water samples from various depths were collected during the up-cast at each CTD Station. The system was adjusted via altimeter to a defined depth in reference to the seabed. The deepest point of closing the bottles was at 2 m $\pm$ 1 m above the sea floor. To achieve a vertical cast at one location, the up-cast speed was 1.5 m s^{-1} and the bottles were closed during the run, which reduced the shift in coordinates caused by ship drifting.

The discrete water samples were analyzed for CH_4 through gas chromatography (Kampbell et al., 1989). Therefore, the water samples were taken immediately from the Niskin bottles and transferred into 22 ml glass vials and crimped tightly with a septum made of Teflon. A head space of 5 mL volume was generated by inserting argon gas. After 5 hours of equilibration, the gas concentration in the head space was analyzed with the gas chromatograph TraceGC (Thermo Finnigan; Waltham, USA) equipped with a flame-ionization detector, and a Porapak Q column was then applied. The GC oven was operated isothermally (100 °C), and the temperature at the sample inlet was 300 °C. Two standard gases (10 ppm and 1000 ppm) were used for the calibration. Based on the CH_4 concentration in the head space and the CH_4 concentration in the aqueous phase, which was computed by the Bunsen coefficient according to Wiesenburg and Guinasso (1979), the CH_4 concentration in the water sample was derived. The overall error of the method is about 5%.

For measuring of the carbon isotopic ratio of CH_4, we took water samples immediately from the Niskin bottles. The dissolved gas was extracted from the water samples by vacuum-ultrasonic treatment (Schmitt et al. 1991). This method achieved 63% recovery of the total dissolved CH_4 (Lammers and Suess 1994). The $\delta^{13}C_{CH4}$

values were determined by a Delta XP plus Finnigan mass spectrometer. The extracted gas was purged and trapped with PreCon equipment (Finnigan) to pre-concentrate the sample. Depending on the CH_4 concentration, the reproducibility derived from duplicates was 0.5-1. All isotopic ratios were given a δ-notation relative to the Pee Dee Belemnite (PDB) standard (Craig 1957).

5.4.5 Sediment observations

For visual detection of the seabed structures and detailed gas bubble recording at the emission sites, we used a digital underwater video camera made by ISITEC[®]. The camera was used in full HD resolution mode with a maximum resolution of 1900 x 1200 pixels. The integrated zoom lens features a 10 x optical zoom and autofocus function. An integrated Ethernet-interface with 100 Mbit s^{-1} allows for a direct connection to a personal computer on board as well as supplying the power through this connection. A SeaLite[®] Sphere from Deepsea[®] was used as an external light source.

To evaluate the number of streams and their bubble emission rate, we used the Sanyo software (VMS-Client). To analyze the bubble sizes of the streams, individual frames were exported to the ImageJ program (Rasband 1997 - 2012). Only the volumes of gas bubbles in close vicinity to the scale bar and with the same focal plane were analyzed. Therefore, the major (a) and minor (b) axes were measured and the volume was calculated by assuming a rotational ellipsoid with an equivalent spherical radius (r_e)(Leifer and Patro 2002).

$$r_e = (a^2 b)^{\frac{1}{3}} \quad (1)$$
$$V = \frac{4}{3}\pi r_e^{\,3} \quad (2)$$

Bubble fluxes (mL min^{-1}) were calculated considering the average bubble volumes and numbers of bubbles rising through the water column. The volume flux was

converted to mass flux (in mol CH_4 min⁻¹) considering the CH_4 compressibility factor (Z) in equation (3) (Römer et al. 2012).

$$PVA = nRTZ \quad (3)$$

P is pressure (Pa), *V* is volume (ml), *n* is the amount of substance, *R* is the ideal gas constant (8.314472 J K⁻¹ mol⁻¹) and *T* is the *in situ* temperature. The values of Z of 0.991 in 41 m water depth and T= 284 K were calculated by the Pipeng online graphing calculator (http://pipeng.com/index.php/gsts/itdmotflup004c/itdtoflup 00424). Due to the short time of investigation, we included a bulk activity time factor A as mentioned in i.e., Schneider von Deimling et al., (2011). Due to the potential errors in the estimation of the mean bubble size and bubble emission frequency, we allowed for a range of uncertainty for the mass flux calculation of $\pm$ 50 %.

A mini multiple sediment corer (MUC) was used to recover undisturbed surface sediment. Due to the sandy sediments sampling of the pore water was not feasible. However, a visual interpretation of the sediment structure was done.

5.4.6 Data synchronization and visualization

To combine all observations and online measurements, the position of the ship (latitude, longitude, and time) was determined by Trimble ship GPS. The coordinates were corrected to the real position of the instruments on board. The time stamps of the instruments were synchronized with the time stamp of the Trimble GPS. In regards to the online measurements by the mass spectrometer, for each single analysis, we also considered the delay time between water sampling at depths and gas analysis, as well as annotating our sampling report. In the sampling report, the sampling depths as well as observations like the occurrence of gas bubbles in the water column were recorded.

For spatial analysis, the entire data set of the study was integrated into the Geo-Information-System ArcGIS 10.0 (ESRI™). The ArcGIS Geospatial Analyst (ESRI™) was applied for the 3-D computation of contour plots of dissolved CH_4 as well as the visualization of the sediment and its features. The inventories of CH_4 within the water column were calculated by MATLAB™.

5.5 Results and discussion

5.5.1 Sediment observation

High resolution bathymetry mapping via multibeam echo sounder from KONGSBERG MARITIM AS reveals two "affected" areas displaying anomalies in the sediment distribution (Fig. 5-3 A). One area is located in the south west corner of the study area, the other in the center. These anomalies are characterized by hummocks up to 2.2 m height, compared to the homogeneous flat bathymetry of ~41 m in the study area. Additionally, two 2.5 m wide and 1.3 m deep depressions are observed near the hummocks. Via hydroacoustic (EK 60), active gas streams in the center area were observed in 2010 (HE337) and 2011 (HE362), while no gas streams occurred in the south-west area. Due to these results, we used detailed video observation of the seafloor (~8400 m²) in the center where sediment anomalies as well as gas streams in the water column occurred. As a result, we observed 113 active CH_4 streams, 4 locations of single bubble release, and dark spots with depressions just centimeters deep, often in combination with white patches, in an area of ~3800 m² in size (Figs. 5-3 A, B, C). In our opinion, the dark spots are currently inactive gas ebullition locations where the uppermost layer of the sediment is disrupted by the intensive gas bubble release, and we suggest that the white spots point towards settled bacterial mats (Fig. 5-3 C). These results are underlined by multiple core samples (Fig. 5-3 D). Visual analysis of the first 12 cm of the sediment reveal that, opposite to the unaffected area (Fig. 5-3 E), the uppermost layer is ~4cm thick, with deep dark sediment occurring underneath, which indicates an anoxic environment. Due to the sandy sediment, we were not able to carry out pore water analyses.
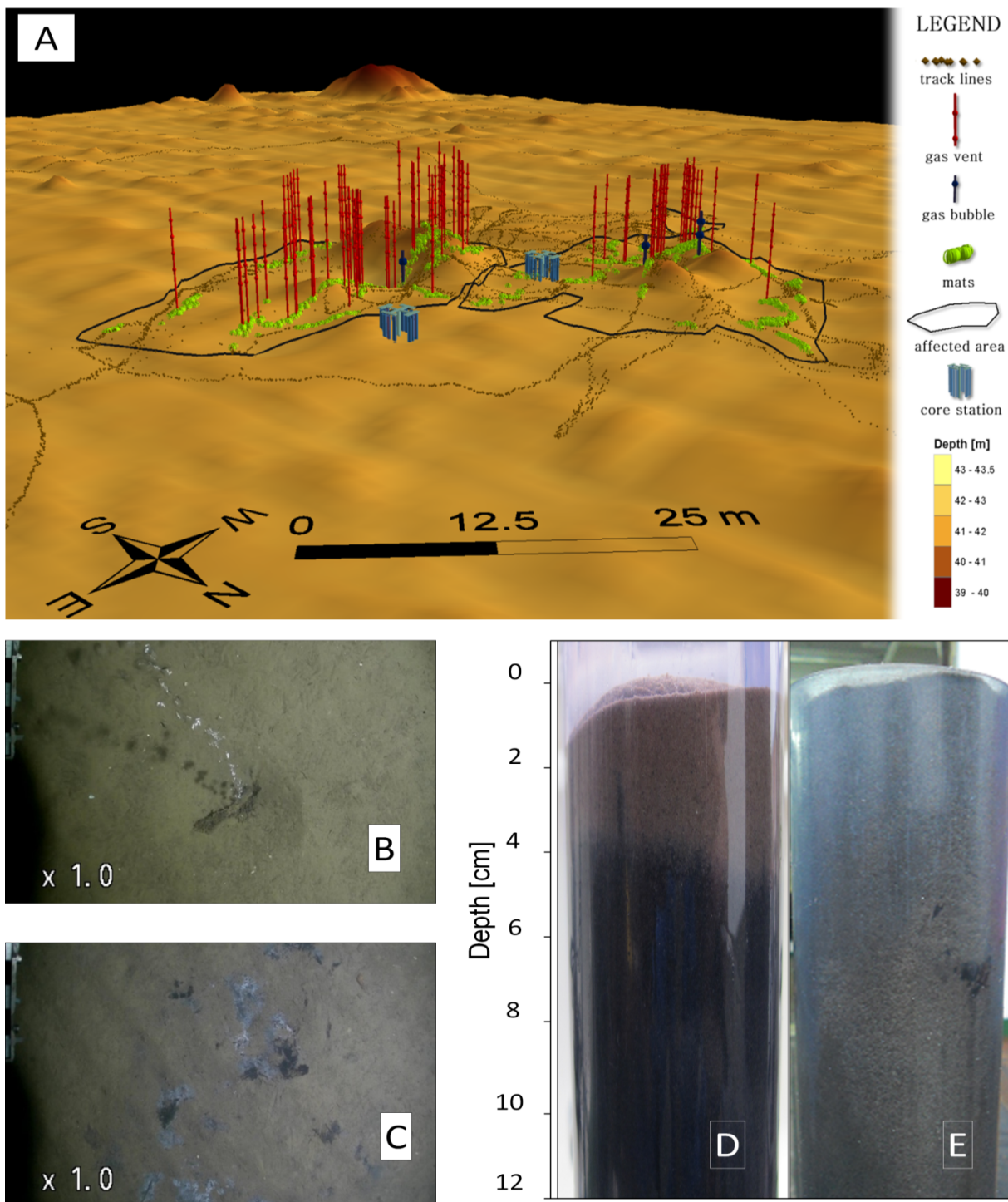
Fig. 5-3 *Sediment observations of the gas seep area (A). The dashed lines show the track lines during observation. The black polygons indicate the affected areas. Location of the streams is shown in B and indicated by red sticks in A. The observations of black spots and potential bacterial mats shown in C are indicated by green dots in A. Sediment core of the "affected area (D) and "unaffected" area (E) shown as blue symbols in A.*

Less than 10 % of the gas streams occur out of the black depressions, while the rest is released from bright sand (Fig. 5-3 B). We suggest that the porosity of the uppermost 4 cm of sediment function as a blockade for gas bubbles and is responsible for the form and size of CH_4 bubble release from the sediment (Leifer and Culling 2010). As the sediment porosity becomes lower, higher pressure and increased bubble size is necessary to migrate through the sediment. Small bubbles do not disturb the sediment, while large bubbles (diameter of ~30 mm) disrupted the sediment surface. This assumption is supported by a video observation we call "a stream is born". In this video, we observe a large bubble, approximately ~30 mm in diameter, being released from the sediment and took over surface sediment. Subsequently, a black hole occurs and a steady flow of smaller gas (diameter < 12 mm) bubbles forms. This result is in coherence with the measurements done by Hovland and Sommerville (1985).

Based on image analyses of all videos, totaling 113 and focusing on various gas streams, the amount of gas bubble released ranged from 0.3 to 40 bubbles s^{-1} (average of 23 bubbles s^{-1}). Detailed investigations at 9 gas streams revealed gas bubbles with a diameter of 4.5 to 16 mm (average 7 mm), larger than diameters observed at other gas ebullition areas (Leifer and Judd 2002; McGinnis et al. 2006; Schneider Von Deimling et al. 2011; Solomon et al. 2009).

On the basis of these observations we estimate a flux of CH_4 28.27 L min^{-1}. Since the determination of gas bubble size as well as its emission frequency was affected by image resolution limitations and the angle view of the camera, we assume an error of up to 50 % for the mass flux estimation. It is important to consider, however, that the amount of gas ebullition into the water column often varies with time. Several of the most intensively studied gas seeps (Greinert 2008; Leifer and Boles 2005; Schneider Von Deimling et al. 2010) exhibited a pulsating behavior, with periods of activity over several minutes. Therefore, according to Schneider von Deimling et al., (2011) we assume an activity time (A) of 70%, which would result in a conservative estimated emission of 35.3 $\pm$ 17.65 t CH_4 yr^{-1} from the sediment into the water column. This result is a first estimate and has to be further clarified in future studies with long-term

measurements. Nevertheless, the results are in order with other gas ebullition areas observed at the continental shelves (Judd 2004), especially compared to those geographically closely located Tommeliten field (Schneider Von Deimling et al. 2011).

5.5.2 *Observation of the gaseous CH$_4$ fraction in the water column*

The gas bubbles in the entire water column were observed by hydroacoustics as well as video observation (Fig. 5-4). The hydroacoustic images show that the gas bubbles penetrate straight forward from the seabed through the entire water column up to the atmosphere (Fig. 5-4 B). The video observations at the seabed in 24 m water depth as well as at the surface corroborate these results (Figs. 5-4 B,C,D). During their rise through the water column, CH$_4$ loaded gas bubbles are supersaturated compared to the ambient water composition, and consequently, CH$_4$ is dissolved into the ambient water until the equilibrium is reached (e.g., Leifer and Judd, 2002). Due to the mass transfer out of the gas bubble, its size is decreasing. Simultaneously, gases like N$_2$, O$_2$ or CO$_2$ dissolved in the seawater are supersaturated with respect to the initial composition of the gas bubble. This causes a mass transfer of these gases into the gas bubble. These processes were modeled by e.g., Leifer and Judd (2002) to estimate the decrease in size and change of gas composition during the ascent of a CH$_4$ loaded gas bubble from the seabed towards the sea surface.

In this study, the dissolved as well as the gaseous CH$_4$ fraction are potential pathways for seabed released CH$_4$ and are considered to be sources for atmospheric CH$_4$. Therefore, both pathways are considered in this study.
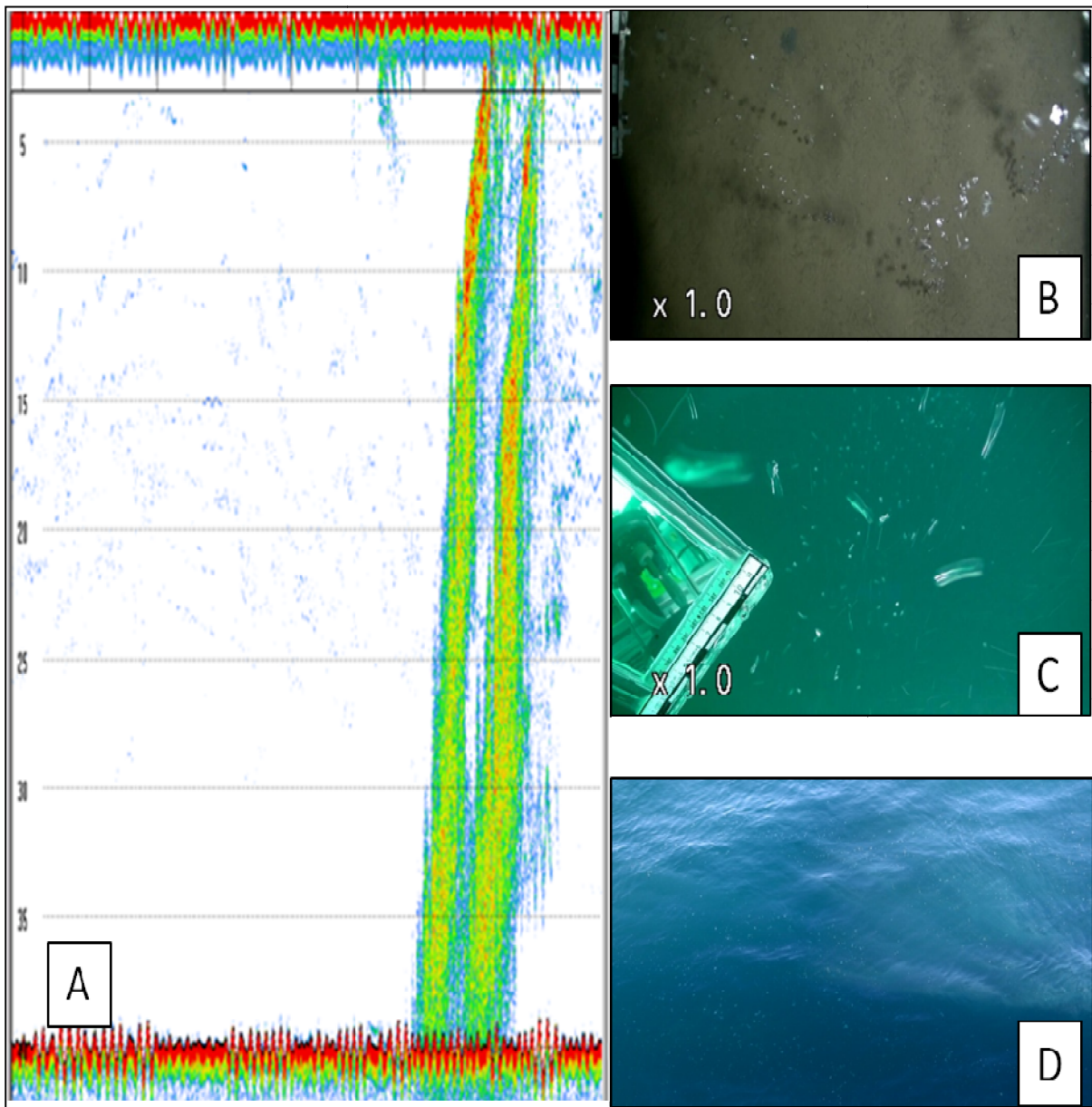
Fig. 5-4 *(A) Hydroacoustic image of the gas streams through the entire water column. Visual observation of gas streams at the same location from the seabed (B) to 24 m water depth (C) and subsequent sea air transition zone (D).*

5.5.3 Hydrography and dissolved CH_4 concentration in the water column

5.5.3.1 Discrete water sampling

The hydrographic conditions at the study area are stable as observed in a 24 hour period (11 August 2011 11:14 till 12 August 10:43), shown in figures 5-5 B and C. Ten CTD cast were conducted within the main gas ebullition area, and four in the corners of a 400 m x 410 m square in the surrounding area (Fig. 5-6). All profiles show similar water column settings. At 27 – 33 m water depth (29 m are utilized for the following distinction of water masses), we observed a distinct pycnocline with strong gradients in temperature of 3 °C as well as potential salinity of 0.7 kg m^{-3}.
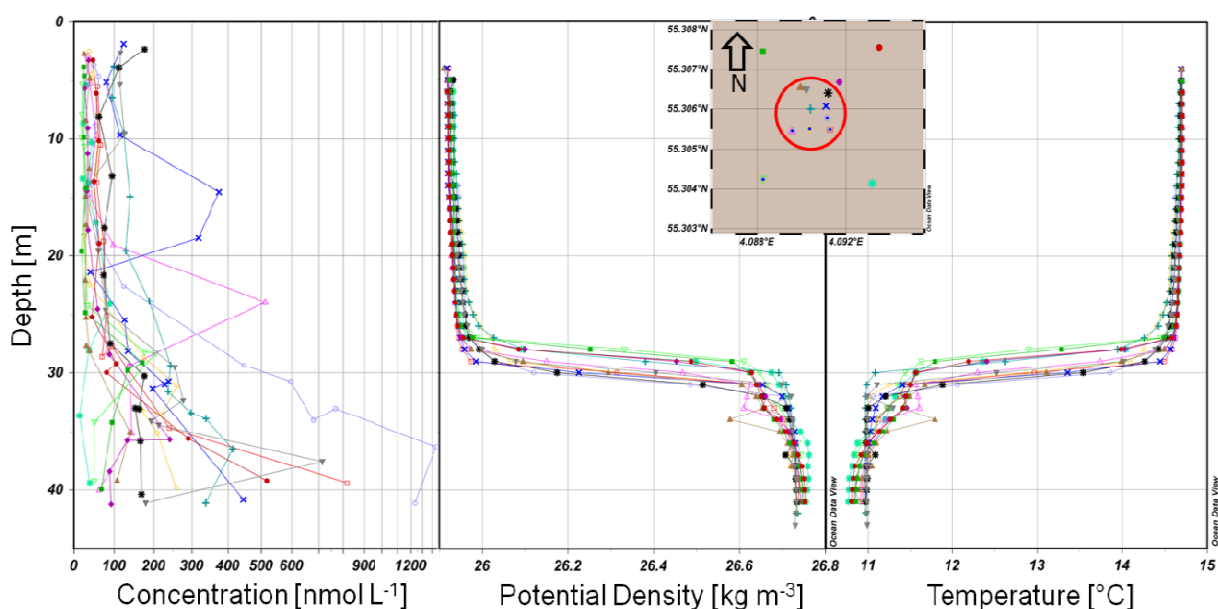
Fig. 5-5 (A) CH_4 concentration profiles in the water column retrieved by discrete water sampling. Potential density (B) as well as the potential temperature (C) derived by CTD casts in the affected areas (red circle) as well as in the surroundings indicate a strong pycnocline at ~29 m.

To reveal horizontal profiles of the dissolved CH_4 concentration, 157 discrete samples were taken during 14 CTD-profiling, and analyzed with conventional methods. Even if the casts are taken very close to each other, the measured CH_4 profiles are very heterogeneous. The result of all measurements revealed that the concentration of dissolved CH_4 varies from 14 to 1447 nmol L^{-1} (Fig. 5-5 A). High concentrations are observed above the gas ebullition area. The concentration varies from 63 to 1447 nmol L^{-1} below and 31 to 512 nmol L^{-1} above the pycnocline. Using the mean

atmospheric CH_4 concentration of November 2009 of 1885 ppm in the study area (Ocean Station M: http://www.esrl.noaa.gov/gmd/ccgg/iadv/, at 66.00 °N, 2.00 °E) and the ambient T and S values (Fig. 5-5), the equilibrium CH_4 concentration in surface layeri s 2.78 nmol L^{-1}, according to Wiesenburg and Guinasso (1979). Compared to this background value, the measured CH_4 concentrations between 24 nmol L^{-1} to 176 nmol L^{-1} (taken 2 m below surface) indicate a saturation of ~ 850 to 6330 %.

During the cruise, the calm weather condition made it possible to take a discrete sample of the gas bubbles at the sea surface to analyze the residual CH_4 content through gas chromatography. After a calculated ascending time of 2.7 min, the gas bubbles at the surface had a residual CH_4 content of up to **25.4 %** which shows the pathway of direct CH_4 transfer via gas bubbles from the seabed to the atmosphere. (McGinnis et al. 2006). With the use of a theoretical model (McGinnis et al., 2006), we were able to support the measured result of the direct CH_4 transport to the surface via bubbles. Input parameters of the model were the initial bubble size of 7 mm (observed by video); initial CH_4 fraction (99.6%) in the gas bubble as estimated by studies of Schroot et al., (2005); salinity, temperature, O_2 concentration (derived via CTD casts); and the CH_4 concentration in the ambient water (taken by discrete water samples and subsequent conventional analysis). Those parameters were set in the graphical user interface SIBGui (Greinert and McGinnis 2009), which implements the numerical model of McGinnis et al., (2006). Beside the results of the amount of direct CH_4 transfer into the atmosphere (29.81 % of residual CH_4 content in surface bubbles), the model calculated that 26.8 % of the initial CH_4 in the bubble was dissolved in the ambient bottom water below the pycnocline. Due to the limitation of vertical transport this CH_4 fraction will be laterally transported and oxidized by time. Therefore, this CH_4 fraction will hardly contribute toward the CH_4 flux into the atmosphere. 43.6 % of the initial CH_4 released at the seabed will be dissolved in the mixed layer above the pycnocline, indicating an indirect pathway of CH_4 reaching the atmosphere.

These important results could not verified by the use of conventional discrete water sampling and subsequent analysis. Additional predictions on the spatial distribution of dissolved CH_4 concentrations in the water column, one objective of the study, do not

become apparent through this rough data set done by CTD casts. Not even with a higher sampling rate due to the inaccuracy of the ship positioning during the profiling and known steep gradient of a view meter. Therefore, the underwater mass spectrometry was applied.

5.5.3.2 In situ CH_4 detection

In close vicinity and above the gas ebullition area, the *in situ* mass spectrometer (Inspectr200-200) was applied three times (each ~3.5 h) in a 24 h period to conduct high resolution mapping of the dissolved CH_4 concentration in various depths. The 3 deployments were adapted to the tide schedule, in order to achieve a high internal correlation of the deployments with respect to the water current changes in the study area. During the deployments, the main water current direction was in easterly direction with a mean speed of 0.06 m s^{-1} to the East and 0.0085 m s^{-1} to the North, below the pycnocline. Above the pycnocline the mean current speed was lower to the East (0.023 m s^{-1}) and nearly zero to the South (0.002 m s^{-1}). The resulting data set contained more than 11000 samples for CH_4 in the entire area, with focus to the gas streams. The operating time was limited to 3.5 h due to the battery power supply.

The first operation ("small transect") determined the CH_4 concentration in the gas ebullition area in water depths of 31 m, 24 m, 18 m, 14 m and 8 m. To map the expansion of the dissolved CH_4 plume from its source, the concentration was measured in the surrounding area ("large transect") at water depths of 31 m, 18 m and 8 m in the second run. During the third run ("sediment observation"), the mass spectrometer and the video system were applied using a towed system 1 m above the seabed (~40 m water depth) to compare the dissolved CH_4 concentration with the observed streams via video. With the aid of vessel speed and latency time of the UWMS we estimated a spatial resolution of our measurements of < 10 m for the water column measurements and < 3 m for the sediment observation. After synchronizing, the data was integrated into the Geo-Information-System ArcGIS 10 (ESRI™).

It became apparent that the highest dissolved CH_4 concentrations were measured via mass spectrometry in the area where hydroacoustics as well as visual observations indicated enlarged gas ebullition into the water column (Fig. 5-6). Related to the limited vertical CH_4 transport by the pycnocline (Fig. 5-6), we assumed a different CH_4 spreading for the water masses which was supported by the observed CH_4 concentrations done by the mass spectrometer in various depths as well as the conventional sampling. Hereafter, the water column will be distinguished in the water mass below the pycnocline (bottom water) and above the pycnocline (mixed water).
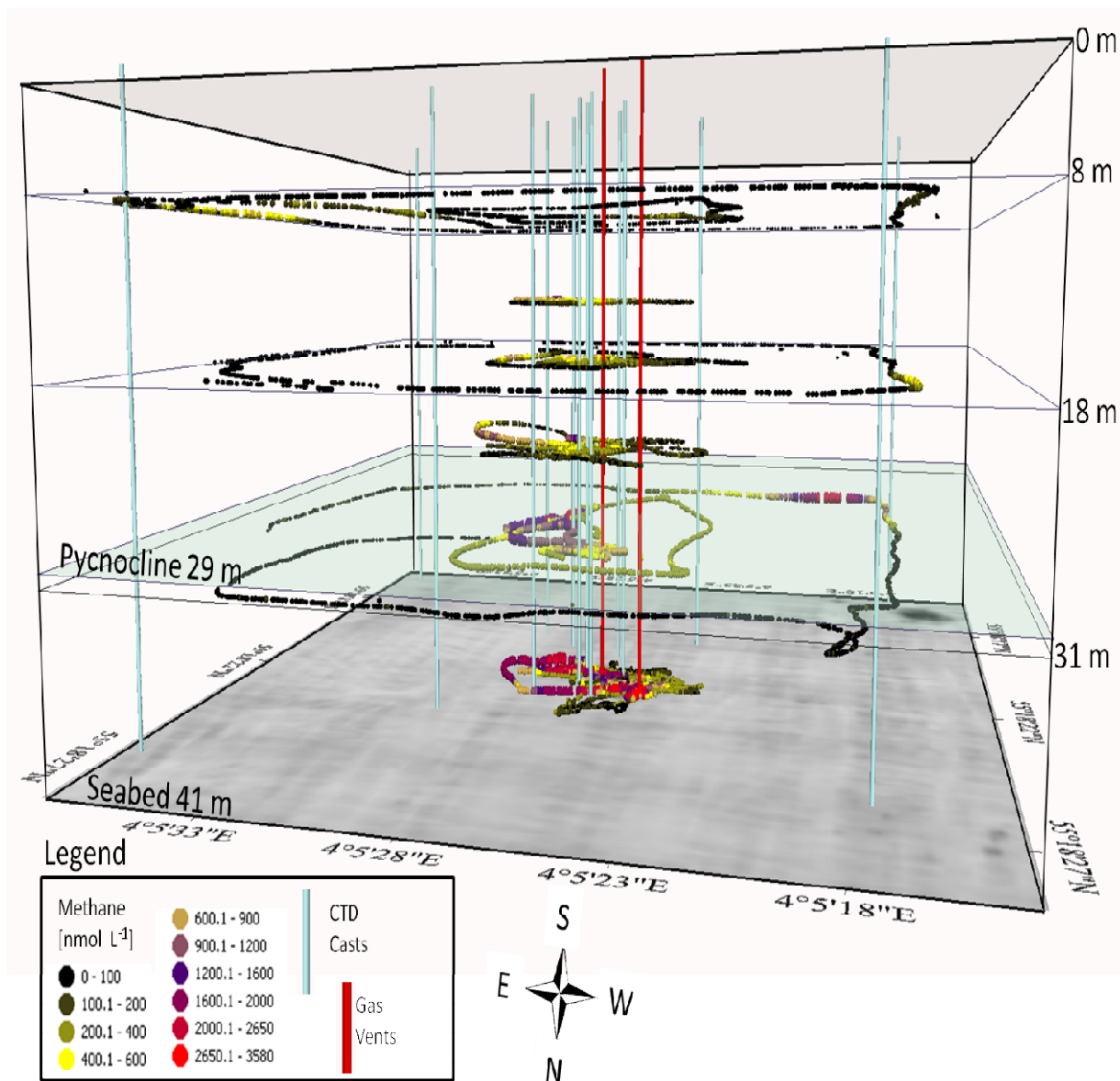
Fig. 5-6 *High resolution 3-D plot of the dissolved* CH_4 *concentration from 11917 samples taken at various depths (41 m, 31 m, 24 m, 18 m, 14 m, 8m), retrieved by the underwater mass spectrometer. Highest concentrations are measured in the bottom water, where anomalies in the bathymetry as well as gas streams are observed.*

In bottom waters (31 m to seabed), the dissolved CH_4 concentration vary between "background concentration" in the surrounding area (< 16 nmol L^{-1}) and higher concentrations ranging from 100 nmol L^{-1} to 3500 nmol L^{-1} at gas streams. Additionally, steep gradients in concentration from 100 nmol L^{-1} to more than 1500 nmol L^{-1} in less than 12 m were measured (Fig. 5-6).

In the mixed water layer (24 m to 8 m) the CH_4 concentration varies between < 16 nmol L^{-1} to 1350 nmol L^{-1}. Highest concentrations are measured in the gas ebullition area at 24 m water depth, which is the deepest point related to the pycnocline. Nevertheless, at 8 m (nearest measured point to the surface) concentrations of up to ~645 nmol L^{-1} were observed. Related to the background value of 2.79 nmol L^{-1} after Wiesenburg and Guinasso (1979) for this region we calculated a saturation of 23200 % and an air sea exchange flux of up to ~210 $\pm$ 63 µmol m^{-2} d^{-1} (Wanninkhof et al. 2009). Hence, additionally to the direct CH_4 transport via gas bubbles, the dissolved CH_4 fraction functions as a contributor to atmospheric CH_4.

In the surrounding area, three locations with enriched dissolved CH_4 concentrations but without indications of gas bubble release had been observed with the aid of hydroacoustics as well as video observations. The mass spectrometer data show a strong signal (up to 2200 nmol L^{-1}) in the upper layer (31 m) below the pycnocline in the S - W corner, with occurring anomalies in the bathymetry. This could indicate dissolved CH_4 release from the seabed via fluid flow or dissolved flux and needs to be verified through further scientific work in the future. In the S - N corner, CH_4 concentrations of up to 641 nmol L^{-1} in 18 m water depth and enhanced concentrations of > 100nmol L^{-1} in the upper layer (8 m) were observed. Due to the water current direction, we suggest that the dissolved CH_4 belongs to an unknown gas source in the West and does not belong to the gas ebullition field we observed. In easterly direction, CH_4 concentrations of up to 645 nmol L^{-1} at water depth of 8 m were observed. Related to the water current direction, these concentrations could result from the observed gas ebullition area.

To corroborate these assumptions and to calculate a detailed inventory of the dissolved CH_4 fraction in the water column above the gas ebullition area, the high-resolution data set was gridded and interpolated to cover the entire study area. The enhanced CH_4 concentrations in the surrounding area not belonging to the observed gas release from the center gas ebullition area were removed. The enhanced CH_4 concentrations in the surrounding area not belonging to the observed gas release from the center gas ebullition area were removed. The high-resolution data set was interpolated by Matlab™ via the Voronoi (natural neighbor interpolation) function into a grid of 2 x 2 x 1 m. Since the lowest sampling depth was 8 m from the surface, the inventory calculation contained the water column between seafloor and 8 m water depth.
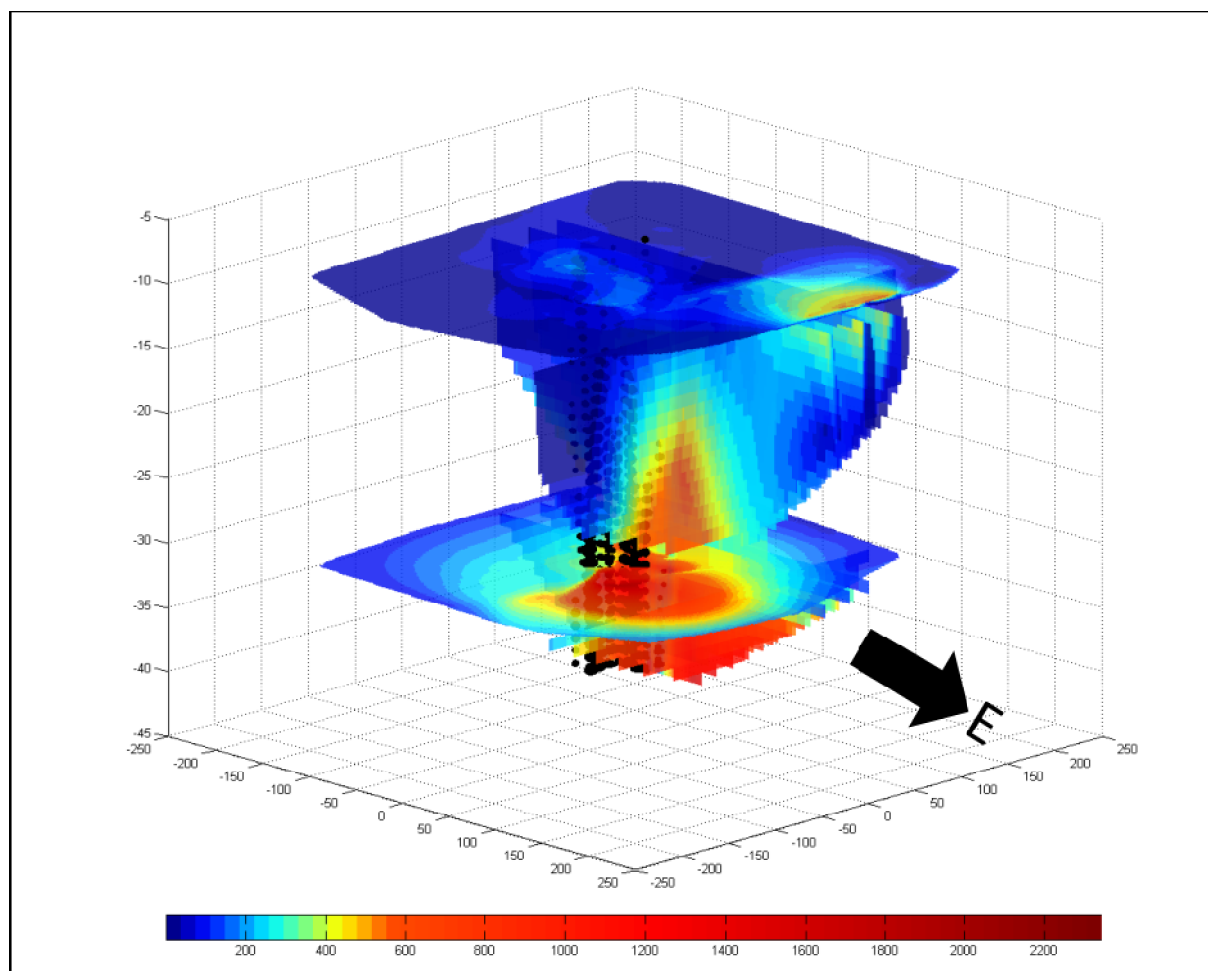
Fig. 5-7. Dissolved CH_4 inventory [nmol L^{-1}] in the water column as well as the gas bubbles observed by hydroacoustic (black dots). The dissolved CH_4 concentration is shown as scatter plots in various depths. The axis are the distance [m] from the center point.

Due to the limitation of the vertical transport of methane by the pycnocline we divided the data set in the water masses ranging from the seabed to 29 m in water depth, which represents the dissolved CH_4 plume below the pycnocline, and from 29 m to 8 m representing the water column above the pycnocline (Fig. 5-7).

By the results of the interpolation, we assume a plume size of ~1000000 m³ (15.6 % of the observed area) with concentrations higher than 200 nmol L^{-1}. The results indicate that, compared to the gas bubbles which cross the water column without any lateral diversion, the dissolved methane load is affected by the eastward flowing water current (dark spots in Fig 5-7). Near the seabed highest dissolved methane concentrations of the plume are measured in close vicinity to the bubble streams (dark spots in Fig 5-7). The plume reach a maximum expansion of 180 m into S – N direction relative to the center point, where gas flares had been observed by hydroacoustic (Fig. 5-7), and a maximum distribution of 310 m into the East at 8 m water depth, and. We assume, that the decreasing methane concentration by increasing plume size is related to mixing (Sauter et al. 2006). Nevertheless, higher dissolved methane concentrations are also observed in 8 m water depth in the surrounding of the gas bubbles but not connected to the higher concentrations of the plume at the same water depth. These results indicate that the gas bubbles are the major source for dissolved methane and most of the gaseous methane is dissolved in the upper part of the water column (McGinnis et al. 2006) and lateral as well as vertical transported in current direction. Nevertheless, methane is also dissolved from the methane loaded gas bubbles at the surface (residual 25.4 % methane from initial) but with lower dissolution rate (McGinnis et al. 2006).

The total dissolved CH_4 concentration from the gas ebullition is calculated to a total the amount of ~$6.2*10^8$ nmol, composed of ~$3.0*10^8$ nmol below and ~$3.2*10^8$ nmol above the pycnocline with respect to 8 m water depth. If we examine the entire water column above the pycnocline (0 – 29 m) we estimate a dissolved CH_4 inventory of ~$3.4*10^8$ nmol.

As we consider a direct CH_4 transport of ~25.4% from the seabed to the atmosphere via gas bubbles, plus an additional ~39.8 % via indirect CH_4 transport through dissolution of gas bubbles above the pycnocline, totalling 65.2 % (23 $\pm$ 11.5 t CH_4 y^{-1}) of the total CH_4 emission, potentially contributing to the atmospheric CH_4 budget.

5.6 Conclusion and outlook

This study shows the first high-resolution data set which maps and quantifies the CH_4 plume distribution above a gas ebullition area of ~3800 m² in size in the southern central North Sea, collected by a novel underwater mass spectrometer (UMS). We employed this new UMS since the spatial and temporal resolution obtainable through conventional methods, as well as the positioning during the sampling, did not fulfill the requirements for this application.. With the UMS Inspectr200-200, more than 11000 *in situ* samples were analyzed, particularly above the gas ebullition, during a 24 hour period, in an area measuring 410 x 400 m. In the study area, the Inspectr200-200 observed dissolved CH_4 concentrations twice as high compared to the 154 discrete samples taken by rosette water sampler. This resulted in a estimated air sea exchange of maximum ~210 $\pm$ 63 µmol m^{-2} d^{-1}. As we considered the gas release, the rise of gas bubbles and partially diffused CH_4 release to represent the source for dissolved CH_4 in the water column (seabed to 8 m water depth), we quantified the amount of dissolved CH_4 in the study area to ~$6.4*10^5$ µmol during the time of measurement. The oceanographic data indicated a pycnocline situated ~10 m above the seafloor, which limits the vertical transport of dissolved CH_4. The dissolved CH_4 in the bottom water would be laterally transported and microbially oxidized over time while the CH_4 reaching the mixed water layer would contribute indirectly via dissolved CH_4 (quantified via mass spectrometer) as well as directly via gas bubbles to the CH_4 flux from the water column into the atmosphere (quantified via discrete samples of the gas bubbles as well as calculated by the hydroacoustic data and a model). These results indicate that 65.2 % (23 $\pm$ 11.5 t CH_4 y^{-1}) of the seafloor-released CH_4 could reach the atmosphere. In winter, the stratification brakes down, and the entire amount of released CH_4 from the seafloor could enter the atmosphere.

Due to the high amount of CH_4 release, the shallow water depth and the pycnocline being close to the seabed, the potential air sea exchange is far above other gas seeps such as the Gulf of Mexico (Solomon et al. 2009), the BlackSea (McGinnis et al. 2006; Schmale et al. 2010), the West Spitsbergen continental margin (Gentz unpublished data) or the geographically close Tommeliten area (Schneider Von Deimling et al. 2011).

5.7   Acknowledgements

References: Chapter 5

Bell, R. J., R. T. Short, F. H. W. Van Amerom, and R. H. Byrne. 2007. Calibration of an in situ membrane inlet mass spectrometer for measurements of dissolved gases and volatile organics in seawater. Environ Sci Technol 41: 8123-8128.

Buffett, B., and D. Archer. 2004. Global inventory of methane clathrate: sensitivity to changes in the deep ocean. Earth Planet Sc Lett 227: 185-199.

Camilli, R., and H. F. Hemond. 2004. NEREUS/Kemonaut, a mobile autonomous underwater mass spectrometer. Trac-Trend Anal Chem 23: 307-313.

Craig, H. 1957. Isotopic standards for carbon and oxygen and correction factors for mass-spectrometric analysis of carbon dioxide. Geochim Cosmochim Ac 12: 133-149.

Etiope, G., and P. Favali. 2004. Geologic Emissions of Methane from lands and seafloor: mud volcanoes and observing systems. Environ Geol 46: 987-987.

Etiope, G., and R. W. Klusman. 2002. Geologic emissions of methane to the atmosphere. Chemosphere 49: 777-789.

Gentz, T., and M. Schlüter. 2012. Underwater cryotrap-membrane inlet system (CT-MIS) for improved in situ analysis of gases. Limnol. Oceanogr. Methods 10: 317-328

Goedecke, E., J. Smed, and G. Tomczak. 1967. Monatskarten des Salzgehaltes der Nordsee, dargestellt für verschiedene Tiefenhorizonte. Deutsches Hydrographisches Institut.

Greinert, J. 2008. Monitoring temporal variability of bubble release at seeps: The hydroacoustic swath system GasQuant. J Geophys Res-Oceans 113.

Greinert, J., and D. F. McGinnis. 2009. Single bubble dissolution model – The graphical user interface SiBu-GUI. Environmental Modelling & Software 24: 1012-1013.

Hemond, H., and R. Camilli. 2002. NEREUS: engineering concept for an underwater mass spectrometer. Trac-Trend Anal Chem 21: 526-533.

Hovland, M., and A. G. Judd. 1988. Seabed Pockmarks and Seepages. Graham and Trotman, London,: 293pp.

Hovland, M., and J. H. Sommerville. 1985. Characteristics of two natural gas seepages in the North Sea. Mar Petrol Geol 2: 319-326.

Intergovernmental Panel on Climate Change (2007) IPCC fourth assessment report (AR4). Working Group 1, The Physical Science Basis

Judd, A., G. Davies, J. Wilson, R. Holmes, G. Baron, and I. Bryden. 1997. Contributions to atmospheric methane by natural seepages on the UK continental shelf. Marine Geology 137: 165-189.

Judd, A. G. 2004. Natural seabed gas seeps as sources of atmospheric methane. Environ Geol 46: 988-996.

Jung, W. Y., and P. R. Vogt. 2004. Effects of bottom water warming and sea level rise on Holocene hydrate dissociation and mass wasting along the Norwegian-Barents Continental Margin. J Geophys Res-Sol Ea 109.

Kampbell, D. H., J. T. Wilson, and S. A. Vandegrift. 1989. Dissolved-Oxygen and Methane in Water by a Gc Headspace Equilibration Technique. Int J Environ an Ch 36: 249-257.

Khalil, M. a. K., and F. P. Moraes. 1995. Linear Least-Squares Method for Time-Series Analysis with an Application to a Methane Time-Series. J Air Waste Manage 45: 62-63.

Kibelka, G. P. G., R. T. Short, S. K. Toler, J. E. Edkins, and R. H. Byrne. 2004. Field-deployed underwater mass spectrometers for investigations of transient chemical systems. Talanta 64: 961-969.

Kuhlmann, G., and T. E. Wong. 2008. Pliocene paleoenvironment evolution as interpreted from 3D-seismic data in the southern North Sea, Dutch offshore sector. Mar Petrol Geol 25: 173-189.

Kvenvolden, K. A., and B. W. Rogers. 2005. Gaia's breath - global methane exhalations. Mar Petrol Geol 22: 579-590.

Lammers, S., and E. Suess. 1994. An improved head-space analysis method for methane in seawater. Marine Chemistry 47: 115-125.

Leifer, I., and J. Boles. 2005. Measurement of marine hydrocarbon seep flow through fractured rock and unconsolidated sediment. Mar Petrol Geol 22: 551-568.

Leifer, I., and D. Culling. 2010. Formation of seep bubble plumes in the Coal Oil Point seep field. Geo-Mar Lett 30: 339-353.

Leifer, I., and A. G. Judd. 2002. Oceanic methane layers: the hydrocarbon seep bubble deposition hypothesis. Terra Nova 14: 417-424.

Leifer, I., and R. K. Patro. 2002. The bubble mechanism for methane transport from the shallow sea bed to the surface: A review and sensitivity study. Continental Shelf Research 22: 2409-2428.

Lloyd, D.; Scott, R. I. Direct measurement of dissolved gases in microbiological systems using membrane inlet mass spectrometry. J. Microbiol. Methods. Vol. 1983, 1, 313–328.

McGinnis, D. F., J. Greinert, Y. Artemov, S. E. Beaubien, and A. Wuest. 2006. Fate of rising methane bubbles in stratified waters: How much methane reaches the atmosphere? J Geophys Res-Oceans 111: -.

Mienert, J., M. Vanneste, S. Bunz, K. Andreassen, H. Haflidason, and H. P. Sejrup. 2005. Ocean warming and gas hydrate stability on the mid-Norwegian margin at the Storegga Slide. Mar Petrol Geol 22: 233-244.

Milkov, A. V. 2000. Worldwide distribution of submarine mud volcanoes and associated gas hydrates. Marine Geology 167: 29-42.

Rasband, W. 1997 - 2012. ImageJ: Image processing and analysis in Java. Astrophysics Source Code Library 1: 06013.

Reshetnikov, A. I., N. N. Paramonova, and A. A. Shashkov. 2000. An evaluation of historical methane emissions from the Soviet gas industry. J Geophys Res-Atmos 105: 3517-3529.

Römer, M., H. Sahling, T. Pape, G. Bohrmann, and V. Spieß. 2012. Quantification of gas bubble emissions from submarine hydrocarbon seeps at the Makran continental margin (offshore Pakistan). Journal of geophysical research 117: C10015.

Sauter, E. J. and others 2006. Methane discharge from a deep-sea submarine mud volcano into the upper water column by gas hydrate-coated methane bubbles. Earth Planet Sc Lett 243: 354-365.

Schlüter, M., and T. Gentz. 2008. Application of Membrane Inlet Mass Spectrometry for Online and In Situ Analysis of Methane in Aquatic Environments. J Am Soc Mass Spectr 19: 1395-1402.

Schlüter, M., P. Linke, and E. Suess. 1998. Geochemistry of a sealed deep-sea borehole on the Cascadia Margin. Marine Geology 148: 9-20.

Schmale, O., S. E. Beaubien, G. Rehder, J. Greinert, and S. Lombardi. 2010. Gas seepage in the Dnepr paleo-delta area (NW-Black Sea) and its regional impact on the water column methane cycle. J Marine Syst 80: 90-100.

Schmitt, M., E. Faber, R. Botz, and P. Stoffers. 1991. Extraction of methane from seawater using ultrasonic vacuum degassing. Anal Chem 63: 529-532.

Schneider Von Deimling, J., J. Greinert, N. R. Chapman, W. Rabbel, and P. Linke. 2010. Acoustic imaging of natural gas seepage in the North Sea: Sensing bubbles controlled by variable currents. Limnol Oceanogr-Meth 8: 155-171.

Schneider Von Deimling, J. S., G. Rehder, J. Greinert, D. F. Mcginnnis, A. Boetius, and P. Linke. 2011. Quantification of seep-related methane gas emissions at Tommeliten, North Sea. Continental Shelf Research 31: 867-878.

Schroot, B. M., G. T. Klaver, and R. T. E. Schuttenhelm. 2005. Surface and subsurface expressions of gas seepage to the seabed - examples from the Southern North Sea. Mar Petrol Geol 22: 499-515.

Schroot, B. M., and R. T. E. Schuttenhelm. 2003a. Expressions of shallow gas in the Netherlands North Sea. Neth J Geosci 82: 91-105.

---. 2003b. Shallow gas and gas seepage: expressions on seismic and other acoustic data from the Netherlands North Sea. J Geochem Explor 78-9: 305-309.

Shakhova, N., I. Semiletov, A. Salyuk, V. Yusupov, D. Kosmach, and Ö. Gustafsson. 2010. Extensive Methane Streaming to the Atmosphere from Sediments of the East Siberian Arctic Shelf. Science 327: 1246-1250.

Short, R. T. and others 2001. Underwater mass spectrometers for in situ chemical analysis of the hydrosphere. J Am Soc Mass Spectr 12: 676-682.

Short, R. T., D. P. Fries, S. K. Toler, C. E. Lembke, and R. H. Byrne. 1999. Development of an underwater mass-spectrometry system for in situ chemical analysis. Meas Sci Technol 10: 1195-1201.

Solomon, E. A., M. Kastner, I. R. Macdonald, and I. Leifer. 2009. Considerable methane fluxes to the atmosphere from hydrocarbon seeps in the Gulf of Mexico. Nat Geosci 2: 561-565.

Tomczak, G., E. Goedecke, and I. Deutsches Hydrographisches. 1962. Monatskarten der Temperatur der Nordsee : dargestellt für verschiedene Tiefenhorizonte. Deutsches Hydrographisches Institut.

Wanninkhof, R., W. E. Asher, D. T. Ho, C. Sweeney, and W. R. Mcgillis. 2009. Advances in quantifying air-sea gas exchange and environmental forcing*. Marine Science 1.

Wenner, P. G. and others 2004. Environmental chemical mapping using an underwater mass spectrometer. Trac-Trend Anal Chem 23: 288-295.

Wiesenburg, D. A., and N. L. Guinasso. 1979. Equilibrium Solubilities of Methane, Carbon-Monoxide, and Hydrogen in Water and Sea-Water. J Chem Eng Data 24: 356-360.

Chapter 6:

~ Synthesis ~

The mass spectrometer deployed in an AUV

6.   Conclusion and outlook

6.1   Conclusions

According to the aim of this study, the *in situ* mass spectrometer was improved in terms of its detection limits with respect to several gases, especially for methane as presented in chapter 3.

In situ mass spectrometry is a useful tool for open questions in marine science. Nevertheless, it is a new technique which needs to be improved and established in the field. In year 2008 we presented a way to calibrate a membrane inlet analyzer like the Inspectr200-200 for methane as well as oxygen based on the volumetric mixture of well-defined standard solutions (Schlüter and Gentz 2008). At this time, the Inspectr200-200 had a detection limit for CH_4 of more than 100 nmol L^{-1} which was not sufficient for many research questions like methane mapping in open waters or the detection of gas plumes in the water column. By implementation of a cryotrap (by cooling ethanol down to -90 ° with liquid nitrogen or a cooling aggregate (Lauda, RP890,Lauda-Königshofen, Germany)) more than 98% of the water vapour in the analytical line is removed, which leads to better conditions for the ionization of the molecules at the ion source (Schlüter and Gentz (2008) and chapter 3 of this thesis). In this way, the detection limits for major and trace gases were considerably improved. Especially, for CH_4 the detection limit was improved by a factor of five to reach ~16 nmol L^{-1}, which allows the measurement of the dissolved CH_4 distribution in the water column above gas seeps as well as in coastal areas.

However, the use of the cryotrap was limited to *ex situ* applications. After unsatisfying tests with Peltier elements (high electrical energy consumption as well as the high waste-heat production) and ethanol cooling by liquid nitrogen (short operational time), the cryotrap was redesigned with a high-end stirling cooler. The stirling cooler is robust, low in power consumption and small in size. After splitting the mass spectrometer in two pressure housings we implemented this cooler in the new "sample unit housing" which also contains the membrane inlet system (MIS).

In contrast to the liquid ethanol cryotrap with cooling systems (e.g., Lauda, RP890) represented in Schlüter and Gentz (2008), the newly designed cryotrap can be used for *in situ* as well as *ex situ* applications and represents the main methodological key result of this thesis. Besides the improvement of the detection limit, the cryotrap represents an important security system in case of a potential rupture of the PDMS membrane. In case of such an incident, the seawater flowing through the $^1/_8$" capillary is instantaneously frozen within the cryotrap. In addition, the analyzer unit from the mass spectrometer was secured mechanically. The free space in the "sensor unit housing" obtained by removing the MIS to the "sample unit housing" was used to install a Pirani pressure sensor (PSG502-S, Inficon™) to measure the absolute pressure in the vacuum line, and a high vacuum solenoid valve (EVI 005 M, Pfeiffer vacuum™). The fast responding Pirani sensor registers the pressure increase in the vacuum section in case of a membrane rupture and triggers the solenoid valve, which uncouples the sensor unit from the sample unit (chapter 3).

Besides the new calibration procedure, the improvement of the detection limits and the implementation of a security system the methodology part contained the comparison of the conventional and novel methods for further investigations. We analyzed the CH_4 concentrations of water samples, parallel to the Inspectr200-200 measurements with gas-chromatography. The results show a close correlation of the methane concentrations between these two techniques.

Chapter 4 deals with the "Quantification of the methane distribution in the water column and its fate in gas ebullition areas".

We conducted a detailed water column study above a gas ebullition area by discrete water sampling for geochemical methods combined with hydroacoustic and oceanographic data. The area is located at the West Spitsbergen continental shelf in ~245 m water depth where we observed 10 active gas flares. The revealed data set allowed the interpretation of the dissolution of methane from submarine released gas bubbles into the water column and the subsequent pathways like microbiological oxidation, dilution by mixing as well as vertical and horizontal transport with regards to

the hydrographic settings. Even though some gas flares were observed rising up to 50 m water depth in this region, we show that ~80 % of the released methane will be trapped by a pycnocline ~20 m above the seafloor which limits the vertical transport and favors horizontal transport. *Ex situ* microbial methane oxidation rates are elevated in the salinity enriched bottom water compared to the upper water column, which suggests ongoing microbial oxidation while the CH_4 load is transported to greater water depth. These results indicate that bubble transport can be excluded as a direct pathway of seabed-released CH_4 to the atmosphere in the study area during the time of measurement. The indirect pathway of seabed-released methane through the water column into the atmosphere by dissolution of gas bubbles and subsequent diffusive flux is indicated by high methane concentrations in the mixed water layer, nevertheless, we assume that the high CH_4 concentrations at the surface originate from the observed gas ebullition area as well as several other sources like inter-granular seepage or micro-seepages occurring widespread over the shelf which makes it difficult to estimate the atmospheric efflux from the observed seepage.

To reach the objective "Detecting, mapping and calculating of the methane inventory in the water column above gas seeps" the obtained results mentioned above were combined (chapter 5).

The acquired knowledge about the limitation of vertical dissolved CH_4 transport due to the pycnocline was used to optimize the sampling strategy during a three day field campaign in a gas seepage area in the Netherland part of the North Sea. Several studies in this part of the North Sea proved the origin of shallow gas, gas chimneys and gas seepage by seismic and other acoustic techniques, but very little is known about the fate and inventory of the seabed-released methane in the water column. The shallow water depth of ~41 m allowed the performance of the improved underwater mass spectrometer in various depths by 3 deployments in between 24 h. In this way we obtained more than 11900 samples directly and simultaneous analyzed for dissolved CH_4 and other gases in a study area of 410 x 400 m where gas ebullition into the water column occurred. This data set presents the first description of dissolved CH_4 in high resolution above a submarine gas seepage visualized in 3-D by ArcGIS[©]. Advantages of the high resolution mapping via mass

spectrometry compared to conventional methods are a higher sampling frequency of up to 750 times which leads to a higher temporal and spatial resolution than would be possible by conventional methods. Furthermore, compared to observation methods like video analysis or model predictions of the gas bubble release the potential diffusive methane flux at the sediment-water-transition-zone is considered. We calculated the dissolved CH_4 inventory to ~$6.4*10^5$ µmol. Due to the unique measurements; these results are not yet comparable with other gas seep areas. Nevertheless, video observations revealed a high gas release by 113 gas streams. Overall we estimate that ~ 65.2 % of the entire seabed-released CH_4 potentially enter the atmosphere via direct and indirect pathways which is far above other observed deep sea gas seeps. Also for gas seeps in shallow water the diffusive flux is higher than the gas seeps observed at Dnepr shelf in the Black Sea, the West Spitsbergen continental margin or the geographically close Tommeliten area. Reasons are the shallow water depth and the observed pycnocline only ~10 m above the seabed. Additional to the high diffusive flux direct transfer of methane into the atmosphere via gas bubble is observed, which is in similarity to the observations at the Coal Oil Point offshore Santa Barbara.

The high resolution measurements by the improved Inspectr200-200 show the importance of new techniques for the understanding of the distribution and fate of methane above gas ebullition areas. As the main result in chapter 5 we consider that the study area in the North Sea is particularly important regarding to the global contribution of submarine gas seeps to the atmospheric methane budget.

6.2   Outlook

The *in situ* mass spectrometry with membrane inlet system is a novel technique and therefore, future work will mainly consist of redesigning some components of the mass spectrometer, optimizing the sampling procedure, and applying the mass spectrometer in combination with other instruments for other scientific questions.

With respect to further investigations of gas ebullition areas, three main improvements are desired.

The Inspectr200-200 is designed for water depths up to 200 m, which is mainly related to the membrane inlet system, but several gas release areas are located in greater water depths (i.e., West Spitsbergen continental margin or Håkon Mosby Mud Volcano). Up to now, the membrane is stretched on a steel spring, which could collapse at a pressure difference of 20 bar (~200 m). Sintered material reveals a high porosity of up to 50 % with a pressure stability of several 100 bar, which would allow the use of the instrument in depths of several thousand meters. Therefore, first prototypes are tested in close cooperation with the Stanford Research Institute (SRI International) to replace the steel spring with sintered metal (material 316L) produced by the Fraunhofer Institute for Manufacturing Technology and Advanced Materials (IFAM).

In the modification of a towed frame, lander or long time mooring system, unmanned underwater vehicles (UUVs) including remote operable vehicles (ROVs) and autonomous underwater vehicles (AUVs) batteries are used for energy supply, which limits the time of operation. As we are not able to optimize the batteries themselves, the power consumption of the mass spectrometer needs to be reduced. This could be done by a redesign of the entire mass spectrometer. Due to the trapped water vapour by the new designed cryotrap, a high vacuum pump with less pump rate and therefore less energy consumption can be used. This leads to a longer time of operation. Additional to the reduced energy consumption, the redesign of the mass spectrometer would result in a smaller housing, which would help to use the instrument in different device holders.

Complementary to the mass spectrometer itself the accuracy of the positioning needs to be optimized. A mismatch of the exact position of the towed frame in the water column related to the ship position is given, which is critical especially in gas ebullition areas where steep gradients over short distances occur. This uncertainty is caused by the influence of i.e., water currents or ship speed on the frame. In water depths of ~40 m the accuracy of the ship coordinates related to the frame position of less than 10 m is sufficient, but a higher uncertainty will be given in greater depths. Therefore an acoustic positioning system (e.g., a transmitter (transducer) on board of the ship and a receiver (transponder) located on the frame) is required. The transducer, with corresponding electronics, calculates an accurate position of the transponder relative to the vessel. This would improve the precision of the frame positioning significantly and would lead to more accurate investigations of the gas distribution in the water column.

Beside the towed frame, other payload carriers are conceivable. Hence, special autonomous underwater vehicles (AUV) get in focus for further investigations. By implementation of the Inspectr200-200 to this payload carrier, large study areas could be investigated in short time. First successful tests in cooperation with an industrial partner have been performed in August/ September 2012. A great advantage of the Inspectr200-200 compared to other methane detection systems is the short response time of ~60 s. Therefore, the immediately measured methane concentrations by Inspectr200-200 could be used for the direct navigation of the AUV to follow i.e., a plume of CH_4 or other gases like CO_2 at natural or anthropogenic induced gas ebullition areas. By this technique a plume mapping could be optimized.

Beside the detection and interpretation of dissolved CH_4 in gas seep areas, another focus of investigations will be the quantification of benthic fluxes by high resolution mapping of major gases (beside the minor gas CH_4) and nutrients. Therefore, the mass spectrometer, which measures continuously and simultaneous gases like N_2, O_2 or CO_2 needs to be combined with benthic chambers and *in situ* sampling systems for analyses of additional nutrients and elements (i.e. NO_3^-, $Si(OH)_4$, PO_4^{3-}, Mn or Fe). Results of a first field applicationare presented in chapter 3.

Additional to the benthic chamber measurements, the mass spectrometer could be combined with a lance system for *in situ* measurements of the pore water in the sediment in various depths. This combination of *in situ* investigations will provide new information about gas and nutrient fluxes at the geochemical important sediment-water-transition-zone.

Acknowledgement / Danksagung

„Wenn man die Forschung nur den Ingenieuren überlässt, hätte man perfekt funktionierende Petroleumlampen, aber keinen elektrischen Strom."

Albert Einstein

Zu Beginn dieser Arbeit wollte ich mein im Ingenieurstudium erlerntes Wissen anwenden, um das Massenspektrometer so weit wie möglich zu optimieren. Während der Dissertation kamen die Einblicke über die Nutzung des Gerätes zum Erhalt neuen Wissens hinzu. Dies hat mir gezeigt hat, wie spannend und wichtig Forschung ist. Für diese Erfahrung bin ich höchst dankbar!

Erklärung

Erklärung gemäß § 6 Abs. 5 der Promotionsordnung der Universität Bremen für die mathematischen, natur- und ingenieurwissenschaftlichen Fachbereiche.

Hiermit versichere ich, dass ich

1. die vorliegende Arbeit ohne unerlaubte fremde Hilfe angefertigt habe,

2. keine anderen als die von mir angegebenen Quellen und Hilfsmittel benutzt habe,

3. die den benutzen Werken wörtlich oder inhaltlich entnommenen Stellen als solche kenntlich gemacht habe.

Bremen, den 3. Januar 2013

Torben Gentz